Dissecting Transcriptional Coactivator Binding Networks To Enable Small Molecule Modulation

by

Andrew Ross Henderson

A dissertation submitted in partial fulfillment of
the requirements for the degree of
Doctor of Philosophy
(Chemical Biology)
in the University of Michigan
2017

Doctoral Committee:

Professor Anna K. Mapp, Chair
Professor Charles L. Brooks, III
Associate Professor Tomasz Cierpicki
Assistant Professor Brent R. Martin

Andrew Ross Henderson

andyhen@umich.edu

ORCID iD: 0000-0002-7955-8538

Acknowledgments

Science is a collaborative process and I have been incredibly lucky to have been surrounded by a fantastic set of conspirators both at the bench and beyond. Without the invaluable contributions of others I would not have been put in a position to accomplish the work presented in this dissertation.

To my parents who taught me the value of curiosity and tolerated an endless stream of questions during our bedtime reading sessions. Thank you. And to my brother who is a complete embodiment of empathy and kindness as well as the funniest person I know.

I am very appreciative of the faculty at Gonzaga University who revealed the excitement and intrigue within biology and chemistry and helped direct me towards graduate school. The risk Professor Tommaso Vannelli took by taking me into his lab was essential in my decision to use grad school as an opportunity to look at the interface between chemistry and biology. Thank you.

I am tremendously grateful to Professor Anna Mapp for her encouragement when applying to graduate school and for letting me work on the complex, challenging, and ultimately fulfilling research questions that have made her lab such an exciting place to be a student. Her guidance has been instrumental in shaping my evolution as a scientist and thinker over the course of my PhD. Thank you.

My development as a scientist was greatly aided by my committee Professor Charles Brooks III, Professor Tomasz Cierpicki, and Professor Brent Martin. Your consistent feedback and thought provoking questions were invaluable. Thank you.

My time in grad school was enriched and eased by fantastic lab mates and collaborators. I owe a tremendous debt to previous lab members especially Paul, Steve, James, and Amanda who taught me so much about how to advance my projects and ask the right questions. Joining the lab at the same time as Matt was such a coup and I have valued his friendship and support throughout. I have also loved working with Matt, Nick, and Amanda and look forward to how they and the rest of the Mapp Lab move our research forward. Thank you all.

To the 2012 Chemical Biology cohort who made grad school bearable at first and exciting throughout. Thank you.

Lastly, I have been gifted a tremendous group of friends accumulated in Seattle, Spokane, and Ann Arbor. Jeff, Nathan, Alex, and Aaron who I have known perhaps too long. Thank you for everything. Time outside of lab in Ann Arbor was enlivened in ways I never imagined by Chris, Mairead, John, Maya, Vik, Elin, and Tim. What a windfall.

Table of Contents

List of Figures

List of Tables

List of Abbreviations

ABD   Activator Binding Domain
AcID   Activator Interaction Domain
ATF6α   Activating transcription factor 6 α CBP CREB Binding Protein
DBD   DNA-Binding Domain
DMEM   Dubelco's modified eagle medium
DMSO   Dimethyl sulfoxide
DNA   Deoxyribonucleic Acid
FBS   Fetal bovine serum
FP   Fluorescence polarization
GACKIX   Gal11, Arc105, CBP/p300, kinase-inducible domain interacting (KIX)
HAT   Histone acetyltransferase
HDAC   Histone deacetylase
HPLC   High-performance liquid chromatography
HSQC   Heteronuclear sing quantum coherence
HSV   Herpes simplex virus
HTS   High-throughput screen
IKK   Inhibitor on kappa b kinase
IPTG   Isopropyl-β-D-1-thiogalactopyranoside
KIX   Kinase inducible domain interacting domain of CBP
MD   Molecular dynamics
MDM2   Murine double minute 2
Med25   Mediator subunit 25
MLL   Multi-lineage leukemia
MMP   Matrix metalloproteinase
mRNA   Messenger RNA
MS   Mass Spectrometry
NF-κB   Nuclear factor kappa B
NMR   Nuclear Magnetic Resonance
NEMO   NF-κB essential modifier
NR   Nuclear receptor
PC4   Positive Cofactor 4
PDB   Protein DataBank
PIC   Preinitiation complex
pKID   Phosphorylated kinase inducible domain (CREB)
PPI   Protein-protein interaction

PrOF	Protein-observed fluorine NMR
RARα	Retinoic acid receptor α
RNA	Ribonucleic acid
RNAPII	RNA Polymerase II
RPM	Revolutions per minute
RT-qPCR	Real time quantitative polymerase chain reaction siRNA Small interfering RNA
siRNA	silencing RNA
shRNA	short hairpin RNA
TAD	Transcriptional Activation Domain
TFIIA	Transcription factor II A
UV/Vis	Ultraviolet/visible spectroscopy
VP16	Herpes simplex virus protein 16
VWA	Von Willebrand Factor Type A

Abstract

The activation of transcription is reliant on the coordinated assembly of multiple dynamic protein complexes at promoter regions of DNA. The composition of this transcriptional machinery varies with cell type and cell cycle allowing for differential gene expression associated with different cellular processes and pathways. Central mediators of transcription are coactivator proteins that form key protein-protein interactions (PPI) with DNA-bound transcriptional activators via activator binding domains (ABD). Due to the requirement of these activator-coactivator interactions for gene expression, dysregulation of both activators and coactivators is associated with many diseases including cancers, metabolic disorders, and developmental defects. Thus, there is great interest in the development of small molecules capable of targeting these dynamic protein interfaces in diseases linked to aberrant activator-coactivator activity. Activator-coactivator interactions are challenging small molecule targets because of the broad, dynamic surfaces that mediate their interactions. Successful targeting of these PPIs has been facilitated by detailed structural and mechanistic characterization of individual activator-coactivator complexes. However, only a small subset of activator-coactivator interactions have been mechanistically characterized leaving many open questions surrounding how differences in ABD structure alter activator-coactivator complex formation.

In this dissertation, we characterize the mechanistic and structural properties of activator interactions with the Activator Interaction Domain (AcID) of Med25. AcID is a structurally unique ABD and we trace the mechanistic features of its interactions with activators to other more

characterized coactivator ABDs including the KIX domain of CBP. We show that although it has a unique protein fold, many of the mechanistic features driving AcID activator interactions are observed in structurally diverse ABDs.

Med25 AcID interacts with multiple transcriptional activators demonstrated to drive gene expression linked to multiple diseases including metastatic cancers. Disrupting these AcID-activator complexes can lead to downregulated expression of these disease-associated genes underscoring the potential of small molecule inhibitors of these interactions. We demonstrate that two native cysteines within the AcID domain of Med25 can be targeted by small molecules and are functionally positioned such that targeting these cysteines with small molecules can inhibit activator-AcID complexes. We next describe the use of Tethering to identify covalent small molecule modulators of AcID function. Through this screen we identified the compound A6, which induces allosteric modulation of the AcID domain and the use of a cell active analog of A6 to inhibit Med25 AcID-dependent gene expression in live cells.

Activator-coactivator interactions that have yet to be fully characterized evade targeted inhibitor discovery strategies. We show that transcriptional activity can be modulated via two different methods of targeting the NF-κB transcriptional activation pathway beyond activator-coactivator interactions. One approach selectively inhibits canonical NF-κB signaling through the use of a novel stabilized peptide (NBD2) that inhibits the IKK-NEMO interface of the IKK kinase complex. We also describe the mechanistic characterization of ketogibberellic acid methyl ester which acts as a potent inhibitor of NF-κB activity.

Chapter 1

INTRODUCTION

1.1 ABSTRACT

Transcriptional activation occurs through the assembly of multimeric protein complexes at promoter regions of DNA leading to gene expression. Transcriptional coactivators act as central hubs in this process by forming protein-protein interactions (PPI) with DNA-bound transcriptional activators and the rest of the transcriptional machinery. These activator-coactivator interactions are mediated by activator binding domains (ABD) within coactivator proteins. These ABDs are a class of structurally diverse tertiary folds united by their function as partners for activator binding. Transcriptional activator activity often becomes dysregulated in disease and as such the protein-protein interfaces between activators and coactivators are useful points for therapeutic intervention with small molecules that can inhibit or modulate these PPIs. Activator-coactivator PPI have been a classically challenging drug development target because of the large surface areas and conformational dynamics characteristic of these interfaces. Successful targeting of activator-coactivator interactions is facilitated by the use of screening strategies well-suited to identifying PPI inhibitors and by a refined understanding of the mechanistic features that drive activator interactions with ABDs.

1.2 TRANSCRIPTIONAL REGULATION – AN OVERVIEW

The maintenance of regulated transcription is essential for the growth and propagation of all organisms. While there are approximately 20,000 protein coding genes in the human genome, a comparatively small subset of these proteins form a complex network that coordinates to convert genetic information stored as DNA into mRNA.[1] The expression of a single gene requires the temporal and spatial arrangement of proteins bearing many different enzymatic and structural functions at a promoter, culminating in the localization of RNA Polymerase II (RNA Pol II) to the target gene and catalyzing the conversion of the gene to RNA (Fig 1.1). For RNA Pol II to effectively bind the upstream promoter of the target gene, chromatin modifying enzymes like histone deacetylases (HDACs) and the general transcription factors TFIIA, TFIIB, TFIID, TFIIE, TFIIF, and TFIIH serve to relax DNA up- and downstream of the gene promoter sequence allowing for the assembly of the preinitiation complex (PIC). While these core PIC components are required for the transcription of nearly all genes, the context specificity and control of gene expression is attributable to a variable set of transcriptional activator and coactivator proteins whose composition is influenced by factors such as cell cycle, cell type, extracellular stimuli, or epigenetic marks. Because of their central role in the recruitment andrganization of the PIC, activator-coactivator protein-protein interactions are essential for the maintenance of healthy phenotypes and defects in their function are implicated in many diseases.

1.3 TRANSCRIPTION IN DISEASE

Regulated transcription, and by extension maintained human health, is dependent upon a complex and extensive network of proteins coordinating their temporal and spatial

arrangement.[2] Diseases can arise from incorrect regulation of chromatin, overexpression or under expression of transcription factors, mutations in transcription factors, chromosomal translocations of transcription factors, coactivator mutations, or defects in upstream signaling pathways.[3-6] In many of these cases, the protein-protein interactions between transcriptional activators and their coactivator binding partners are key for propagation of the disease phenotype and thus represent valuable, if challenging, sites for therapeutic intervention.

One important coactivator-mediated transcriptional pathway is the Wnt signaling network that regulates the expression of numerous genes involved in cell differentiation, proliferation, and survival.[7] β-Catenin acts as a coregulatory hub in the Wnt pathway via protein-protein interactions with transcriptional activators and other coactivator partners including CREB-binding protein (CBP) and Mediator complex subunits.[8,9] Upregulated or constitutive Wnt signaling is implicated in many cancers including, most notably, colorectal cancers.[9,10] Targeting protein-protein interactions between β-Catenin and transcription factors or other coactivators such as CBP or Mediator can disrupt overactive Wnt signaling leading to downregulation of oncogene expression.[11] For example, a stapled peptide targeting the β-Catenin interaction with the TCF transcriptional activator downregulates TCF-dependent gene expression.[8]

A second example is the complex formed between the master coactivator p300 and the transcription factor c-Myb. Under normal conditions, the transcription factor c-Myb is required for hematopoietic differentiation through interactions with several coregulatory binding partners.[12-16] In acute myeloid leukemia (AML), c-Myb coordinates gene expression essential for the maintenance of the leukemic state induced by the oncogenic fusion transcription factor, MLL-AF9 (Fig 1.2).[17] Interactions of c-Myb and MLL with p300 are critical for the induction of AML

oncogenes and occur via binding with the GACKIX (KIX) domain.[18] Genetic studies have shown

that knockdown of c-Myb expression or mutations within the c-Myb activation domain that

disrupt c-Myb-p300 interactions inhibit MLL-AF9-induced leukemic transformations.[19,20] The

demonstration that blocking the Myb-p300 interaction stops AML proliferation highlights the

therapeutic potential of blocking activator-coactivator interactions.
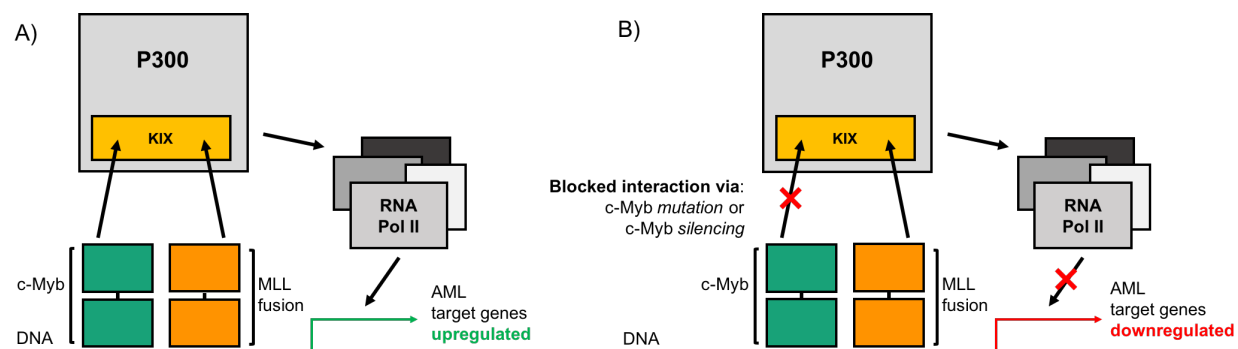
Figure 1.1 Role of p300-activator interactions in leukemogenesis A. The KIX domain of p300 is binding partner of c-Myb and MLL both of which drive expression of AML oncogenes. B. Downregulation of c-Myb expression inhibits leukemic transformations driven by MLL-fusion proteins. Blocking the p300-Myb interaction via c-Myb mutation also inhibits AML oncogene expression.[18,20]

In diseases resulting either from aberrant Wnt-signaling or p300-Myb-MLL mediated

leukemogenesis, blocking activator-coactivator interactions results in cell death underscoring the

therapeutic potential of these PPIs. Even in the mechanistically defined, KIX-Myb system, the

identification of small molecules has been challenging. In less defined activator-coactivator

interaction networks, answering the open structural and mechanistic questions surrounding

activator-coactivator complex formation are necessary to guide the discovery and development

of new molecules targeting diverse disease-associated transcriptional pathways.[21]

1.4 TRANSCRIPTIONAL COACTIVATORS

The transcriptional preinitiation complex is composed of multiple activator-interacting protein complexes required for the recruitment of RNA Pol II and activated gene expression (Table 1.1). These coactivators perform multiple tasks including enzymatic modification of histones and DNA or scaffolding and recruitment roles. Many of these coactivators are hubs able to directly contact multiple transcriptional activators bound at gene promoter and enhancer elements integrating these signals into the assembly and activity of the PIC. CBP, and its paralog p300, are multidomain proteins that interact with over 400 transcriptional activators and can directly modulate chromatin structure via an enzymatic histone acetyl transferase domain (HAT).[22,23] Mediator is a megadalton multi-subunit protein complex that makes direct contact with RNA Pol II and the associated general transcription factors.[24-26] SRC-1 mediates transcriptional response to androgen and other hormones by directly binding nuclear receptors and through intrinsic histone modifying activity.

Activator interactions with coactivators occur via activator binding domains (ABDs). ABDs are conformationally dynamic protein folds that exist within all of the above mentioned coactivator proteins and enable interaction with the multitude of transcriptional activators that regulate the expression of protein coding genes. Despite the importance of activator-coactivator interactions and their demonstrated role in disease, very few ABDs have been structurally or mechanistically defined. Further mechanistic definition will add to our understanding of transcriptional activation and aid in the development of novel therapeutics.

Table 1.1: Activator-interacting coactivator complexes

Coactivator	Function
CBP/p300	Multi-domain hub with activator binding and histone modifying properties[27]
Mediator Complex	Multi-subunit complex that bridges transcriptional activators and RNA Pol II[28]
SRC-1	Nuclear receptor binding protein[29]
β-catenin	Hub for activator and CBP/Mediator binding[7]
SAGA	Multi-subunit complex that binds transcriptional activators and modifies histones[30]

1.5 STRUCTURAL DIVERSITY OF COACTIVATOR ACTIVATOR BINDING DOMAINS

Unlike transcriptional activators that only adopt secondary structure upon binding a protein interaction partner, activator binding domains within transcriptional coactivators exist as folds with tertiary structures even when unbound by activators.[31] Solution NMR studies have revealed large structural diversity across several ABDs (Fig 1.3). Although ABDs are a structurally diverse group, many of the characterized ABDs are largely α-helical. In the KIX domain of CBP/p300, activators make critical contacts with residues on α-helices inducing allosteric rearrangement of the three helix bundle.[32,33] Additionally, flexible unstructured loops link secondary structural elements. A much rarer secondary structural feature is the presence of β-sheets in PC4 and a 7-stranded β-barrel in the AcID motif of AcID.[34-37] The presence of β-sheet architecture in these domains is unique and how they alter their activator binding properties remains an open question.

CBP KIX
2LXS

Med25 AcID
2XNF

CBP Taz1
1U2N

PC4
2PHE

CBP Taz2
1F81

CBP iBid
2KKJ
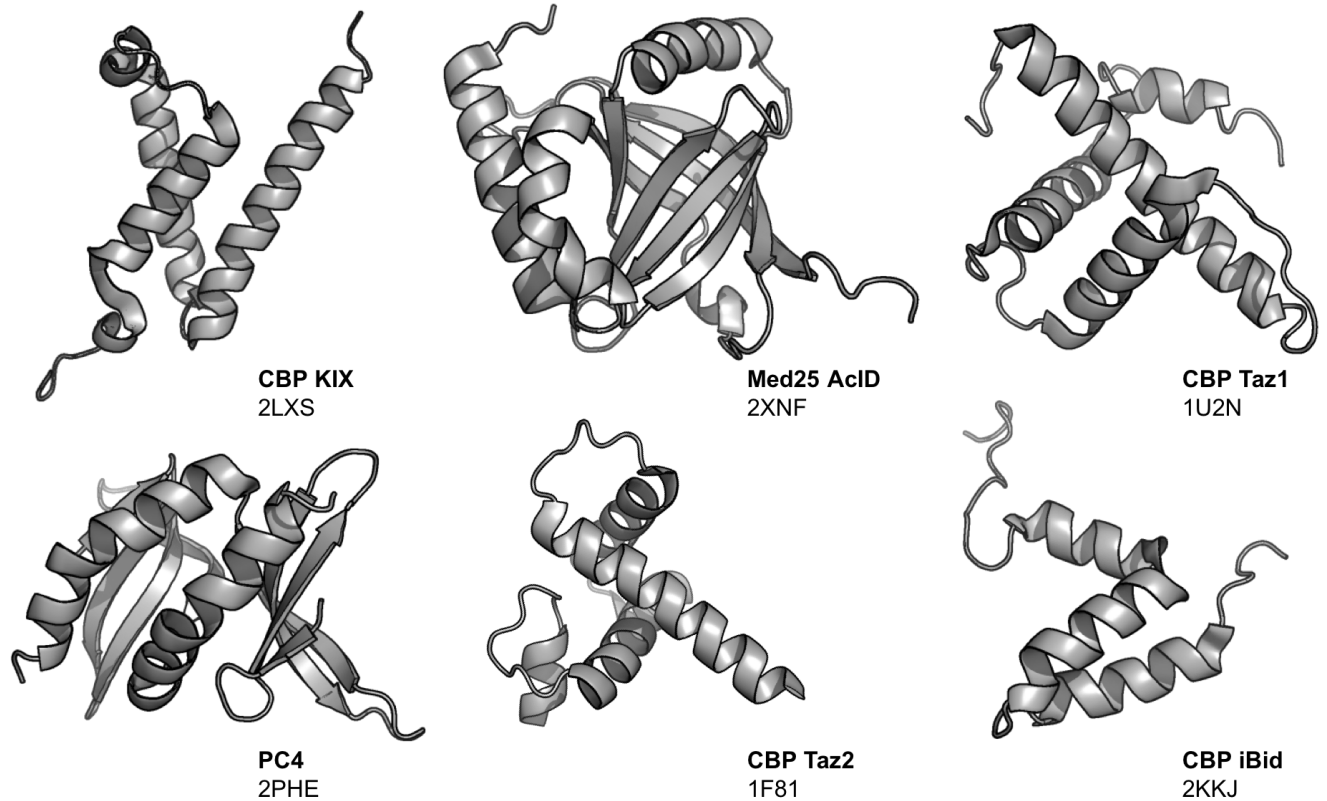
Figure 1.2 Activator binding motifs of transcriptional coactivators are structurally diverse ABDs are structurally diverse despite their shared function. ABDs possess a high degree of α-helicity and multiple unstructured loop regions are common. PC4 and Med25 AcID possess notable β-sheet structures.[12,33,34,37-40]

Despite this structural diversity, ABDs of transcriptional coactivators all serve the same nominal function: to link DNA-bound activators to RNA Pol II and its associated complex network of co-factors and co-regulators. A second feature is that they are able to form particular binary and ternary complexes with many different transcriptional activators. This raises the question of how structure dictates or guides the function and mechanism of activator-coactivator complex formation. Mechanistic characterization of activator-coactivator complex formation has focused on only a subset of the known activator-coactivator interactions known to occur in biology with most of these studies performed on a single activator binding domain. Those mechanistic details

have been outlined below and will be used as a means of comparison to a structurally diverse set of activator-coactivator complexes throughout this dissertation.

1.6 MECHANISTIC UNDERPINNINGS OF ACTIVATOR-COACTIVATOR INTERACTIONS

Conformational heterogeneity in ABDs

ABDs can use the same group of amino acids to interact with a diverse set of transcriptional activators. The Taz1 domain of CBP interacts with upwards of 12 different transcription factors while the iBid domain of CBP complexes with 7 activators.[41] The KIX domain of CBP interacts with at least 13 activators between two non-overlapping binding sites (Fig 1.4). The KIX-targeting activators pKID and MLL bind to opposite sites on KIX and differentially perturb the KIX structure.[33,42] This conformational heterogeneity observed with activators bound at opposite KIX binding sites and at other ABDs within CBP/p300 results from the high degree of intrinsic disorder in both activators and ABDs.[23] This intrinsic disorder paradoxically enables both specificity and promiscuity in activator-coactivator interactions, allowing for distinct activators to compete for the same binding surface during transcriptional activation only remaining bound until adequate levels of their transcriptional products have been produced.
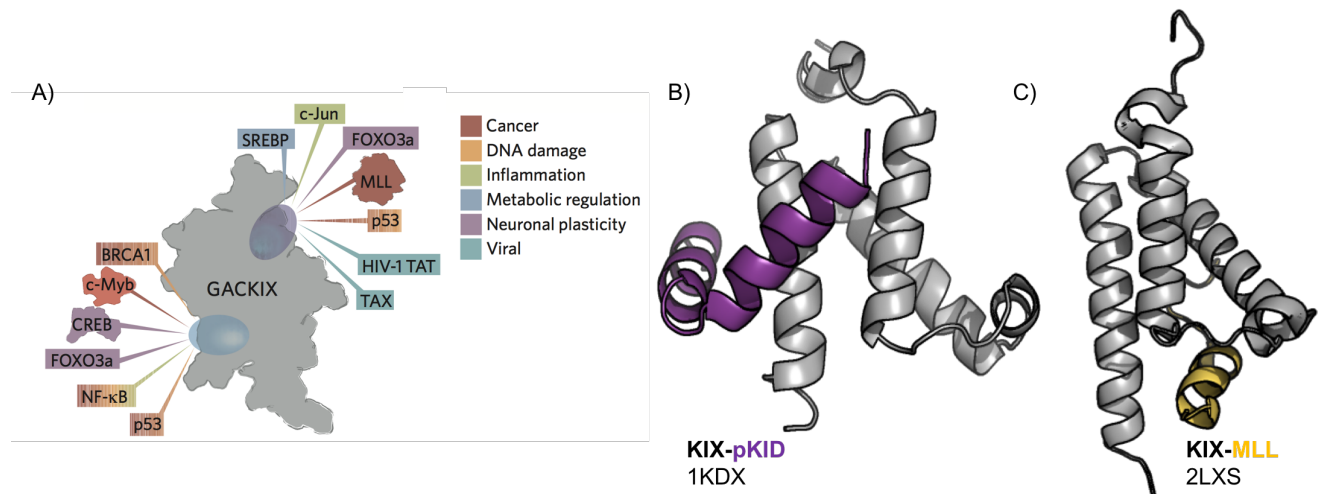
Figure 1.3 Conformational heterogeneity in KIX molecular recognition A. GACKIX of CBP interacts with over 13 activators at two discrete binding surface. B. The structure of KIX-pKID is distinct from the KIX-MLL complex (C.) highlighting the conformational heterogeneity within the domain.[33,42] Modified from Mapp et al., *Nat. Chem. Bio.* **2015**, 11, 891-894.[21]

Ternary complex formation at ABDs

Structural studies have revealed the presence of multiple activator binding surfaces on many ABDs. In some cases these isolated binding sites can be simultaneously occupied by a single bidentate activation domain. VP16 has two functionally independent activation domains in its 77-amino acid sequence that have been shown to simultaneously bind two discrete binding surfaces of Med25 AcID.[12,37] Another bidentate activator, FoxO3a, simultaneously binds both binding surfaces on CBP KIX.[43] KIX and Taz2 of CBP can also be simultaneously bound by both activation domains of p53.[44-46] Formation of ternary complexes involving two distinct activators bound at the opposite binding surfaces on KIX has been described for several activator pairs including c-Myb and MLL.[47-50] The in vivo significance of these ternary complexes has been a challenging question to answer, but several elegant experiments have pointed to the existence

of the KIX allosteric network as means of enabling selective ternary complex formation dependent upon activator sequence and identity.[51,52]

Allostery and Cooperativity in ABDs

Given that ABDs such as KIX, Taz1, and Taz2 can interact with a multitude of activators at non-overlapping binding sites, allosteric communication offer another means for specificity in activator-ABD ternary complex formation.[50] This could lead to specific enhancement of certain transcriptional products given a particular cellular signal or context.[53] The existence of allostery in activator binding motifs is a much less well characterized phenomenon with its description and characterization limited to the KIX domain of CBP.[54] Cooperative binding within the KIX domain has been described for several activator pairs with cooperativity values ranging from 1.4 to 18.[52] The MLL-KIX complex preferentially forms an MLL-KIX-CREB complex over MLL-KIX-cMyb by a factor of two and by a factor of 18 over MLL-KIX-HBZ.[52,55] A host of biochemical, NMR, and computational studies have been completed to define the KIX allosteric network and how it contributes to the positive cooperativity observed in KIX ternary complexes.

Tollinger and colleagues have used a combination of NMR and molecular dynamics (MD) simulations to show that KIX undergoes a significant conformational change upon MLL binding followed by a subtle rearrangement of the KIX hydrophobic core upon pKID binding to form a stable ternary complex.[33] Allosteric coupling in KIX has also been proposed to involve preferential selection of specific "excited state" conformations of KIX (<7 % of KIX conformers) by MLL upon binary complex formation. Further, MLL binding to KIX causes a redistribution of conformational substates towards those that favor pKID binding.[33,56] In line with these finding, Brooks and

colleagues used computational simulations to show that MLL binding to KIX "prepays the entropic penalty" of cMyb binding, essentially increasing the favorability of ternary complex formation.[57]

Because KIX has served as the only model system for cooperativity and allostery in ABDs, it remains to be seen how conserved these mechanisms are across structurally distinct ABDs.

Kinetic mechanisms of activator-coactivator complex formation

Kinetic assessment of binary and ternary complex formation involving activators and ABDs provide another essential insight into molecular recognition by ABDs and how allostery is regulated within them. Stopped-flow transient kinetics experiments showed that c-Myb, a highly-disordered peptide prior to binding, association to KIX was an order of magnitude faster ($2.2 \pm 0.1 \times 10^7$ $M^{-1}s^{-1}$) than its predicted value if it were to be a folded protein.[58,59] As activator binding to KIX is proposed to be a coupled binding and folding process, this remarkable association speed may lower the activation barrier between bound and unbound states thereby making each collision more likely to result in binary complex formation.[31,47,60,61] Electrostatics offer a strong contribution to activator binding to ABDs and this has also been demonstrated to lead to significantly enhanced association rates.[62,63] The combination of electrostatics and intrinsic disorder combine to make activator-coactivator complex formation among the fastest protein-protein association events ever recorded.[59]

While complex formation between activators and coactivators is characterized by extremely fast association, the kinetic basis of cooperativity in ternary complex formation is modulated through changes in dissociation kinetics. Mapp and colleagues performed transient kinetic analysis of ternary activator-KIX complexes and observed a 30% reduction in k_{off} for pKID from KIX-MLL than from KIX alone.[51] Notably, in studies involving a covalent small molecule, the

fragment 1-10, tethered at the MLL site on KIX, they observed negative cooperativity with pKID binding, a much rarer phenomenon. Negative cooperativity was found to be directed through both a decrease in pKID association and increased dissociation rates. This reduction in dissociation kinetics was also observed by Clarke and colleagues for several KIX-activator ternary complexes capable of inducing positive allostery.[52]

1.7 THE ACID DOMAIN OF MED25 – A UNIQUE ABD STRUCTURE

Mediator subunit 25 (Med25) is conserved in metazoans and is a linchpin of PIC assembly for many transcription factors via a nuclear receptor recognition sequence (NR Box) and the Activator Interaction Domain (AcID) (Fig 1.3). AcID is a novel protein fold composed of a 7-stranded β-barrel flanked by 3 α-helices and flexible loops that is observed in only one other protein, Prostate Tumor Overexpressed Variant 1 (PTOV1).[64,65] The AcID motif is an ABD for activators that mediate cellular differentiation (ERM), oxidative stress response (ATF6α), and viral infection (VP16).[12,36,66,67] In addition to the virulent VP16 activator, AcID binding partners control disease-associated gene expression such as metastasis (ERM) or diabetes and neurodegeneration (ATF6α).[68,69] Because of its association with disease, targeting activator-AcID interactions with small molecules is a promising therapeutic strategy. The development of high quality inhibitors of these interactions will be aided by the mechanistic definition of key aspects of AcID-activator complex formation. By mechanistically characterizing activator-AcID complex formation, important questions about conservation of mechanistic details of activator-coactivator interactions across structurally diverse domains can be answered.

1.8 MODULATING ACTIVATOR-COACTIVATOR INTERACTIONS

Targeting the protein-protein interfaces of activator-coactivator complexes with small molecules is challenging. But the mechanistic complexity of activator-coactivator complex formation offers several means by which small molecules can modulate these interactions. First, orthosteric inhibitors of individual binding surfaces on ABDs offer a means to block activator binding at that location. More interesting would be molecules that access the structural plasticity and disorder inherent to ABDs to modulate their structure. Small molecules capable of engaging the allosteric network of an ABD could tune binding at both activator binding surfaces simultaneously. As all ABDs interact with multiple activators at shared binding surfaces, the ability to selectively inhibit a subset of these interactions while leaving others intact or even enhanced would be an extremely valuable means of targeting disease pathways while leaving the core biological functions mediated by a given ABD intact. Molecules designed to exploit the conformational heterogeneity of coactivators by stabilizing certain coactivator conformations thereby inhibiting a subset of activators while favoring the interactions of a different subset would be a useful way to inhibit disease-associated activator interactions while not interfering with the activation activity or normal pathways.

The ability to identify molecules that target ABDs in this manner will be facilitated by further mechanistic studies of activator-coactivator complexes especially in those for which little mechanistic information is known. Mechanistic details can also be further probed by the discovery of small molecules that modulate ABDs in these specific ways.

Activator-coactivator protein-protein interfaces are characterized by their often broad surface areas, These are in direct contrast to the deep, small surface area (300-500 Å^2) binding

interfaces observed for enzyme-substrate reactions.[70,71] As a result, while medicinal chemists have had great success identifying small-molecule enzyme inhibitors, the discovery of novel molecular scaffolds suited to the inhibition of PPIs has been a more arduous process. Despite these challenges, the development of chemical probes capable of targeting transcriptional PPI would have enormous potential as mechanistic probes and more importantly as novel therapeutics for the numerous diseases stemming from dysregulated transcription. Advances in PPI inhibitor development have come from enhanced understanding of PPI characteristics and mechanisms, novel screening strategies, and the development of new small-molecule and peptide-based scaffolds with unique activity at PPI interfaces.

Features of protein-protein interfaces influence inhibitor development success

Notwithstanding the difficulty, extensive progress has been made this century in identifying and developing chemical modulators of PPIs. The expansive growth in this field is illustrated by databases of PPI inhibitors like the 2P2Idb database which catalogues PPI inhibitors for which structural information is available.[72-74] Upon its release in 2010, 2P2Idb contained 31 inhibitors of 8 distinct protein-protein complexes.[75] An update in 2016 has seen this database grow to cover 27 protein-protein interfaces inhibited by 242 distinct molecules.[72,75,76] Several reviews have used these databases to examine trends in PPI inhibitor development based on the affinity and surface area of each protein-protein complex.[21,77,78] This analysis revealed that PPIs exist across a continuum of affinity and surface area (Fig 1.5). The greatest number of identified inhibitors have been those that target PPIs that more closely resemble enzyme-substrate like interactions of small surface area (< 1700 Å^2) and high affinity (< 500 nM) such as the p53-MDM2

interface.[79,80] The larger (1700-5000 $Å^2$) and weaker affinity (> 1 µM) targets have proven more elusive, yet new inhibitors have continued to emerge that target within this regime (Fig 1.5).
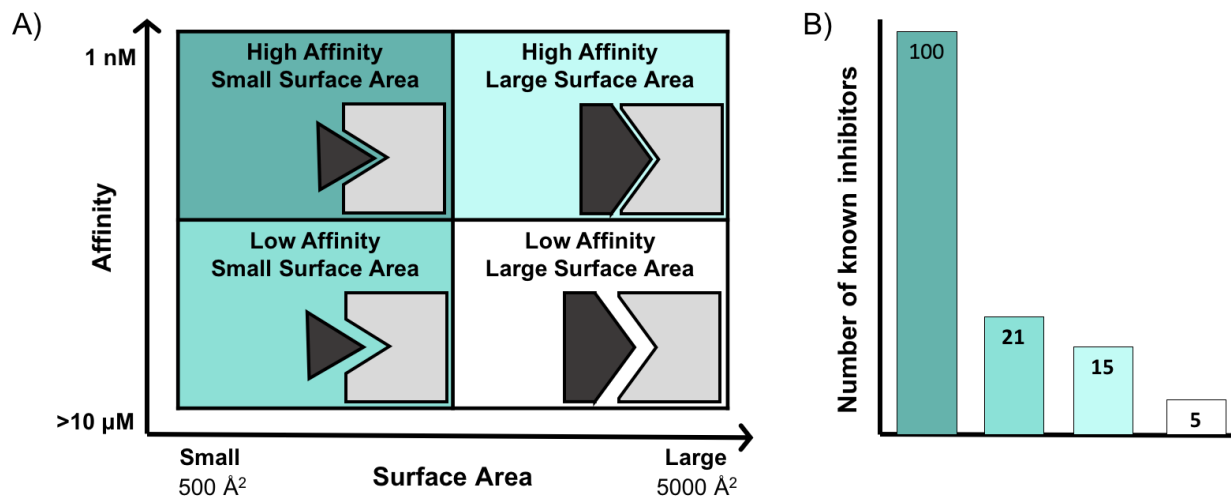
Figure 1.4 Targetability of different classes of protein-protein interactions A. PPIs can be grouped according to their affinity (y-axis) and surface area (x-axis). B. The number of reported PPI inhibitors for each class of PPI.[21,77,78]

Examples of Activator-cofactor inhibitors

A variety of activator-cofactor interfaces are the focus of several active inhibitor discovery campaigns. The interaction between the transcriptional activator p53 and its masking protein MDM2 has been very successfully targeted by small molecules due to its high affinity and small surface area.[80] p53 is a critical regulator of cell cycle progression and apoptosis and is silenced by MDM2 under non-stress conditions. MDM2 is overexpressed in many malignancies leading to inappropriate silencing of p53 activity.[81] Vassilev and coworkers at Roche identified the Nutlin class of inhibitors that selectively target the p53-MDM2 interface leading to a rescue of p53 function and induction of senescence in cancer cells (Table 1.2).[82] Wang and colleagues used structure-based design and modeling to identify a natural product derived MDM2 inhibitor.[83]

Stapled peptides have proven to be effective activator-coactivator inhibitors. Verdine and colleagues identified a series of 17-mer stapled peptides capable of inhibiting the TCF-β-catenin interaction. These StAx peptides are cell permeable and inhibit β-catenin-mediated transcription.[8] Additionally, the inhibition of the ICN-MAML complex necessary for NOTCH signaling via a 17-mer stapled peptide. This peptide inhibited genome-wide expression of NOTCH-activated genes in leukemia cells.[84]
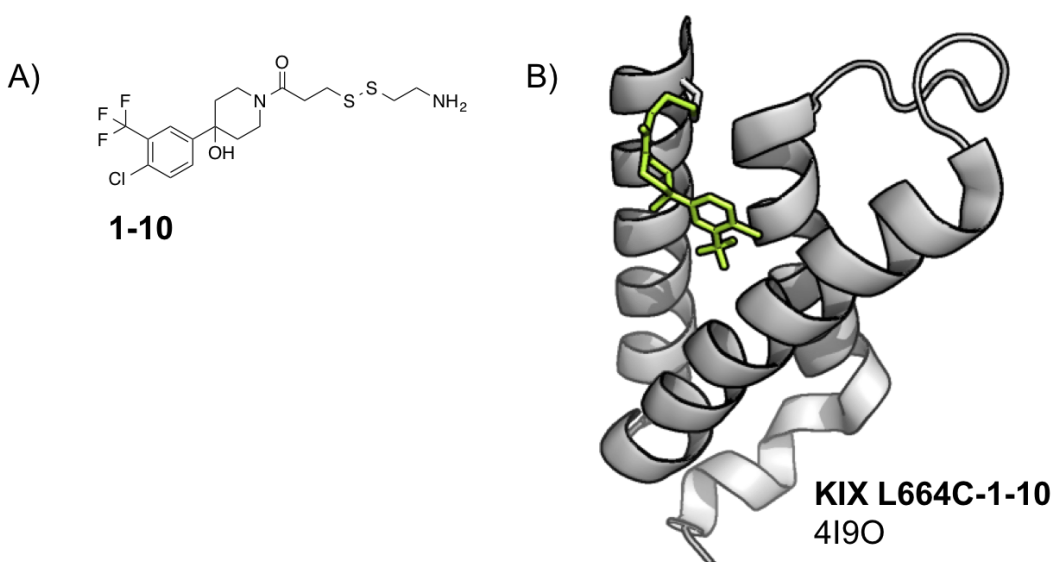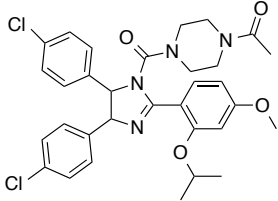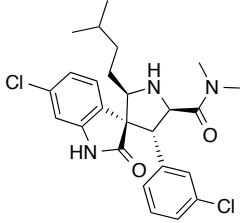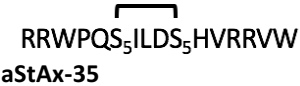
Figure 1.5 Figure 1.6 1-10 is an allosteric modulator of KIX A) The fragment 1-10 was identified from a tethering screen of the KIX-MLL interaction. B) A 1-10 stabilized complex resulted in the first crystal structure of KIX.
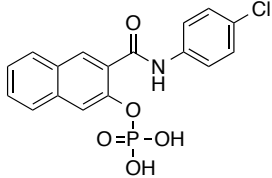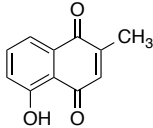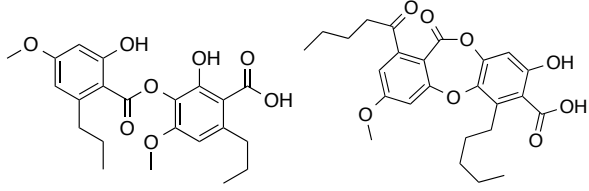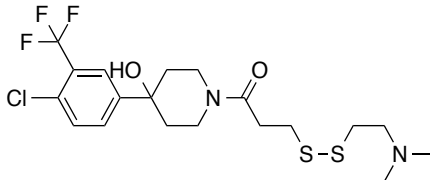
KIX has also served as a hub of active small molecule inhibitor research. The KIX-pKID interaction was originally screened via NMR and KG-501 was identified as a 115 μM inhibitor of the complex capable of disrupting KID-KIX interactions in cells.[85] Sekikaic and lobaric acids function as dual orthosteric allosteric inhibitors of pKID-KIX and MLL-KIX interactions through binding at the MLL site.[86] A tethering screen of the KIX-MLL interaction identified the fragment 1-10 that has proven to be an extremely useful chemical modulator of KIX function (Fig 1.6).[51,87]

This low molecular weight fragment was an effective orthosteric inhibitor of MLL binding (KD) but also an allosteric modulator capable of inducing positive and negative binding cooperativity in activators targeting the opposite pKID binding site on KIX. This fragment was also a stabilizer of KIX structure and allowed for the first ever crystal structure of KIX to be obtained (Fig 1.6).

Targeting the KIX domain has been aided by the extensive mechansitic and structural information that has been obtained through decades of study. These molecules, in turn, have added to our understanding of KIX funtion both in vitro and in vivo. The identification of molecules targeting other ABDs, such as AcID, will benefit from additional mechansitic studies that preceed a molecule screening campaign.

Table 1.2 Inhibitors of Activator-Cofactor interactions

Molecule	Target	Method	Reference
Nutlin-1	p53-MDM2	HTS Screening	Vassilev et al. *Science*, **2004**, 303, 844-848.
Compound 1f	p53-MDM2	Structure-based design and modeling	Ding et al. *JACS*, **2005**, 127, 10130-10131.
RRWPQS$_5$ILDS$_5$HVRRVW aStAx-35	TCF-β-catenin	Stapled Peptide	Grossmann et al. *PNAS*, **2012**, 109, 17942-17947.
βAla-ERLRRRIS$_5$LCRS$_5$HHST SAHM1	ICN-MAML	Stapled Peptide	Moellering et al. *Nature*, **2009**, 462, 182-190.

\n**KG-501**	pKID-KIX	NMR-based screen	Best et al. *PNAS*, **2004**, 101, 17622-17627.
\n**Plumbagin**	Myb-KIX	Cell-based screen	Uttarkar et al. Mol Cancer Ther, **2016**, 15, 2905-2915.
\n**Sekikaic acid**　　**Lobaric Acid**	MLL-KIX-pKID	Natural products extract screen	Majmudar et al. *Angew. Chem. Int. Ed.* **2012**, 51, 11258-11262.
\n**1-10**	MLL-KIX	Disulfide Tethering	Wang et al. *J. Am. Chem. Soc.*, **2013**, 135, 3363-3366.

1.9 DISSERTATION SUMMARY

The overarching goal of my research has been to identify small molecules capable of targeting transcriptional activator-coactivator interactions as a means of regaining control of aberrant transcriptional activity in diseased cells. To that end, I have focused on the structurally unique AcID domain of Med25 which serves as a necessary binding partner of several disease-associated activators. To facilitate our small molecule discovery efforts, I have first sought to better define the mechanistic details surrounding activator-AcID interactions. Because AcID is such a novel fold we demonstrate the extent of conservation of activator-coactivator mechanistic details across coactivators of diverse structures using a combination of site-specific covalent peptides, solution NMR, and stopped-flow kinetics. Building on this enhanced understanding of

the mechanistic behavior of the AcID domain, I screened an activator-AcID interaction in pursuit of new small molecule modulators of AcID activity. I identified molecules that both structurally perturb AcID and function as cell-active modulators of Med25-dependent transcription.

Because of the challenges inherent in targeting activator-coactivator interactions, I also describe work developing inhibitors of other transcriptional protein-protein interactions. This work has focused on targeting aspects of the NF-κB signaling pathway and describes the identification of a peptidic inhibitor of canonical NF-κB signaling as well as the mechanistic characterization of small molecule inhibitor of NF-κB activity.

1.10 REFERENCES

1   Djebali, S. *et al.* Landscape of transcription in human cells. *Nature* **489**, 101-108, doi:10.1038/nature11233 (2012).

2   Lee, T. I. & Young, R. A. Transcriptional regulation and its misregulation in disease. *Cell* **152**, 1237-1251, doi:10.1016/j.cell.2013.02.014 (2013).

3   Baker, R. G., Hayden, M. S. & Ghosh, S. NF-kappaB, inflammation, and metabolic disease. *Cell Metab* **13**, 11-22, doi:10.1016/j.cmet.2010.12.008 (2011).

4   Gasi Tandefelt, D., Boormans, J., Hermans, K. & Trapman, J. ETS fusion genes in prostate cancer. *Endocr Relat Cancer* **21**, R143-152, doi:10.1530/ERC-13-0390 (2014).

5   Chen, T. & Dent, S. Y. Chromatin modifiers and remodellers: regulators of cellular differentiation. *Nature reviews. Genetics* **15**, 93-106, doi:10.1038/nrg3607 (2014).

6   Rahl, P. B. & Young, R. A. MYC and transcription elongation. *Cold Spring Harb Perspect Med* **4**, a020990, doi:10.1101/cshperspect.a020990 (2014).

7   Clevers, H. & Nusse, R. Wnt/beta-catenin signaling and disease. *Cell* **149**, 1192-1205, doi:10.1016/j.cell.2012.05.012 (2012).

8   Grossmann, T. N. *et al.* Inhibition of oncogenic Wnt signaling through direct targeting of beta-catenin. *Proceedings of the National Academy of Sciences of the United States of America* **109**, 17942-17947, doi:10.1073/pnas.1208396109 (2012).

9   Yuan, H. *et al.* Knockdown of mediator subunit Med19 suppresses bladder cancer cell proliferation and migration by downregulating Wnt/beta-catenin signalling pathway. *J Cell Mol Med*, doi:10.1111/jcmm.13229 (2017).

10   Fearnhead, N. S., Wilding, J. L. & Bodmer, W. F. Genetics of colorectal cancer: hereditary aspects and overview of colorectal tumorigenesis. *Br Med Bull* **64**, 27-43 (2002).

11   Nusse, R. & Clevers, H. Wnt/beta-Catenin Signaling, Disease, and Emerging Therapeutic Modalities. *Cell* **169**, 985-999, doi:10.1016/j.cell.2017.05.016 (2017).

12   Milbradt, A. G. *et al.* Structure of the VP16 transactivator target in the Mediator. *Nature structural & molecular biology* **18**, 410-415, doi:10.1038/nsmb.1999 (2011).

13   Mucenski, M. L. *et al.* A functional c-myb gene is required for normal murine fetal hepatic hematopoiesis. *Cell* **65**, 677-689 (1991).

14   Nomura, T. *et al.* Oncogenic activation of c-Myb correlates with a loss of negative regulation by TIF1beta and Ski. *The Journal of biological chemistry* **279**, 16715-16726, doi:10.1074/jbc.M313069200 (2004).

15   Jin, S. *et al.* c-Myb binds MLL through menin in human leukemia cells and is an important driver of MLL-associated leukemogenesis. *J Clin Invest* **120**, 593-606, doi:10.1172/JCI38030 (2010).

16   Dai, P. *et al.* CBP as a transcriptional coactivator of c-Myb. *Genes & development* **10**, 528-540 (1996).

17   Zuber, J. *et al.* An integrated approach to dissecting oncogene addiction implicates a Myb-coordinated self-renewal program as essential for leukemia maintenance. *Genes & development* **25**, 1628-1640, doi:10.1101/gad.17269211 (2011).

18   Pattabiraman, D. R., Sun, J., Dowhan, D. H., Ishii, S. & Gonda, T. J. Mutations in multiple domains of c-Myb disrupt interaction with CBP/p300 and abrogate myeloid

transforming ability. *Molecular cancer research : MCR* **7**, 1477-1486, doi:10.1158/1541-7786.MCR-09-0070 (2009).

19   Pattabiraman, D. R. *et al.* Interaction of c-Myb with p300 is required for the induction of acute myeloid leukemia (AML) by human AML oncogenes. *Blood* **123**, 2682-2690, doi:10.1182/blood-2012-02-413187 (2014).

20   Anfossi, G., Gewirtz, A. M. & Calabretta, B. An oligomer complementary to c-myb-encoded mRNA inhibits proliferation of human myeloid leukemia cell lines. *Proceedings of the National Academy of Sciences of the United States of America* **86**, 3379-3383 (1989).

21   Mapp, A. K., Pricer, R. & Sturlis, S. Targeting transcription is no longer a quixotic quest. *Nature chemical biology* **11**, In Press (2015).

22   Bedford, D. C., Kasper, L. H., Fukuyama, T. & Brindle, P. K. Target gene context influences the transcriptional requirement for the KAT3 family of CBP and p300 histone acetyltransferases. *Epigenetics* **5**, 9-15 (2010).

23   Dyson, H. J. & Wright, P. E. Role of Intrinsic Protein Disorder in the Function and Interactions of the Transcriptional Coactivators CREB-binding Protein (CBP) and p300. *The Journal of biological chemistry* **291**, 6714-6722, doi:10.1074/jbc.R115.692020 (2016).

24   Poss, Z. C., Ebmeier, C. C. & Taatjes, D. J. The Mediator complex and transcription regulation. *Critical reviews in biochemistry and molecular biology* **48**, 575-608, doi:10.3109/10409238.2013.840259 (2013).

25   Asturias, F. J., Jiang, Y. W., Myers, L. C., Gustafsson, C. M. & Kornberg, R. D. Conserved structures of mediator and RNA polymerase II holoenzyme. *Science* **283**, 985-987 (1999).

26   Nozawa, K., Schneider, T. R. & Cramer, P. Core Mediator structure at 3.4 A extends model of transcription initiation complex. *Nature* **545**, 248-251, doi:10.1038/nature22328 (2017).

27   Thakur, J. K., Yadav, A. & Yadav, G. Molecular recognition by the KIX domain and its role in gene regulation. *Nucleic acids research* **42**, 2112-2125, doi:10.1093/nar/gkt1147 (2014).

28   Allen, B. L. & Taatjes, D. J. The Mediator complex: a central integrator of transcription. *Nature reviews. Molecular cell biology* **16**, 155-166, doi:10.1038/nrm3951 (2015).

29   Amin, M. B. *et al.* The critical role of the pathologist in determining eligibility for active surveillance as a management option in patients with prostate cancer: consensus statement with recommendations supported by the College of American Pathologists, International Society of Urological Pathology, Association of Directors of Anatomic and Surgical Pathology, the New Zealand Society of Pathologists, and the Prostate Cancer Foundation. *Arch Pathol Lab Med* **138**, 1387-1405, doi:10.5858/arpa.2014-0219-SA (2014).

30   Samara, N. L. & Wolberger, C. A new chapter in the transcription SAGA. *Current opinion in structural biology* **21**, 767-774, doi:10.1016/j.sbi.2011.09.004 (2011).

31   Sugase, K., Dyson, H. J. & Wright, P. E. Mechanism of coupled folding and binding of an intrinsically disordered protein. *Nature* **447**, 1021-1025, doi:10.1038/nature05858 (2007).

32   Radhakrishnan, I. *et al.* Solution structure of the KIX domain of CBP bound to the transactivation domain of CREB: a model for activator:coactivator interactions. *Cell* **91**, 741-752 (1997).

33   Bruschweiler, S., Konrat, R. & Tollinger, M. Allosteric communication in the KIX domain proceeds through dynamic repacking of the hydrophobic core. *ACS chemical biology* **8**, 1600-1610, doi:10.1021/cb4002188 (2013).

34   Jonker, H. R., Wechselberger, R. W., Boelens, R., Folkers, G. E. & Kaptein, R. Structural properties of the promiscuous VP16 activation domain. *Biochemistry* **44**, 827-839, doi:10.1021/bi0482912 (2005).

35   Eletsky, A. *et al.* Solution NMR structure of MED25(391-543) comprising the activator-interacting domain (ACID) of human mediator subunit 25. *Journal of structural and functional genomics* **12**, 159-166, doi:10.1007/s10969-011-9115-1 (2011).

36   Bontems, F. *et al.* NMR structure of the human Mediator MED25 ACID domain. *Journal of structural biology* **174**, 245-251, doi:10.1016/j.jsb.2010.10.011 (2011).

37   Vojnic, E. *et al.* Structure and VP16 binding of the Mediator Med25 activator interaction domain. *Nature structural & molecular biology* **18**, 404-409, doi:10.1038/nsmb.1997 (2011).

38   De Guzman, R. N., Wojciak, J. M., Martinez-Yamout, M. A., Dyson, H. J. & Wright, P. E. CBP/p300 TAZ1 domain forms a structured scaffold for ligand binding. *Biochemistry* **44**, 490-497, doi:10.1021/bi048161t (2005).

39   De Guzman, R. N., Liu, H. Y., Martinez-Yamout, M., Dyson, H. J. & Wright, P. E. Solution structure of the TAZ2 (CH3) domain of the transcriptional adaptor protein CBP. *Journal of molecular biology* **303**, 243-253, doi:10.1006/jmbi.2000.4141 (2000).

40   Kjaergaard, M., Teilum, K. & Poulsen, F. M. Conformational selection in the molten globule state of the nuclear coactivator binding domain of CBP. *Proceedings of the National Academy of Sciences of the United States of America* **107**, 12535-12540, doi:10.1073/pnas.1001693107 (2010).

41   Lin, C. H. *et al.* A small domain of CBP/p300 binds diverse proteins: solution structure and functional studies. *Molecular cell* **8**, 581-590 (2001).

42   Campbell, K. M. & Lumb, K. J. Structurally distinct modes of recognition of the KIX domain of CBP by Jun and CREB. *Biochemistry* **41**, 13956-13964 (2002).

43   Wang, F. *et al.* Structures of KIX domain of CBP in complex with two FOXO3a transactivation domains reveal promiscuity and plasticity in coactivator recruitment. *Proceedings of the National Academy of Sciences of the United States of America* **109**, 6078-6083, doi:10.1073/pnas.1119073109 (2012).

44   Lee, C. W., Arai, M., Martinez-Yamout, M. A., Dyson, H. J. & Wright, P. E. Mapping the interactions of the p53 transactivation domain with the KIX domain of CBP. *Biochemistry* **48**, 2115-2124, doi:10.1021/bi802055v (2009).

45   Jenkins, L. M. *et al.* Two distinct motifs within the p53 transactivation domain bind to the Taz2 domain of p300 and are differentially affected by phosphorylation. *Biochemistry* **48**, 1244-1255, doi:10.1021/bi801716h (2009).

46   Arai, M., Ferreon, J. C. & Wright, P. E. Quantitative analysis of multisite protein-ligand interactions by NMR: binding of intrinsically disordered p53 transactivation subdomains

with the TAZ2 domain of CBP. *Journal of the American Chemical Society* **134**, 3792-3803, doi:10.1021/ja209936u (2012).

47   Vendel, A. C. & Lumb, K. J. Molecular recognition of the human coactivator CBP by the HIV-1 transcriptional activator Tat. *Biochemistry* **42**, 910-916, doi:10.1021/bi0270034 (2003).

48   Vendel, A. C., McBryant, S. J. & Lumb, K. J. KIX-mediated assembly of the CBP-CREB-HTLV-1 tax coactivator-activator complex. *Biochemistry* **42**, 12481-12487, doi:10.1021/bi0353023 (2003).

49   Ramirez, J. A. & Nyborg, J. K. Molecular characterization of HTLV-1 Tax interaction with the KIX domain of CBP/p300. *Journal of molecular biology* **372**, 958-969, doi:10.1016/j.jmb.2007.06.062 (2007).

50   Goto, N. K., Zor, T., Martinez-Yamout, M., Dyson, H. J. & Wright, P. E. Cooperativity in transcription factor binding to the coactivator CREB-binding protein (CBP). The mixed lineage leukemia protein (MLL) activation domain binds to an allosteric site on the KIX domain. *The Journal of biological chemistry* **277**, 43168-43174, doi:10.1074/jbc.M207660200 (2002).

51   Wang, N., Lodge, J. M., Fierke, C. A. & Mapp, A. K. Dissecting allosteric effects of activator-coactivator complexes using a covalent small molecule ligand. *Proceedings of the National Academy of Sciences of the United States of America* **111**, 12061-12066, doi:10.1073/pnas.1406033111 (2014).

52   Shammas, S. L., Travis, A. J. & Clarke, J. Allostery within a transcription coactivator is predominantly mediated through dissociation rate constants. *Proceedings of the National Academy of Sciences of the United States of America* **111**, 12055-12060, doi:10.1073/pnas.1405815111 (2014).

53   Shaywitz, A. J., Dove, S. L., Kornhauser, J. M., Hochschild, A. & Greenberg, M. E. Magnitude of the CREB-dependent transcriptional response is determined by the strength of the interaction between the kinase-inducible domain of CREB and the KIX domain of CREB-binding protein. *Molecular and cellular biology* **20**, 9409-9422 (2000).

54   Ernst, P., Wang, J., Huang, M., Goodman, R. H. & Korsmeyer, S. J. MLL and CREB bind cooperatively to the nuclear coactivator CREB-binding protein. *Molecular and cellular biology* **21**, 2249-2258, doi:10.1128/MCB.21.7.2249-2258.2001 (2001).

55   Cook, P. R., Polakowski, N. & Lemasson, I. HTLV-1 HBZ protein deregulates interactions between cellular factors and the KIX domain of p300/CBP. *Journal of molecular biology* **409**, 384-398, doi:10.1016/j.jmb.2011.04.003 (2011).

56   Korkmaz, E. N., Nussinov, R. & Haliloglu, T. Conformational control of the binding of the transactivation domain of the MLL protein and c-Myb to the KIX domain of CREB. *PLoS Comput Biol* **8**, e1002420, doi:10.1371/journal.pcbi.1002420 (2012).

57   Law, S. M., Gagnon, J. K., Mapp, A. K. & Brooks, C. L., III. Prepaying the entropic cost for allosteric regulation in KIX. *Proceedings of the National Academy of Sciences of the United States of America*, doi:10.1073/pnas.1405831111 (2014).

58   Gianni, S., Morrone, A., Giri, R. & Brunori, M. A folding-after-binding mechanism describes the recognition between the transactivation domain of c-Myb and the KIX domain of the CREB-binding protein. *Biochemical and biophysical research communications* **428**, 205-209, doi:10.1016/j.bbrc.2012.09.112 (2012).

59   Shammas, S. L., Travis, A. J. & Clarke, J. Remarkably fast coupled folding and binding of the intrinsically disordered transactivation domain of cMyb to CBP KIX. *J Phys Chem B* **117**, 13346-13356, doi:10.1021/jp404267e (2013).

60   Zor, T., De Guzman, R. N., Dyson, H. J. & Wright, P. E. Solution structure of the KIX domain of CBP bound to the transactivation domain of c-Myb. *Journal of molecular biology* **337**, 521-534, doi:10.1016/j.jmb.2004.01.038 (2004).

61   Huang, Y. & Liu, Z. Kinetic advantage of intrinsically disordered proteins in coupled folding-binding process: a critical assessment of the "fly-casting" mechanism. *Journal of molecular biology* **393**, 1143-1159, doi:10.1016/j.jmb.2009.09.010 (2009).

62   Schreiber, G. & Fersht, A. R. Rapid, electrostatically assisted association of proteins. *Nat Struct Biol* **3**, 427-431 (1996).

63   Dogan, J., Schmidt, T., Mu, X., Engstrom, A. & Jemth, P. Fast association and slow transitions in the interaction between two intrinsically disordered protein domains. *The Journal of biological chemistry* **287**, 34316-34324, doi:10.1074/jbc.M112.399436 (2012).

64   Canovas, V., Lleonart, M., Morote, J. & Paciucci, R. The role of prostate tumor overexpressed 1 in cancer progression. *Oncotarget* **8**, 12451-12471, doi:10.18632/oncotarget.14104 (2017).

65   Benedit, P. *et al.* PTOV1, a novel protein overexpressed in prostate cancer containing a new class of protein homology blocks. *Oncogene* **20**, 1455-1464, doi:10.1038/sj.onc.1204233 (2001).

66   Landrieu, I. *et al.* Characterization of ERM transactivation domain binding to the ACID/PTOV domain of the Mediator subunit MED25. *Nucleic acids research* **43**, 7110-7121, doi:10.1093/nar/gkv650 (2015).

67   Sela, D. *et al.* Role for human mediator subunit MED25 in recruitment of mediator to promoters by endoplasmic reticulum stress-responsive transcription factor ATF6alpha. *The Journal of biological chemistry* **288**, 26179-26187, doi:10.1074/jbc.M113.496968 (2013).

68   Baert, J. L. *et al.* Expression of the PEA3 group of ETS-related transcription factors in human breast-cancer cells. *International journal of cancer. Journal international du cancer* **70**, 590-597 (1997).

69   Ron, D. & Walter, P. Signal integration in the endoplasmic reticulum unfolded protein response. *Nature reviews. Molecular cell biology* **8**, 519-529, doi:10.1038/nrm2199 (2007).

70   Fuller, J. C., Burgoyne, N. J. & Jackson, R. M. Predicting druggable binding sites at the protein-protein interface. *Drug Discov Today* **14**, 155-161, doi:10.1016/j.drudis.2008.10.009 (2009).

71   Smith, R. D. *et al.* Exploring protein-ligand recognition with Binding MOAD. *J Mol Graph Model* **24**, 414-425, doi:10.1016/j.jmgm.2005.08.002 (2006).

72   Basse, M. J., Betzi, S., Morelli, X. & Roche, P. 2P2Idb v2: update of a structural database dedicated to orthosteric modulation of protein-protein interactions. *Database (Oxford)* **2016**, doi:10.1093/database/baw007 (2016).

73   Higueruelo, A. P. *et al.* Atomic interactions and profile of small molecules disrupting protein-protein interfaces: the TIMBAL database. *Chem Biol Drug Des* **74**, 457-467, doi:10.1111/j.1747-0285.2009.00889.x (2009).

74   Higueruelo, A. P., Jubb, H. & Blundell, T. L. TIMBAL v2: update of a database holding small molecules modulating protein-protein interactions. *Database (Oxford)* **2013**, bat039, doi:10.1093/database/bat039 (2013).

75   Bourgeas, R., Basse, M. J., Morelli, X. & Roche, P. Atomic analysis of protein-protein interfaces with known inhibitors: the 2P2I database. *PloS one* **5**, e9598, doi:10.1371/journal.pone.0009598 (2010).

76   Basse, M. J. *et al.* 2P2Idb: a structural database dedicated to orthosteric modulation of protein-protein interactions. *Nucleic acids research* **41**, D824-827, doi:10.1093/nar/gks1002 (2013).

77   Cesa, L. C., Mapp, A. K. & Gestwicki, J. E. Direct and Propagated Effects of Small Molecules on Protein-Protein Interaction Networks. *Front Bioeng Biotechnol* **3**, 119, doi:10.3389/fbioe.2015.00119 (2015).

78   Thompson, A. D., Dugan, A., Gestwicki, J. E. & Mapp, A. K. Fine-tuning multiprotein complexes using small molecules. *ACS chemical biology* **7**, 1311-1320, doi:10.1021/cb300255p (2012).

79   Wang, S. *et al.* SAR405838: an optimized inhibitor of MDM2-p53 interaction that induces complete and durable tumor regression. *Cancer research* **74**, 5855-5865, doi:10.1158/0008-5472.CAN-14-0799 (2014).

80   Zhang, B., Golding, B. T. & Hardcastle, I. R. Small-molecule MDM2-p53 inhibitors: recent advances. *Future Med Chem* **7**, 631-645, doi:10.4155/fmc.15.13 (2015).

81   Momand, J., Jung, D., Wilczynski, S. & Niland, J. The MDM2 gene amplification database. *Nucleic acids research* **26**, 3453-3459 (1998).

82   Vassilev, L. T. *et al.* In vivo activation of the p53 pathway by small-molecule antagonists of MDM2. *Science* **303**, 844-848, doi:10.1126/science.1092472 (2004).

83   Ding, K. *et al.* Structure-based design of potent non-peptide MDM2 inhibitors. *Journal of the American Chemical Society* **127**, 10130-10131, doi:10.1021/ja051147z (2005).

84   Moellering, R. E. *et al.* Direct inhibition of the NOTCH transcription factor complex. *Nature* **462**, 182-188, doi:10.1038/nature08543 (2009).

85   Best, J. L. *et al.* Identification of small-molecule antagonists that inhibit an activator: coactivator interaction. *Proceedings of the National Academy of Sciences of the United States of America* **101**, 17622-17627, doi:10.1073/pnas.0406374101 (2004).

86   Majmudar, C. Y. *et al.* Sekikaic acid and lobaric acid target a dynamic interface of the coactivator CBP/p300. *Angewandte Chemie* **51**, 11258-11262, doi:10.1002/anie.201206815 (2012).

87   Wang, N. *et al.* Ordering a dynamic protein via a small-molecule stabilizer. *Journal of the American Chemical Society* **135**, 3363-3366, doi:10.1021/ja3122334 (2013).

Chapter 2

ASSESSING MECHANISTIC FEATURES OF MED25-ACTIVATOR INTERACTIONS[1]

2.1 ABSTRACT

The Activator Interaction Domain (AcID) of the coactivator Med25 is a structurally unique motif. The vast majority of activator binding domains (ABDs) use helices connected by flexible loops to access a variety of conformations; this conformational heterogeneity enables complex formation with activators of diverse sequence composition and, in some cases, confers allosteric communication between distinct binding surfaces. An ABD present only in metazoans, AcID contains large and topologically flat activator binding surfaces comprised of a 7-stranded beta barrel with some contribution by flanking helices. Here, we dissect key mechanistic details of activator-AcID complexes and demonstrate that, despite its stabile fold, there is also heterogeneity in activator-AcID complex formation. Additionally, we find that there are two binding surfaces within AcID that are allosterically linked. Transient kinetic analysis of activator binding to AcID reveal that activator-AcID association events are consistent with a coupled

---

[1] The research described in chapter 2 is a collaborative effort. A.R. Henderson synthesized and purified VP16 peptides, expressed Med25 and Med25 variants for NMR, performed peptide labeling experiments, and performed direct binding experiments. NMR was performed in collaboration with Prof. Tomasz Cierpicki and Brian Linhares. Matthew Henley performed kinetics experiments and assisted in peptide synthesis and NMR experiments. Matthew Beyersdorf contributed peptides for study via NMR. Nicholas Foster assisted in peptide synthesis. Manuscript in progress.

binding and folding mechanism. Thus, despite its disparate structural features and presumably more recent emergence, AcID utilizes an analogous mechanism as the more conserved helical activator-binding motifs. This enhanced mechanistic understanding of AcID will be important in the development of small molecule modulators of activator-AcID protein-protein interactions.

2.2 BACKGROUND

Transcriptional activation occurs through a tightly regulated protein-protein interaction network encompassing proteins with varied enzymatic and structural roles[3-6]. Amongst these proteins, transcriptional coactivators act as linchpins between DNA-bound transcriptional activators and the rest of the transcriptional machinery (Figure 2.1). Coactivators perform a diverse set of functions and can exist as individual proteins such as CBP/P300 or as multiprotein complexes such as Mediator[7-9]. Therapeutics capable of selectively targeting individual coactivator interaction surfaces have an opportunity to afford nuanced control of transcriptional output. In pursuit of this goal it will be necessary to better understand the molecular basis of protein-protein interactions that involve coactivator complexes.
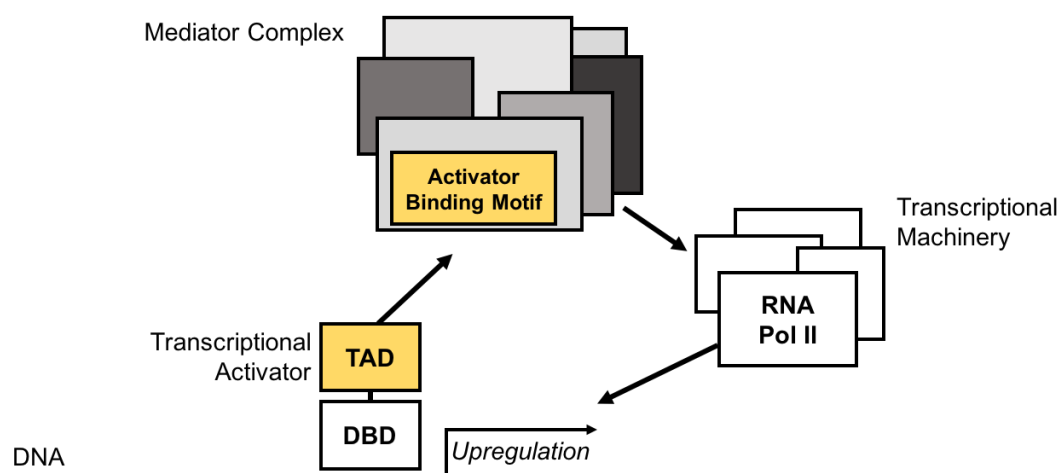
Figure 2.1 The Mediator complex is a multicomponent coactivator The multi subunit Mediator complex interacts RNA Pol II and associated general transcription factors. Promoter-bound transcriptional activators interact with Mediator subunits via activator binding domains.

The Mediator complex is a hub in transcriptional activation

The Mediator complex is a megadalton, multiprotein coactivator complex found in eukaryotes. The composition of Mediator is species-dependent, with 21 subunits observed in the yeast *S. pombe* and 31 subunits in mammals.[10-12]. Mediator composition simplifies in differentiated cells with cell-type dependent downregulated expression of individual subunits. For example, a comparison of liver progenitor cells to fully differentiated hepatocytes saw the loss of several Mediator subunits including Med1, Med6, and Med14.[13] The loss of certain subunits enables more specific and finely-tuned gene expression in these cells due to the loss of their ability to interact with transcription factors or coregulatory partners [13,14]. Regardless of composition, Mediator serves as a key conduit between DNA-associated activators and RNA Polymerase II (RNA Pol II). As a key member of the transcriptional pre-initiation complex (PIC), Mediator makes extensive contacts with RNA Pol II and plays a role in stabilizing chromatin architecture bringing enhancer regions of genomic DNA into proximity with their correspondent promoter region[15-17].

Many Mediator subunits contain ABDs that enable direct interaction with a variety of promoter-bound transcriptional activators[18]. The canonical LxxLL nuclear receptor recognition motif is found in both Med1 and Med25[19,20]. Additionally, the KIX domain of Med15 interacts with a variety of activators including Gcn4 (master yeast regulator) and Pdr1 (*S. cerevisiae* drug resistance)[21,22]. The AcID domain of Med25 is used to interact with at least 4 transcriptional activators.

Several recent studies have sought to define the quaternary structure of Mediator and identify the protein-protein interaction network linking Mediator subunits within this larger structure.[23,24] The Cramer Lab recently published an elegant study combining x-ray crystallography and cryo-electron microscopy to produce a 3.4 Å model of the yeast preinitiation complex (PIC) (Fig 2.2) [23]. Notably, the overall structure of Mediator is quite dynamic and is highly influenced by interactions with associated cofactors including CDK8 or polymerase[12,25,26]. For example, human Mediator undergoes large-scale structural rearrangement upon association with RNA Pol II primarily via extensive contacts between Pol II and the Mediator tail module.[25]
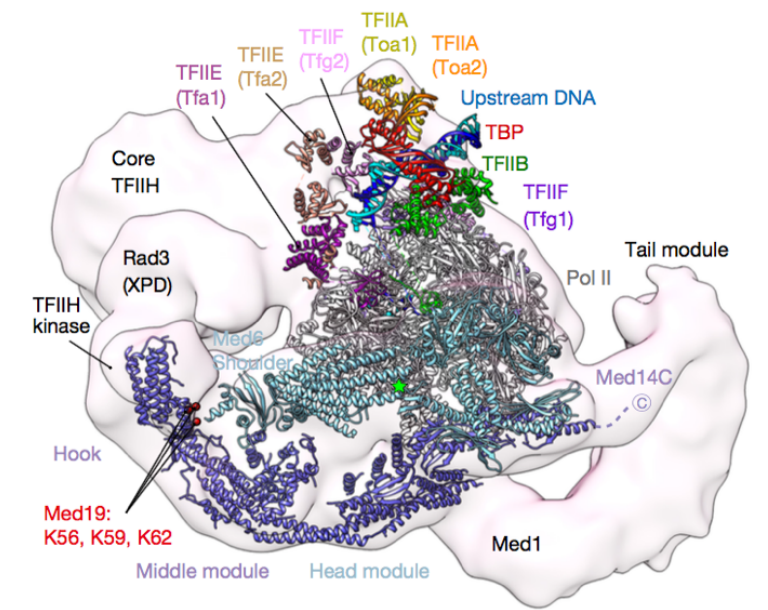
Figure 2.2 A 3.4 Å model of the yeast preinitiation complex Crystal structure of the core Mediator complex docked into cro-EM model of the entire PIC. Atomic model of Mediator reveals specific connections between Mediator subunits and PIC components. Modifed from Nozawa et al., *Nature* **2017**, 545, 248-251.[23]

Because of the central role Mediator plays in regulating transcription, targeting individual Mediator subunits with small molecules is an attractive therapeutic strategy[27-29]. Studies aimed

at better understanding the structure and biochemical mechanism of protein-protein interactions of individual Mediator subunits will enable efforts to identify small molecule modulators or inhibitors that can alter transcriptional output.

Med25 is a unique Mediator subunit

Mediator subunit 25 of the Mediator complex occurs only in higher eukaryotes and is ubiquitously expressed in essentially all human tissue types[30]. Med25 forms direct interactions with multiple transcription factors (VP16, ERM, ATF6α) and cofactors (CBP/p300) linking them to Mediator and the rest of the PIC[31-35]. Within the 747-amino acid Med25 are three distinct domains (Figure 2.3). The N-terminal von Willebrand factor type-A domain (VWA) links Med25

A)

B)
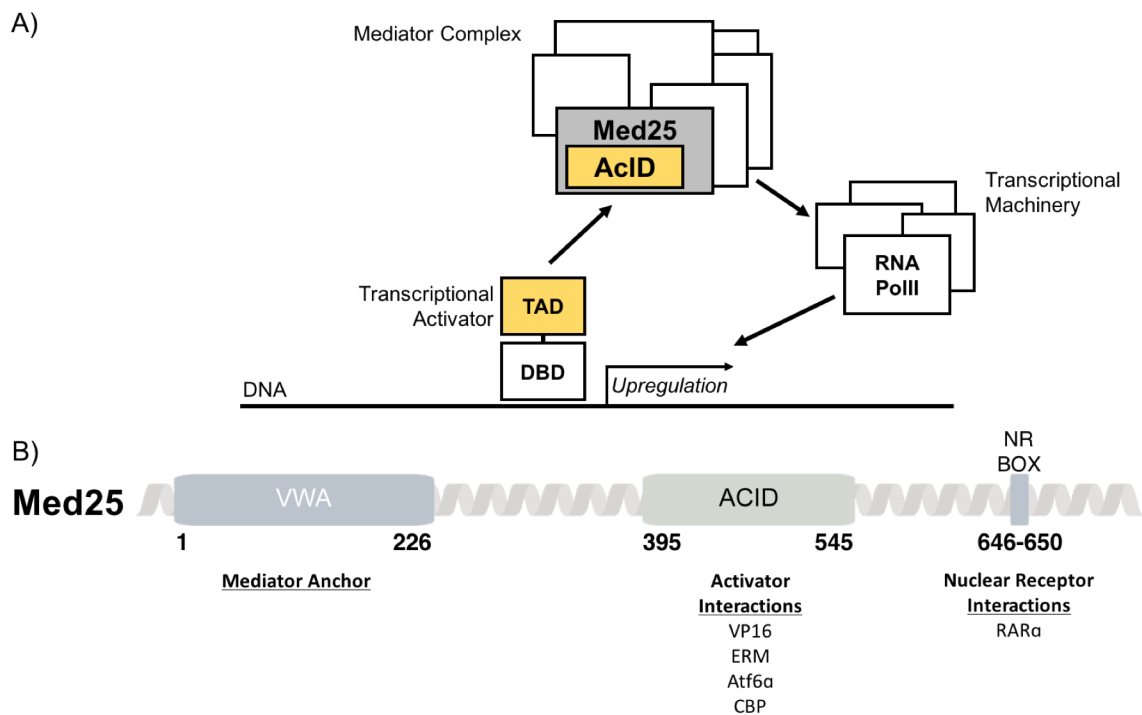
Figure 2.3 Med25 is an activator interacting Mediator subunit A. Med25 interacts with transcriptional activators via its AcID domain. B. Med25 is composed of at least three subdomains with identified roles: 1) von Willebrand factor type-A (VWA) serves to anchor Med25 to the Mediator complex 2) Activator Interaction Domain (AcID) interacts with a diverse set of transcriptional activators 3) canonical LxxLL Nuclear Receptor (NR) box is a recognition motif for nuclear receptors including retinoic acid receptor alpha (RARα).

to the rest of Mediator[36]. The NR box, is a 5-amino acid LxxLL motif recognized by nuclear receptors including Retinoic Acid Receptor[35,37]. Finally, Med25 contains the 151-amino acid Activator Interacting Domain (AcID) domain which is a binding region for transcription factors which regulate multiple cellular processes and are implicated in a variety of human diseases.[38-40]

As with several other transcriptional coactivator ABDs, AcID interacts with transcriptional activation domains (TADs) of transcription factors using two discrete binding surfaces. These two binding surfaces occur on opposite faces of the AcID fold, a unique ABD motif found in only one other protein, PTOV1[1,2]. AcID is a 7-stranded β-barrel flanked by three alpha helices and several loop regions (Figure 2.4)[41,42]. To develop potent and specific small molecule inhibitors of activator-AcID interactions there is a need to understand the molecular mechanisms that govern AcID-activator binary and ternary complex formation.

Figure 2.4 The AcID domain of Med25 is a unique activator binding motif AcID is a 7-stranded β-barrel flanked by three α-helices and several flexible loops. Activators bind AcID at two surfaces on opposite faces of AcID. Colored regions are those contacted by VP16 H1 (Blue) and VP16 H2 (Gold).[1,2] PDB: 2XNF

The Med25-VP16 Interaction

The herpes simplex viral activator VP16 forms specific contacts with both activator binding sites on AcID (Figure 2.5)[1,2]. Upon infection, VP16 hijacks the transcriptional apparatus of host cells to induce expression of viral genes.[43-45] VP16 interacts with a number of coactivator proteins complexes including: Mediator, CBP/P300, SAGA, SWI/SNF, and the general transcription factors[40]. The activation domain of VP16 contains two tandem and homologous sequences capable of independently activating transcription (Figure 2.5). A pair of recent papers used protein NMR and a suite of biochemical experiments to establish an initial model of the VP16-AcID interaction. NMR chemical shift perturbation analysis reveals that the full length VP16 TAD interacts with both AcID binding sites and when the TAD is bisected the N-terminal TAD (VP16 H1) binds AcID H1 while the C-terminal TAD (VP16 H2) binds AcID H2. This putative model establishes a preliminary binding location for each half of the VP16 TAD but does not comment on key aspects of activator-ABD interactions including binding kinetics, binding orientation, or allosteric communication linking the two AcID binding surfaces.

VP16 H1$_{413-452}$ VP16 H2$_{453-490}$

413 --APPTDVSLGDELHLDGEDVAMAHADALD<u>DFDLDMLGDGDS</u>PGPGFTPHDSAPYGALD<u>MADFEFEQMFTDALGID</u>EYGG- 490

Underline=predicted region of helicity

Figure 2.5 The VP16 transcriptional activation domain VP16 is composed of N- and C-terminal activation domains, VP16 H1 and H2 respectively, each capable of independently activating transcription. Underlined residues are predicted to become alpha helical upon binding to AcID.

Through this work we aimed to further refine our mechanistic and structural understanding of Med25-activator complex formation. We sought to understand how activator

complex formation with the structurally unique AcID domain compares to structurally unrelated coactivator motifs like KIX and TAZ1. This refined mechanistic understanding has and will aid in efforts to identify small molecules capable of targeting the AcID domain altering the protein-protein network it participates in, thereby altering downstream transcriptional output. Because of AcID's central role as a transcriptional regulator of many diverse processes, these molecules have therapeutic potential in the treatment of a variety of diseases.

2.3 RESULTS AND DISCUSSION

The novel structural fold of AcID relative to other ABDs has left many open questions surrounding how AcID-activator complex formation differs from the other more mechanistically defined activator binding domains like KIX or Taz1. Mechanistic definition of activator-AcID complexes will increase insight into the role of Med25 in transcriptional activation. This increased knowledge will be directly applicable to attempts to develop small molecule inhibitors of activator-AcID complexes that can target or leverage certain mechanistic features of AcID.

STRUCTURAL ANALYSIS OF ACID-ACTIVATOR INTERACTIONS

While the VP16-AcID interaction was recently described, there are many structural details of this interaction that remain unknown including binding orientation and the presence of allosteric communication between the two binding sites. To help further understand and clarify the AcID-VP16 interaction we utilized ^{1}H,^{15}N HSQC NMR (Heteronuclear Single Quantum Coherence Nuclear Magnetic Resonance Spectroscopy) to examine various VP16-AcID complexes. These 2D experiments measure the correlation between the ^{1}H proton and the ^{15}N

nitrogen that comprise each amide bond, with the exception of proline, in the protein backbone. In all cases we used ^{15}N-labeled Med25 AcID and monitored changes to those amide resonances induced by interactions with activator peptides (Figure 2.6).
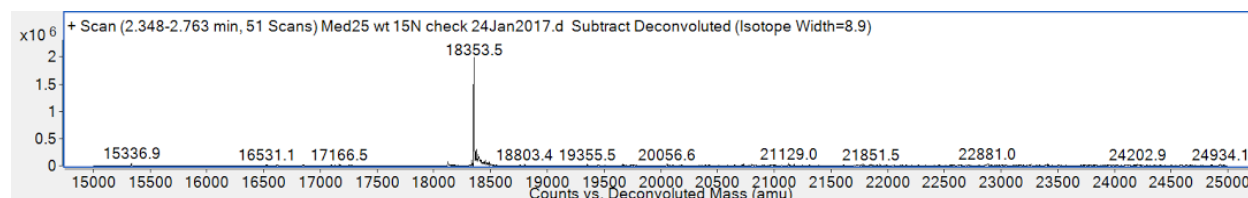
Figure 2.6 Confirmation of [15]N Med25 Expression Mass spectrum showing the expected mass for ^{15}N-labeled Med25 AcID

Assignment of Med25 AcID HSQC Spectra

In order to meaningfully interpret our HSQC data we first correlated peaks in the HSQC spectra to their corresponding amino acid in Med25 AcID using triple resonance experiments and ^{1}H,[13]C,[15]N labeled protein (Fig 2.7).[46] An AcID assignment from Patrick Cramer's lab was used as a means of comparison. Our assignment was in high agreement with the Cramer assignment, but we were able to assign residues on helix three that were not assigned by Cramer et al.
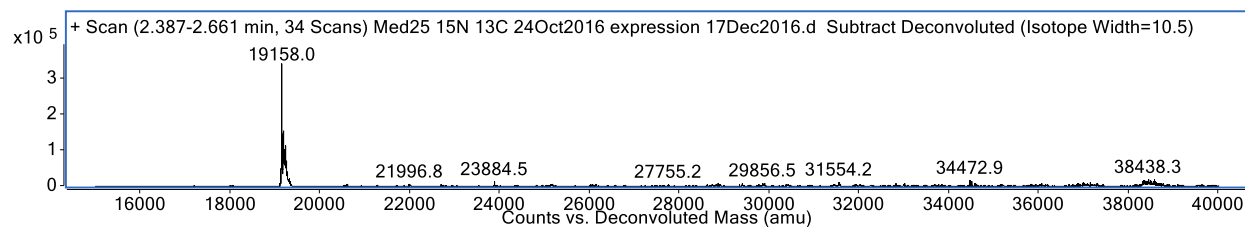
Figure 2.7 Confirmation of ^{13}C,[15]N Med25 Expression Mass spectrum showing the expected mass for ^{13}C,[15]N-labeled Med25 AcID.

VP16 L2L3 recapitulates the full length VP16 TAD interaction with Med25 AcID

Previous work combined with decades of functional studies indicate that the amino terminus of VP16 is dispensable for binding and function. In fact, the N-terminal 24 residues

34

VP16$_{413-437}$ (VP16 L1) very weakly binds Med25 with a K_d greater than 50 μM. To test if that were

true in this case, we synthesized and evaluated a variety of shortened versions of VP16. To assess

how well shortened constructs of the VP16 TAD compare to full length VP16, the full length VP16

TAD was synthesized via microwave-assisted SPPS. This peptide and the N' terminally truncated

VP16 L2L3 were titrated against Med25 AcID in an HSQC experiment. The HSQC spectra of AcID

saturated with either 3 equivalents of full VP16 or VP16 L2L3 show very high agreement in the

perturbations they induce to AcID (Figure 2.8). In addition, Fluorescein labeled VP16 L2L3 binds

AcID with a K_d of 65 nM which is close to the values reported for full VP16 (50 nM).[1]
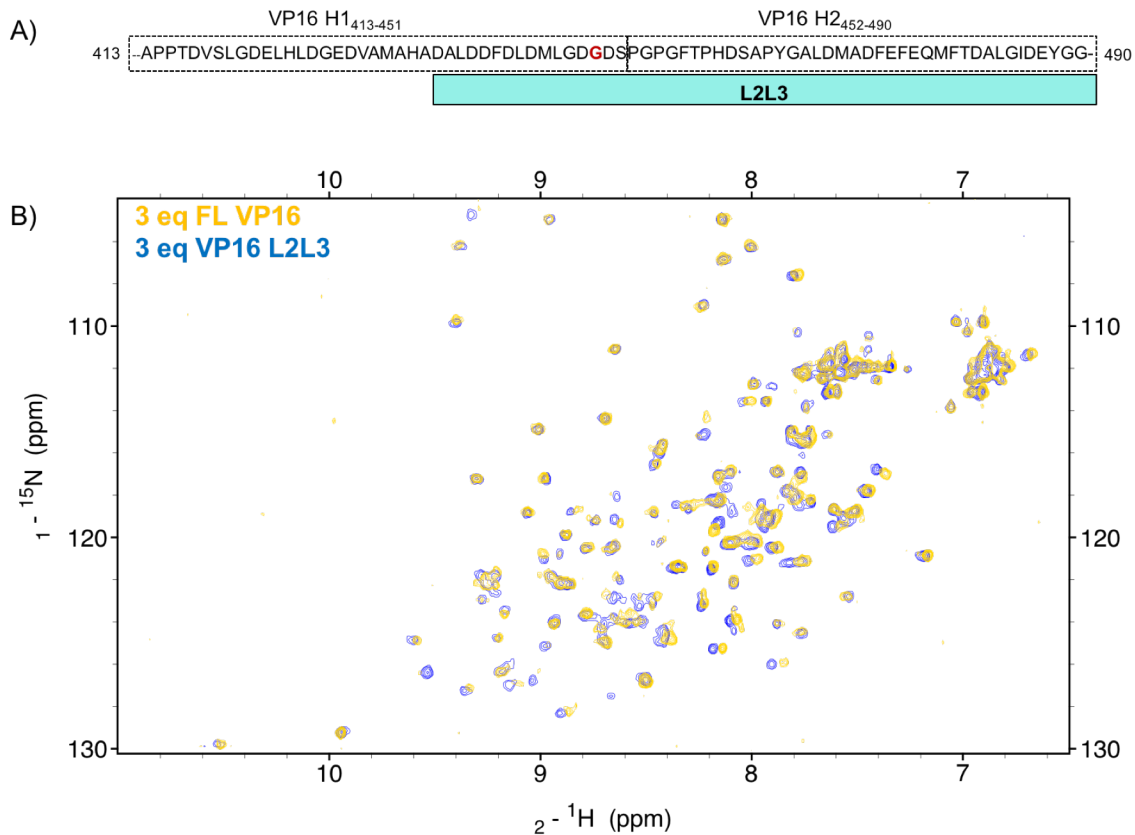
Figure 2.8 VP16 L2L3 overlays largely recapitulates the full length VP16 TAD-AcID interaction
A. The VP16 TAD and the L2L3 construct. B. The HSQC spectra for AcID in the presence of saturating (3 eq) full VP16 TAD or VP16 L2L3 agree well. Full VP16 shows a higher degree of peak broadening perhaps due to higher overall binding affinity. Performed with Matthew Henley.

VP16 L2L3 binds both faces of AcID

As demonstrated above, VP16 L2L3 is a useful full VP16 TAD surrogate. When titrated against ^{15}N Med25 AcID in an HSQC experiment we see binding saturation above 2 equivalents which reflects the high affinity of this interaction (Fig 2.9). While most residues in this titration are perturbed along a linear vector, several residues, notably D529, showed different perturbation patterns above and below 0.8 equivalents (Figure 2.9.C). This deviation from

linearity can be indicative of a ligand that binds in multiple modes or at multiple binding sites.[41] While VP16 L2L3 appears to bind in one major mode, there appears to be contributions from alternate binding modes. This observation is consistent with the direct binding data presented above and in line with other reported examples of activator-coactivator complexes where multiple binding modes are supported.

The K_d for VP16 L2L3 was calculated from the titration data of 7 different peaks and two different values of 4.9 and 30.4 µM were determined. Notably, the lower K_d correlates to residues located on the H2 face of AcID (Q456, V471, and G524), while the higher value correlates to residues on the H1 face (N438, L448, V498, G536). This may indicate that the C-terminal TAD of VP16 binds with a tighter affinity and thus drives the VP16-AcID interaction.
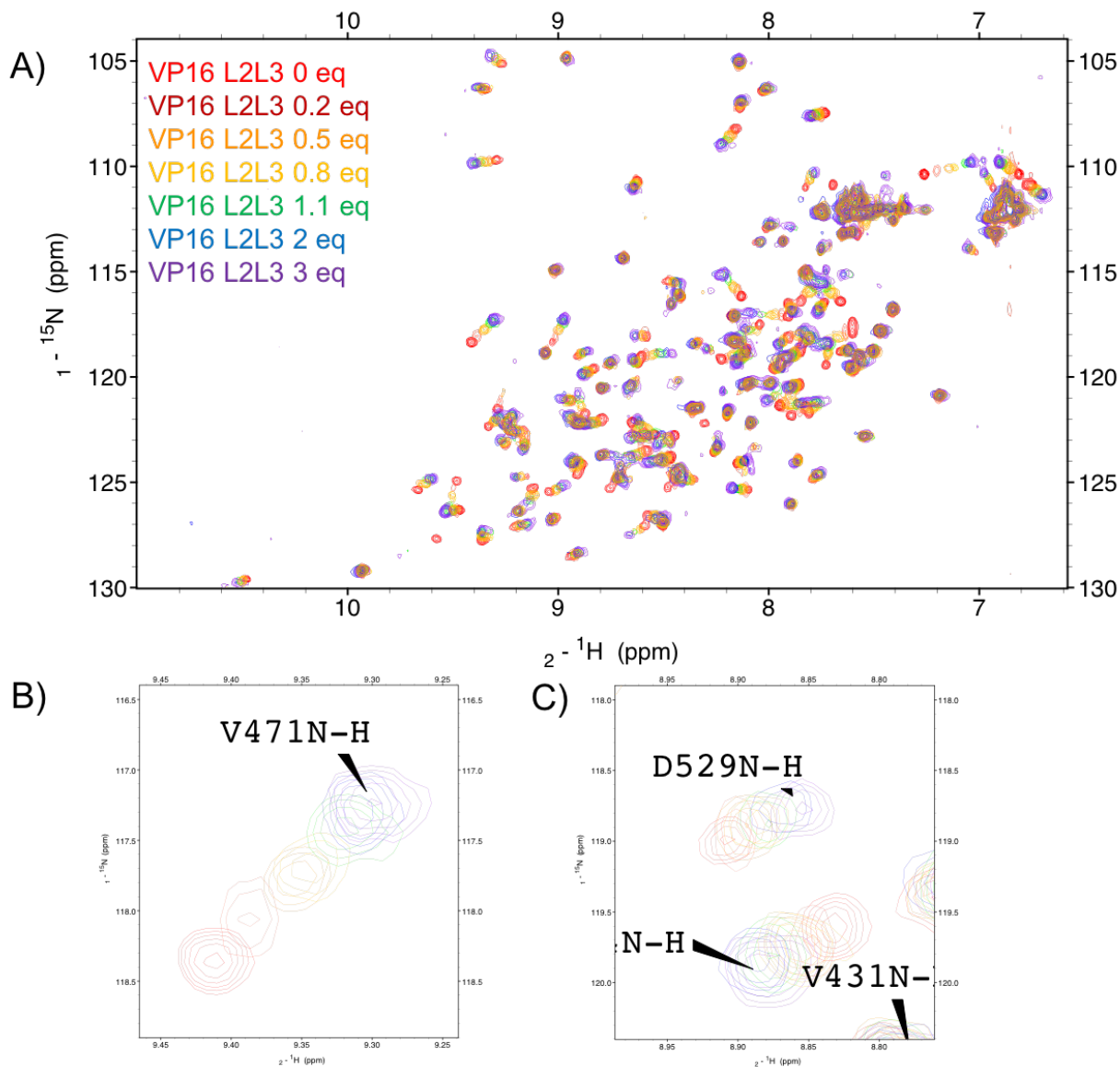
Figure 2.9 Titration of VP16 L2L3 A. Titration of 0, 0.2, 0.5, 0.8, 1.1, 2 and 3 equivalents of VP16 L2L3 with Med25 AcID. B. Residue V471 is illustrative of a linear perturbation pattern. C. D529 displays subtle curvature consistent with multiple binding modes.

Mapping these perturbations to the surface of AcID reveal binding at both activator binding surfaces, H1 and H2 (Figure 2.10). These perturbation patterns are consistent with previously published work. This NMR data with VP16 L2L3 and the above direct binding

experiments show that it effectively reconstitutes the affinity and overall binding mode of the VP16 TAD and its interaction with AcID.

CSP > 1 StDev
CSP > 2 StDev
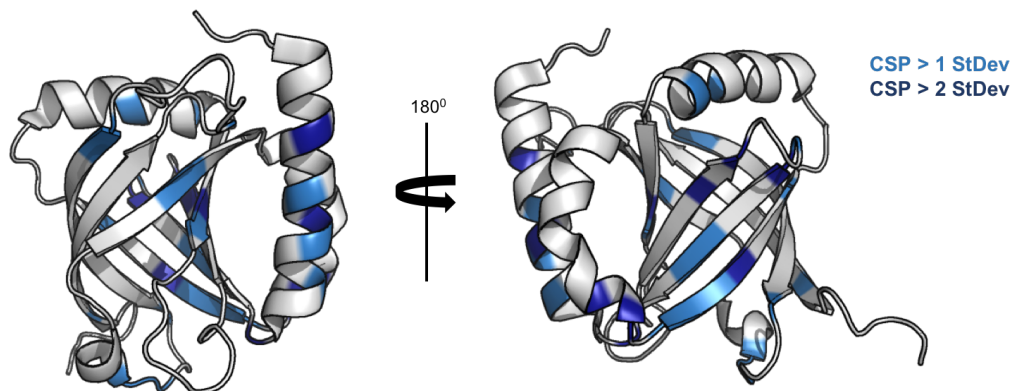
Figure 2.10 VP16 L2L3 induces perturbations on both faces of Med25 AcID HSQC perturbations induced by VP16 L2L3 on ^{15}N Med25 AcID.

ACTIVATOR-ACID COMPLEXES ARE CONFORMATIONALLY HETEROGENEOUS

Many activator binding domains, such as KIX, TAZ1, and TAZ2, interact with multiple activators using a shared group of amino acids.[47-50] Although ABDs use a shared set of amino acids for activator binding, it has been demonstrated that different activator sequences lead to different conformations of the coactivator upon binding.[51,52] Figure 2.11 displays structural perturbations induced by several activators of divergent sequence. VP16 H1 and ERM have been reported to predominantly target the H1 face of AcID while VP16 H2, ATF6α, and CBP target the H2 face. A comparison of VP16 H1 and ERM titrations reveals a stark difference in binding mode. ERM induces a high degree of peak broadening across a large number of residues, while VP16 H1 induces comparatively little broadening. This broadening of ERM is characteristic of an electrostatically-driven interaction where ERM weakly scans the surface of AcID in several modes. Alternatively, this could result from ERM binding at two different sites on AcID.[21,33] Despite these

two activators targeting the same face of AcID their interactions are distinct. Activators targeting H2 also induced different perturbation patterns. ATF6α and CBP both predominately use the H2 face for AcID binding, but CBP makes more extensive contacts with the small helical loop that wraps underneath the AcID β-barrel.

ERM: 38-DLAHDSEELFQDLSQLQEAWLAEAQVPDDEQ-68
ATF6α: 38-FTDTDELQLEAANETYENNFDNLDFDL-64
CBP: 20-PGFSANDSTDFGSLFDLENDLPDEL-44
VP16 H1: 413-APPTDVSLGDELHLDGEDVAMAHADALDDFDLDMLGDGDSPG-451
VP16 H2: 452-PGPGFTPHDSAPYGALDMADFEFEQMFTDALGIDEYGG-490
VP16 L2L3: 437-DALDDFDLDMLGDGDSPGPGPGFTPHDSAPYGALDMADFEFEQMFTDALGIDEYGG-490
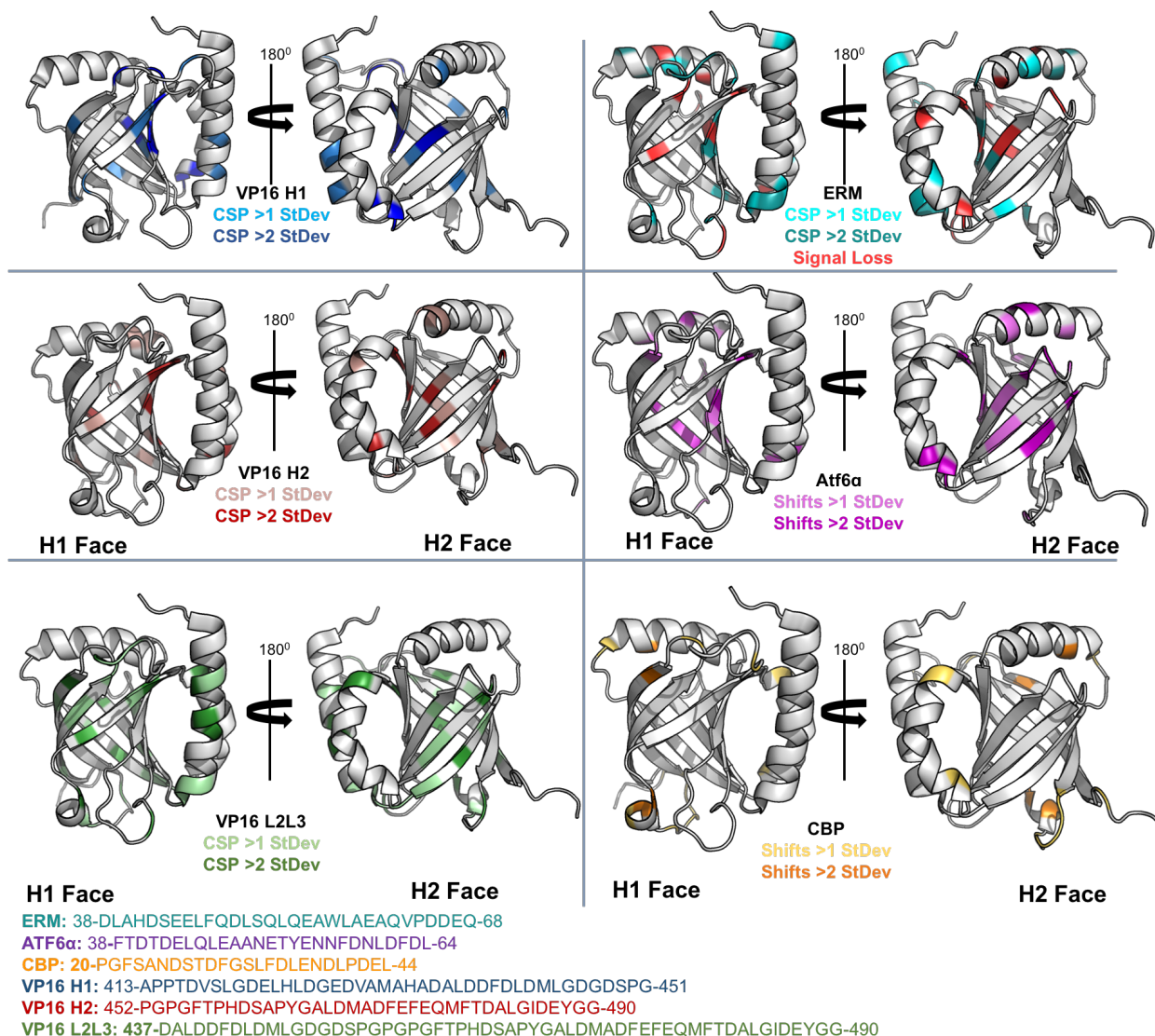
Figure 2.11 Conformational heterogeneity in activator-AcID complexes Perturbation patterns induced by different activator sequences as measured by HSQC. CSPs greater than 1 and 2 standard deviations mapped for the indicated colors. All perturbations gathered at saturating conditions. Performed with Matt Beyersdorf and Brian Linhares.

COVALENT ACTIVATOR-ACID COMPLEXES FACILITATE MECHANISTIC DEFINITION

As activator-coactivator interactions are often "fuzzy" allowing an activator to bind in multiple conformations or locations on a coactivator, the ability to study individual activator-coactivator binary complexes would be quite useful[21,53,54]. Because the H1 face of AcID contains two native cysteines, we sought to form activator-AcID complexes tethered through a disulfide bond. This disulfide Tethering approach to studying protein-protein interactions was elegantly demonstrated by Sadowsky et al. where they examined an allosteric site on PDK1 kinase[55]. This PPI tethering is a direct extension from the Tethering small-molecule screening strategy developed by Prof. Jim Wells and co-workers[56-58]. The ability to form homogenous covalent VP16-Activator complexes greatly simplify the interpretation of experiments involving VP16 binding to AcID because we know with high confidence where the activator is bound. This strategy has also allowed us to better map the VP16 binding site on AcID. We have used these covalent VP16-Med25 complexes to measure direct binding of activators, in stopped-flow kinetics studies, protein NMR, and other experiments to characterize mechanistic details of VP16-AcID complex formation.

Peptide synthesis

Several studies have indicated that, when bound by coactivators, VP16 adopts an α-helical structure. Milbradt and colleagues demonstrated that the N-terminal TAD of VP16 (VP16 H1$_{413-452}$) primarily induces perturbations of residues located within the H1 face of AcID [59,60]. Further, a mutation of AcID Q451E significantly inhibits binding of VP16$_{413-452}$. Because VP16$_{413-452}$ has been shown to interact with the H1 face of AcID, we initially utilized a minimal sequence of the N-terminal TAD, VP16 αH1 (VP16$_{438-454}$) that still retains binding affinity to AcID. A

fluorescently (FITC) tagged variant of this 17-amino acid peptide binds Med25 with a dissociation

constant of 1.5 μM. Each residue in the helical region of this sequence was iteratively mutated

to cysteine. All peptides were N-terminally acetylated and the cysteine thiol was capped with

cystamine (Figure 2.12).
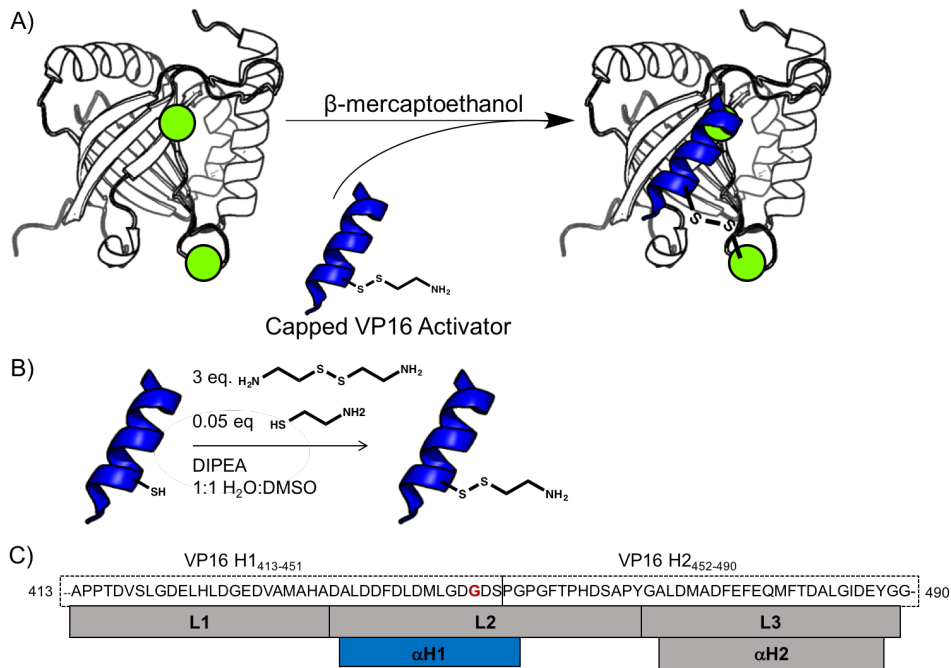
Figure 2.12 Disulfide tethered activator-coactivator complexes A. A disulfide-capped cysteine transcriptional activator peptide is incubated with Med25 containing two cysteines. B. Synthesis of disulfide-capped cysteine peptides. Reaction of the VP16 peptide with cystamine results in quantitative conversion. C. Constructs of VP16 used in this dissertation. Initial tethering experiments were performed with VP16 αH1 (blue).

VP16 αH1 binds Med25 with a unidirectional orientation

　　　To assess how well each disulfide-capped cysteine VP16 peptide could interact with the

two native AcID cysteines, labeling experiments were conducted and labeling efficiency was

assessed by mass spectrometry (MS). The disulfide-capped cysteine VP16 peptides were

incubated with wt Med25 AcID in the presence of a competitor thiol, β-mercaptoethanol (β-ME)

Analysis by MS revealed a strong orientational preference in reactivity (Fig 2.13). Labeling efficiency increased from the N- to the C-terminus with a significant increase in labeling observed for residues 450 to 454.
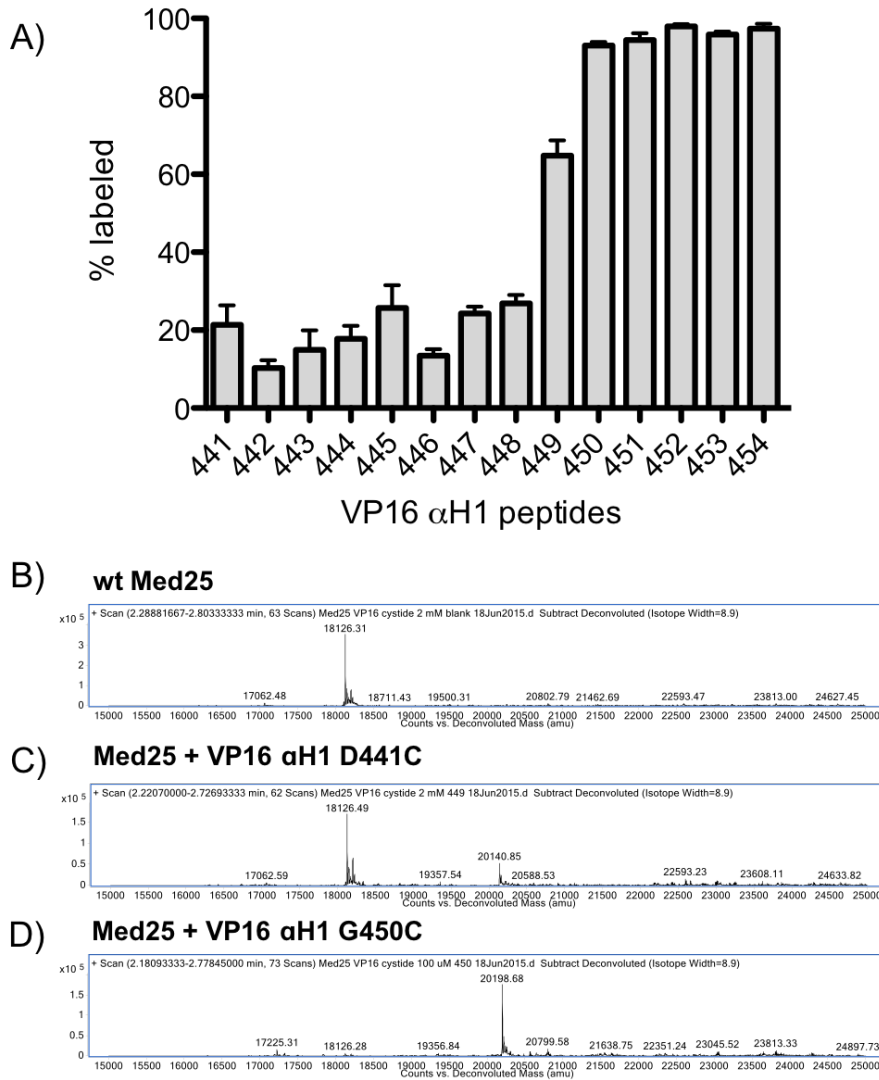
Figure 2.13 Mass spectrometry labeling analysis of VP16 αH1 cys-capped peptides A. Labeling efficiency of each cys mutant peptide for wt Med25. 10 μM Med25 was incubated with 40 μM peptide and 20 μM β-ME for 4 hrs at 20 °C. B. Mass spectrum showing unlabeled Med25. C. Mass spectrum showing Med25 + VP16 D441C. D. Mass spectrum showing Med25 + VP16 G450C. Mass Spectra were obtained on an Agilent Q-TOF LC/MS.

The large increase in labeling efficiency that occurred in the C-terminal residues indicates that this VP16 αH1 peptide interacts with Med25 quite specifically. If this peptide bound AcID in multiple orientations one would expect higher labeling of the N-terminal cysteine peptides. Instead, low labeling efficiencies are observed for residues 441-448. The complete labeling of residues 450-454 indicate that VP16 αH1 binds Med25 H1 with these residue in close proximity to one of the native AcID cysteines. This result suggests that VP16 binds the H1 face of AcID with a strong orientational preference.

VP16 αH1 binds Med25 AcID at C506 on a flexible loop

Because Med25 AcID has two cysteines in the H1 face, we next sought to determine which of these two cysteines were tethered by VP16. Site-directed mutagenesis (SDM) was used to individually replace each cysteine with alanine. Alanine substitution was chosen because it is a non-bulky, chemically inert side chain. Each mutant AcID variant was expressed, purified and incubated with VP16 αH1 G450C (Figure 2.14). The VP16 αH1 peptides were able to form covalent complexes with C506 but not C497. In fact, C497 did not display disulfide exchange with the excess β-ME suggesting that it is less accessible to solvent than C506.
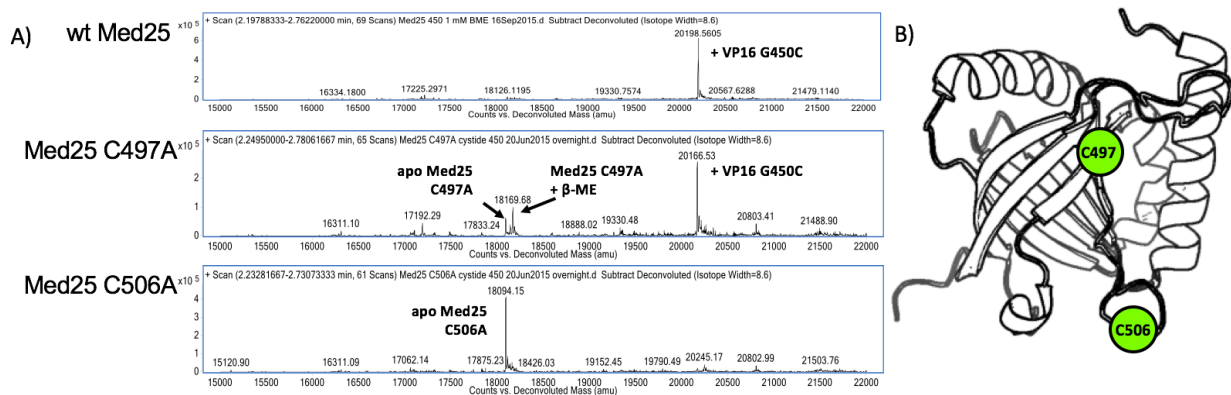
Figure 2.14 VP16 αH1 peptides target Med25 C506 A. VP16 αH1 G450C was incubated with wt Med25, Med25 C497A, and C506A. B. Location of C497 and C506 on the H1 face of AcID.

Because VP16 αH1 can be tethered to C506 but not C497, the Tethering data reveals information about binding orientation of the VP16 N-terminal TAD. While the Wagner and Cramer groups helped establish the ability of VP16 to simultaneously bind both faces of Med25 AcID, how the TAD bridges the two binding sites is unknown. The C-terminal portion of VP16 αH1 must be near AcID C506 presumably leaving the region of VP16 N-terminal of G450C to interact with the β-barrel and flexible loop at the top of the H1 face. The portion of VP16 C-terminal of G450C might then wrap along the bottom of AcID before binding AcID H2.

VP16 αH1 G450C inhibits activator binding to Med25 AcID

The high labeling efficiency exhibited by VP16 αH1 G450C enabled us to readily synthesize and purify the covalent Med25 AcID-VP16 αH1 G450C complex. Using this complex in a fluorescence polarization (FP) binding assay allowed us to assess how the presence of tethered VP16 αH1 peptides altered binding of non-covalent activator peptides. The ability to selectively bind, and therefore block, one face of AcID allowed us to dissect binding of activator peptides at both faces of AcID.   In line with VP16 αH1 being tethered at C506 and bound at the H1 face of Med25, a 5-fold reduction in binding was observed for FITC-VP16 H1 to 5 different Med25-VP16 complexes (Fig 2.15). A larger effect was observed for ERM$_{38\text{-}38}$ which also binds the AcID H1 face. Alternatively, VP16 H2 was less perturbed, consistent with the model that it preferentially binds the H2 face of AcID.
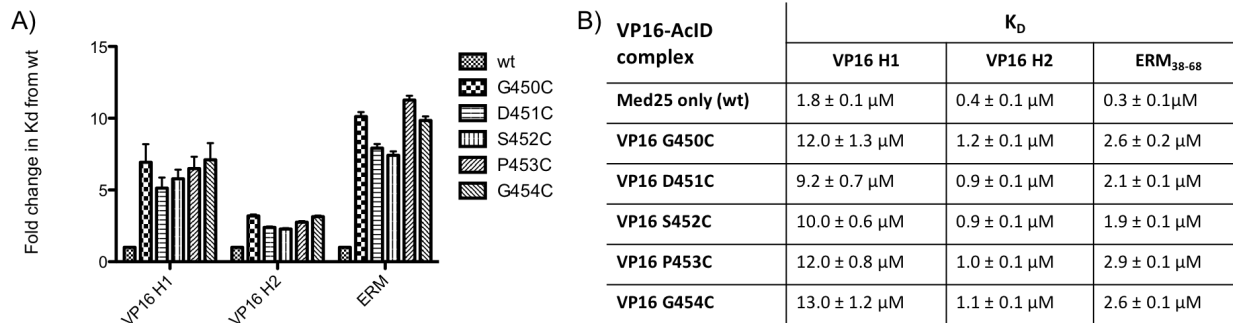
Figure 2.15 FP-inhibition assays of activators for covalent Med25-VP16 αH1 complexes A. Fold changes in K_d observed for three fluorescent tracers in the presence of wt Med25 and 5 different covalent Med25-VP16 complexes with the location of tethering at AcID C506 and VP16 αH1 450-454. B. K_d and error of each tracer for each Med25-VP16 complex.

While the presence of tethered VP16 αH1 did inhibit binding of VP16 H1 and ERM$_{38-68}$, the degree of inhibition was lower than might be expected given the large size of the tethered peptide. The presence of such a large covalently bound molecule should occlude most of the H1 binding face. A possible explanation for this is that activators can bind either surface of AcID which is also supported by the NMR titration of VP16 L2L3 (Fig 2.9). This is illustrated by examining the binding of shorter tracers to AcID. We looked at the change in binding affinity that was observed for FITC-VP16 αH1 and FITC-VP16 αH2 to a covalent AcID-VP16 αH1 G450C complex (Figure 2.16). These shorter peptides were significantly less inhibited than the full length VP16 H1 and H2 peptides. Because the N- and C-terminal TADs of VP16 are homologous, the shorter, α-helical region peptides, αH1 and αH2 peptides are likely less selective for one binding surface over another.

A)

Activator		K_d (µM)	Fold Change
VP16 αH1	+ G450C	3.44 ± 0.24	1.9
	wt	1.87 ± 0.09	
VP16 αH2	+ G450C	0.70 ± 0.04	1.2
	wt	0.57 ± 0.05	

B)

```
VP16 αH1  ALD--DFDLD-MLGD--GDSPG
          ::: ::...:. :  : .
VP16 αH2  ALDMADFEFEQMFTDALGIDEY
```

: = identical
· = similar

Figure 2.16 Fold change in affinity of VP16 αH1 and αH2 to Med25 AcID-VP16 αH1 G450C A. Fold change in shorter VP16 αH1 and αH2 peptides. B. Alignment showing high similarity between VP16 αH1 and αH2.[61]

The high similarity between the two shorter peptides likely allows them to promiscuously bind at both faces of AcID to a larger degree than the full N- and C-terminal VP16 TADs. This explains the lower overall inhibition observed using these peptides. This observation also lends support to a model where VP16 can bind in multiple orientations which would counter the precedent established in the literature, but is something that has been observed for other activator-coactivator complexes. Notably, p53 can bind the coactivator TAZ1 of CBP, which also has two activator binding faces, in two opposite orientations[62,63].

Extended VP16 G450C complexes further inhibit activator binding

The relatively low inhibition observed with the tethered VP16 αH1 G450C complex led us to wonder how binding of activators would be altered by extending the length of the tethered VP16 peptide. Two extended constructs were prepared. First, an N-terminally extended species was synthesized that encompassed the entire H1 VP16 TAD. Additionally, VP16 αH1 G450C was extended to the C-terminus to create VP16 L2L3 G450C. Both extended peptides readily labeled AcID and could be prepared in large quantities. Extended constructs were more adept at inhibiting both VP16 αH1 and αH2 with inhibition levels increasing as construct length increased.

VP16 L2L3 G450C offered almost complete inhibition indicative of its ability to fully bind both surfaces of AcID.
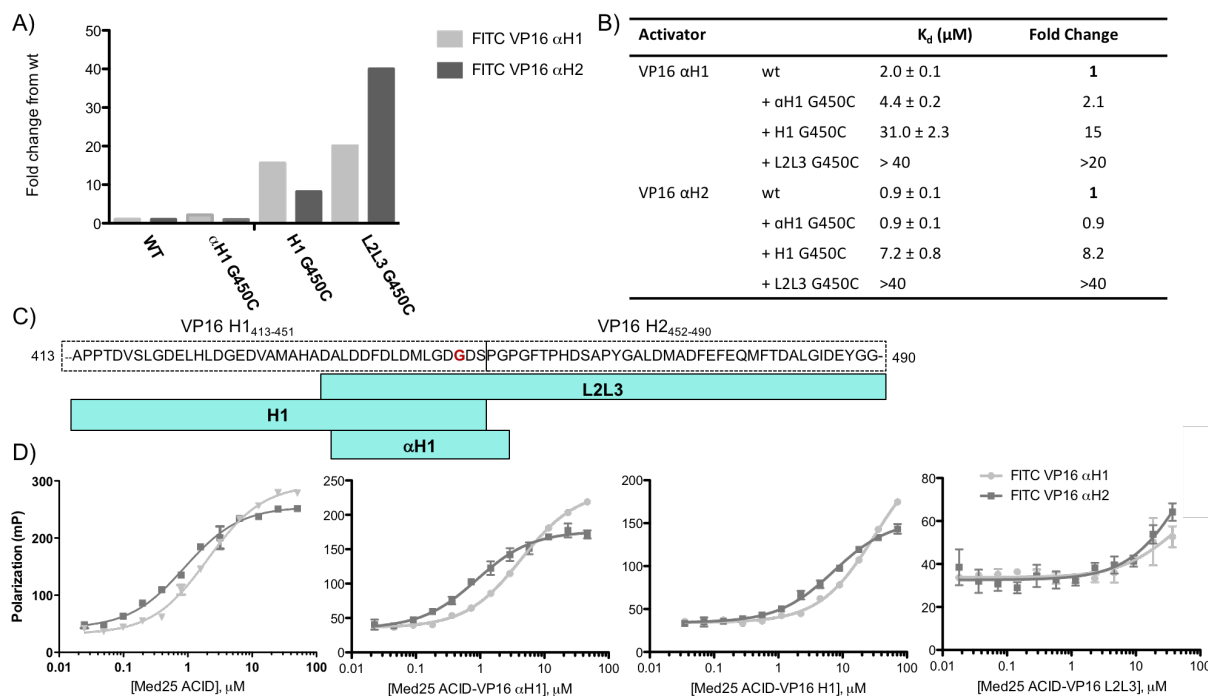
Figure 2.17 Effect of extended tethered constructs on VP16 binding A. Fold change in VP16 αH1 and αH2 binding in the presence of progressively longer VP16 G450C constructs. B. Table listing K_d and fold changes for VP16 αH2 and αH2. C. Full VP16 TAD sequence. Length of G450C peptide constructs graphically illustrated by teal bars. D) From left to right: FP curves of wt AcID, AcID-VP16 αH1, AcID-VP16 H1, AcID-VP16 L2L3.

VP16 L2L3 G450C recapitulates the native VP16 L2L3 interaction with Med25 AcID

With the ability to tether VP16 to Med25 AcID C506, we sought to see how well covalently tethered complexes recapitulate native activator-AcID interactions. Comparing HSQC spectra of VP16 L2L3 titrated against a VP16 L2L3 G450C tethered variant reveal spectra of high similarity indicating that the presence of the disulfide tether does not capture a highly non-natural conformation or induce large non-natural perturbations to the AcID structure (Figure 2.18). The covalently tethered L2L3 construct did produce a greater number of significant perturbations

which is consistent with it being a covalently bound ligand and thus more likely to remain in the

bound state making additional molecular contacts more favorable.
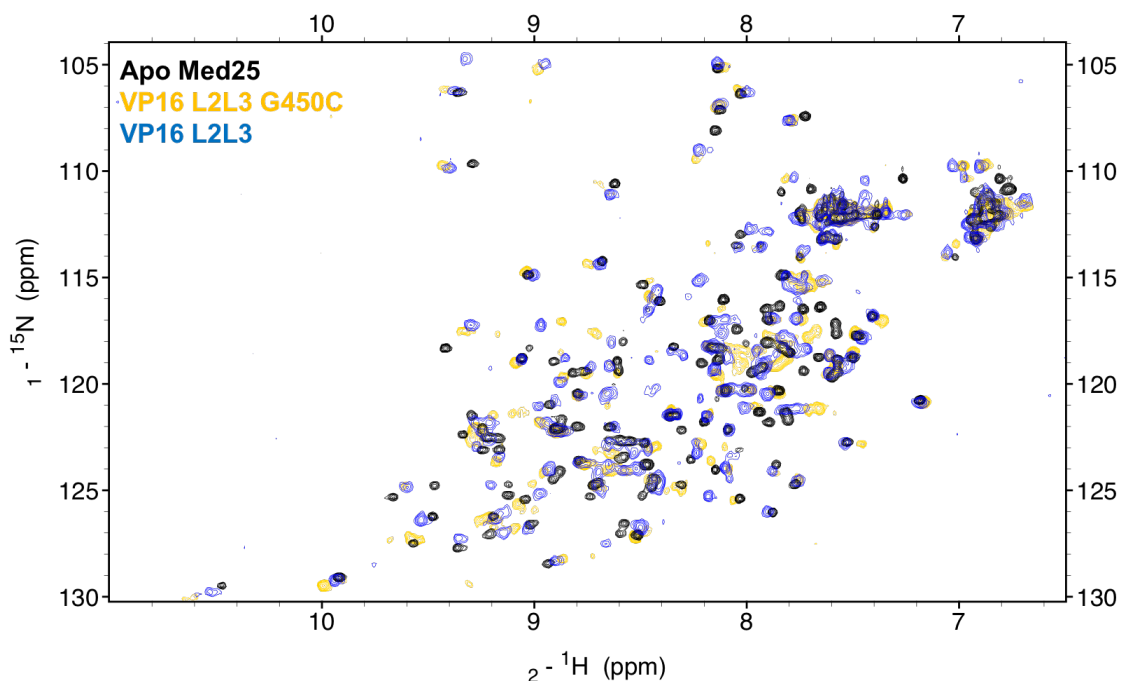
Figure 2.18 VP16 L2L3 and covalent VP16 L2L3 G450C induce similar perturbations Overlaid HSQC spectra of apo Med25 AcID (black), a covalent VP16 L2L3 G450C-AcID complex (gold), 3 eq VP16 L2L3 (blue).

Mapping the perturbations of the covalent VP16 L2L3 complex on to the surface of AcID

(Figure 2.19.B) compare favorably to the free acetylated VP16 L2L3 peptide titration (figure

2.19.A). In both complexes it is notable that the helix bounding the left side of the H2 face (helix

1) is not highly perturbed. This appears to indicate that this helix is not a significant participant

in binding of ligands at this face.
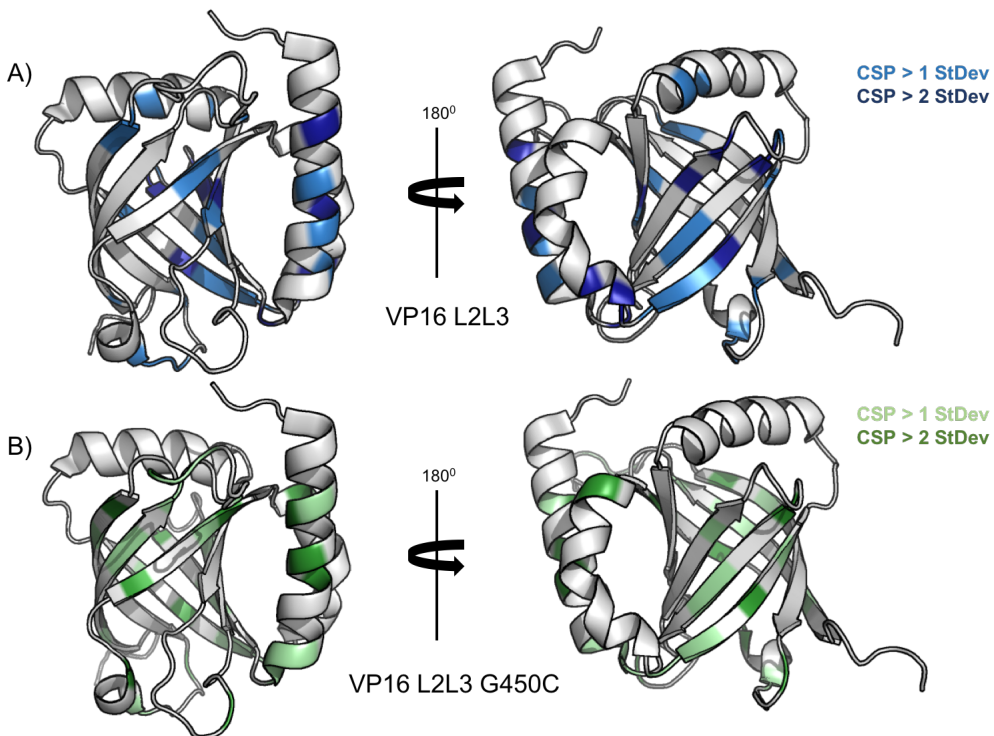
Figure 2.19 VP16 L2L3 and covalent VP16 L2L3 G450C overlaid perturbations A. Perturbations induced by acetylated VP16 L2L3 (3 equivalents) on AcID. Perturbations greater than 1 standard deviation are indicated in light blue while perturbations 2 standard deviations and greater are marked in dark blue. B. Perturbations induced by covalent VP16 L2L3 G450C on AcID. Perturbations great than 1 standard deviation are indicated in light green while perturbations 2 standard deviations and greater are marked in dark green.

KINETICS OF ACTIVATOR-MED25 COMPLEX FORMATION

While much information can be extracted from equilibrium binding experiments, stopped-flow kinetics is a highly sensitive technique that enables the quantification of individual kinetic parameters that contribute to a binding event between two proteins. Transient kinetics enable the detection and quantification of different bound states between activators and coactivators and how these states interconvert. These subtleties are invisible in equilibrium binding experiments. We utilized this technique to establish a mechanism of VP16-Med25 complex formation.

Electrostatics play a significant role in the Med25-VP16 interaction. Titration of increasing concentrations of salt significantly attenuate VP16 binding to AcID. From a kinetic perspective, the significant contribution from electrostatics in an interaction often results in extremely high on-rates.[64,65] In order to effectively measure such a fast interaction we utilized the fluorophore 4-*N*,*N*-dimethylamino-1,8-napththalimide (4-DMN) (Fig 2.20.A). 4-DMN is very environmentally sensitive exhibiting low fluorescence in an aqueous environment, but becoming extremely fluorescent as the environment becomes more hydrophobic (such as a protein interface).[66-68] This solvatochromic character made it an ideal fluorophore for kinetic studies and was attached to the N' terminus of VP16 L2L3.

Association experiments between Med25 AcID and 4-DMN VP16 L2L3 display biphasic kinetics which is indicative of a two-state association mechanism at minimum (Fig 2.20.b). The fast, initial phase was determined to be linearly dependent on Med25 concentration while the slow phase appears to be concentration independent (Fig 2.20.c). This suggests that in Med25 VP16 complex formation there is a fast initial bimolecular association followed by a slower unimolecular conformational change after binding. The k_{on} was determined to be $1.1 \pm 0.1 \times 10^9$ $M^{-1}s^{-1}$ which is very fast and consistent with electrostatics playing a significant role in VP16-Med25 complex formation. For comparison, this association is two orders of magnitude faster than the association of c-Myb to KIX ($2.2 \pm 0.1 \times 10^7$ $M^{-1}s^{-1}$).[69]

Dissociation kinetics experiments also revealed a biphasic process. The fast phase is attributable to direct dissociation of VP16 from Med25 AcID while the slower phase is the reverse of the slow conformational phase determined in the association kinetics experiments.
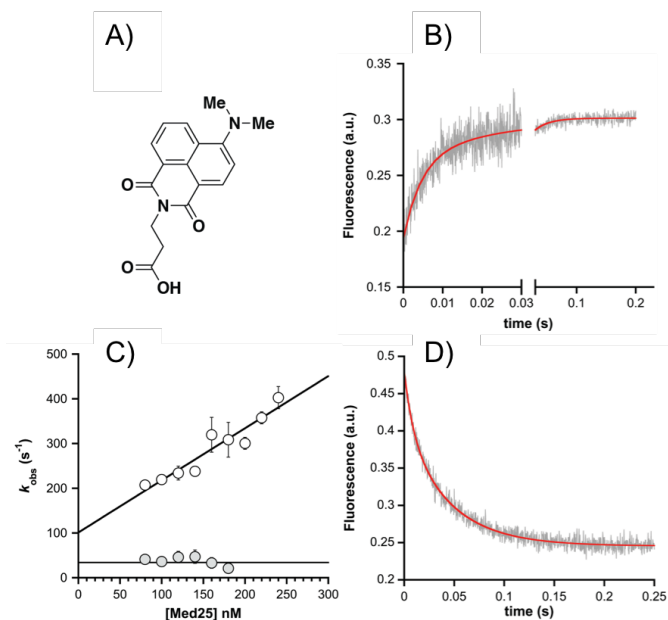
Figure 2.20 Association and dissociation kinetics of Med25-VP16 using the 4-DMN fluorophore
A. 4-DMN was used and added to the N' terminus of VP16 L2L3. B. Association kinetics of VP16 with Med25 reveal a two-step association. C. The fast association step is linearly dependent on Med25 concentration while the slow phase is concentration independent. D. Dissociation kinetics of the VP16-AcID complex. Performed by Matthew Henley

Microscopic rate constants were calculated using the exact solution for a two-step induced-fit mechanism.[70] The overall mechanism with rate constants is displayed in Figure 2.21.
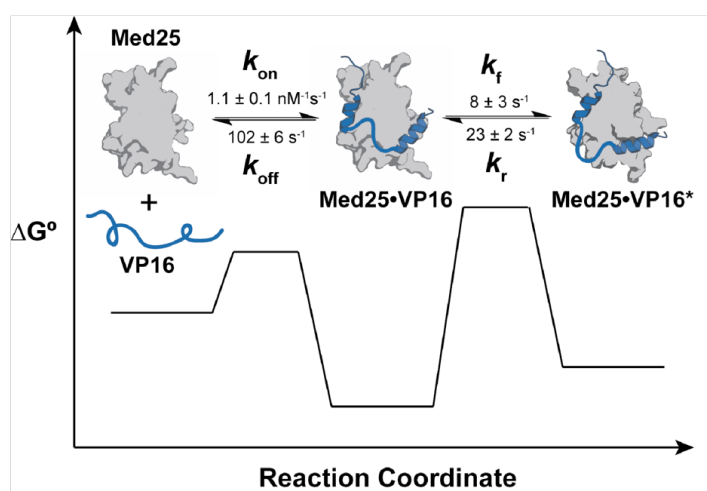
Figure 2.21 Overall kinetic mechanism of VP16-Med25 complex formation

MED25 ACID BINDING SURFACES ARE IN COMMUNICATION

AcID, despite its distinct structure, is similar to the KIX and TAZ1 domains in that they all possess two activator binding surfaces that can be used to bind a variety of transcription factors. A notable feature of the KIX domain is the allosteric network linking the two binding surfaces leading to positive binding cooperativity for specific activator pairs when they form ternary complexes involving KIX. This positive cooperativity can range from 2 to 18-fold depending on which two activator pairs are involved. The presence of the two activator binding surfaces in AcID led us to wonder if these two surfaces are 1) in communication and 2) able to participate in positive or negative cooperativity during ternary complex formation.

To address this first question we tethered VP16 αH1 G450C to AcID at C506 and performed HSQC NMR experiments. Interestingly, perturbations were observed both within the AcID H1 face and at distal regions of the protein including the Med25 H2 face (Figure 2.22) Specifically, the α-helix flanking the H2 face of AcID was perturbed as were residues on the β-barrel in close proximity to that helix. This can most likely be attributed the direct interactions between VP16 and the H1 face helix propagating to the H2 helix and surrounding residues. This represents the clearest demonstration that targeting one site of AcID can be used to alter or change the opposite binding site which would have utility in the design of small molecules capable of inducing or stabilizing certain AcID conformations in both an orthosteric and allosteric manner.
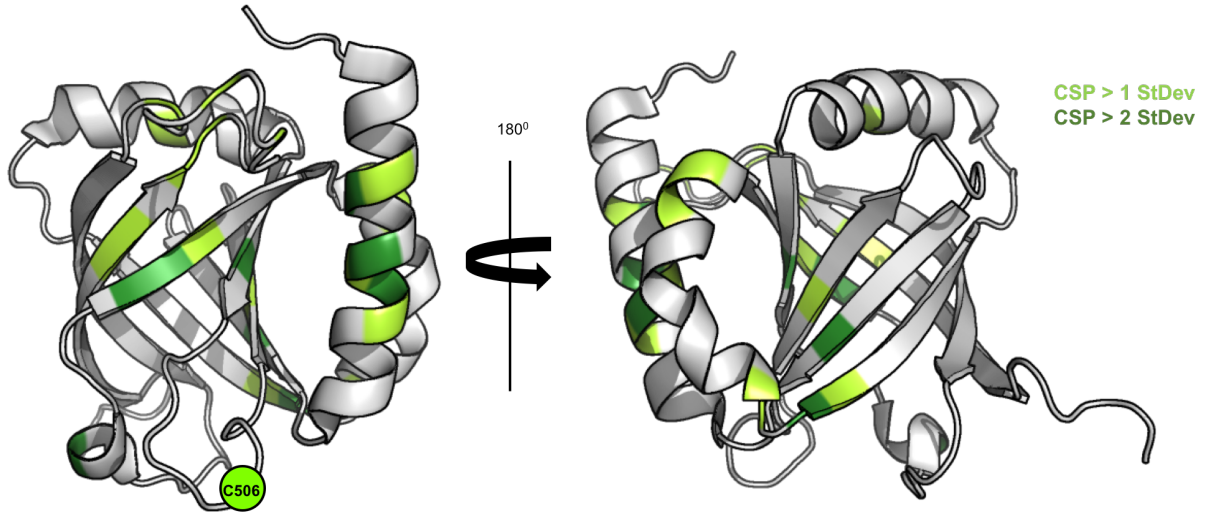
Figure 2.22 Med25 AcID binding surfaces are in communication A. Perturbations induced by VP16 αH1 G450C tethered to AcID. Chemical shifts greater than 1 standard deviation are indicated in pale green and those greater than two deviations are indicated in dark green.

ALLOSTERY IN MED25 ACID

We next wanted to assess what cooperativity, if any, existed between activators binding

at both AcID surfaces using the two VP16 TADs as a model system. Unlike KIX, the two AcID

binding surfaces are topologically very similar and the two VP16 TADs possess high sequence
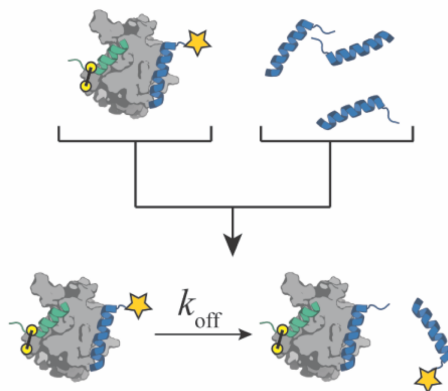
Figure 2.23 Dissociation kinetics experiment with tethered AcID-VP16 complexes Schematic of stopped-flow kinetics dissociation experiments. Pre-bound 4-DMN VP16 αH2 is competed from tethered VP16 αH1-AcID with acetylated VP16 H2 allowing for kinetic rates, notably k_{off} to be determined.

homology and similar dissociation constants. These features of both AcID and VP16 make it difficult to link experimental outcomes to a specific binding event.

VP16 H1 and VP16 H2 can bind both faces of AcID to some degree. To counter this problem we utilized VP16 αH1 cysteine mutants tethered to the AcID H1 face in stopped-flow kinetics experiments to measure binding of ligands at the AcID H2 face (Figure 2.23) A 4-DMN labeled VP16 αH2 peptide was competed with acetylated VP16 H2 to determine k_{off} values. Previous work has found that allosteric communication between activator-coactivator-activator ternary complexes is primarily mediated through a reduction of k_{off} with little appreciable change in k_{on} values.[71] Like the fast association rates of VP16-Med25 complexes, dissociation of VP16 αH2 from apo Med25 AcID is quite fast (k_{off} = 517 ± 11 s^{-1}) (Fig 2.24). A second small amplitude kinetic phase was also detected (k_r = 74 ± 3 s^{-1}) indicative of a conformational change similar to the change observed in VP16 L2L3. When VP16 αH1 is tethered to the AcID H1 face, a 20 % and 35 % reduction was observed in k_{off} and k_r, respectively. This reduction in the dissociation kinetics induced by tethered VP16 αH1 is indicative of allosteric stabilization with the most dominant contribution stemming from the decreased k_{off}. This represents the first example of positive cooperativity occurring between the AcID binding surfaces. The magnitude of this reduction in k_{off} is consistent with the reduction in k_{off} observed for pKID dissociation from KIX ternary complexes involving either KIX-MLL or KIX bound to the covalent molecule 1-10.
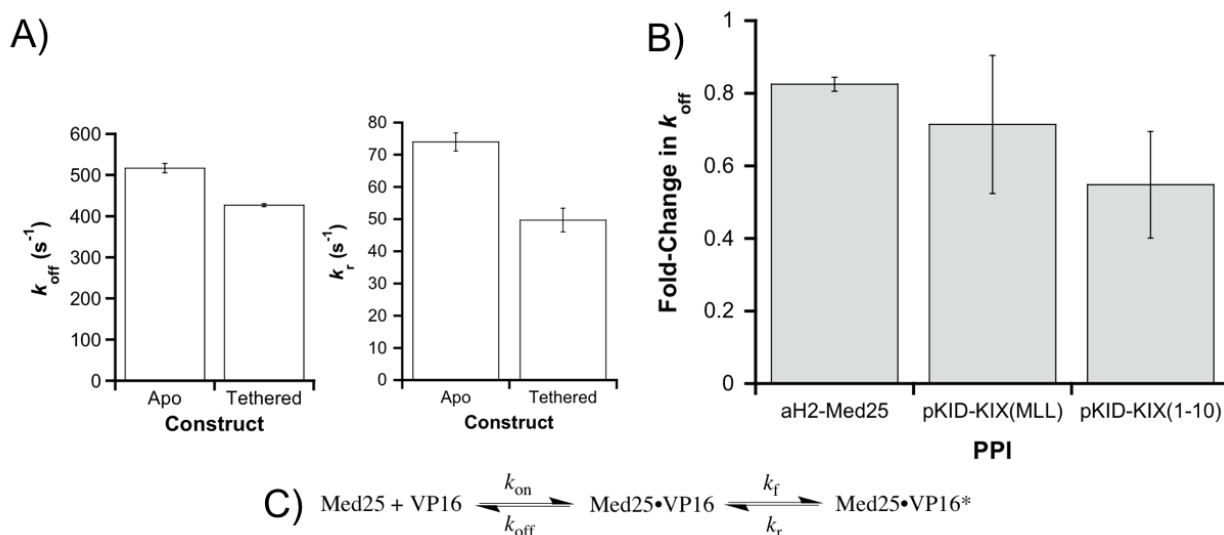
Figure 2.24 Positive cooperativity in VP16-AcID complexes A. Tethered VP16 αH1 induces positive cooperativity in VP16 αH2 binding as measured by reductions in both k_{off} and k_r. B. Reduction in k_{off} of VP16 αH2 from tethered Med25-VP16 αH1 is in line with reduction in k_{off} observed for pKID from either a KIX-MLL or 1-10 tethered KIX. C. Mechanism of Med25-VP16 complex formation. Performed by Matthew Henley.

VP16 BINDS TO THE ACID H2 FACE IN MULTIPLE ORIENTATIONS

The covalent tethering strategy has enabled a host of mechanistic and structural studies that have allowed us to better understand how AcID interacts with activators and revealed an allosteric network linking two binding sites on AcID. While the native placement of two native cysteines within the H1 face of AcID enabled us to easily probe binding at that location with covalent cysteine-containing VP16-derived peptides, we still sought to investigate activator binding at the H2 face. In an analogous fashion to the H1 studies, a panel of cysteine mutant peptides were prepared based on the alpha helical portion of VP16 H2 (Fig 2.25).

Because the H2 face of AcID contains no native cysteines, we utilized site-directed mutagenesis to add them at various locations. We replaced all three native cysteines with alanine before adding new cysteines at specific locations on the H2 face of AcID. In the 10 cysteine

mutations that were prepared, protein expression yield ranged from 25 to 100% that of wild type Med25. Based on both published and our own NMR data, we initially placed cysteines on helix 1 flanking the left edge of the H2 face (Fig 2.25). Residues were chosen where side chains appeared both solvent-exposed and projected towards the H2 binding surface.
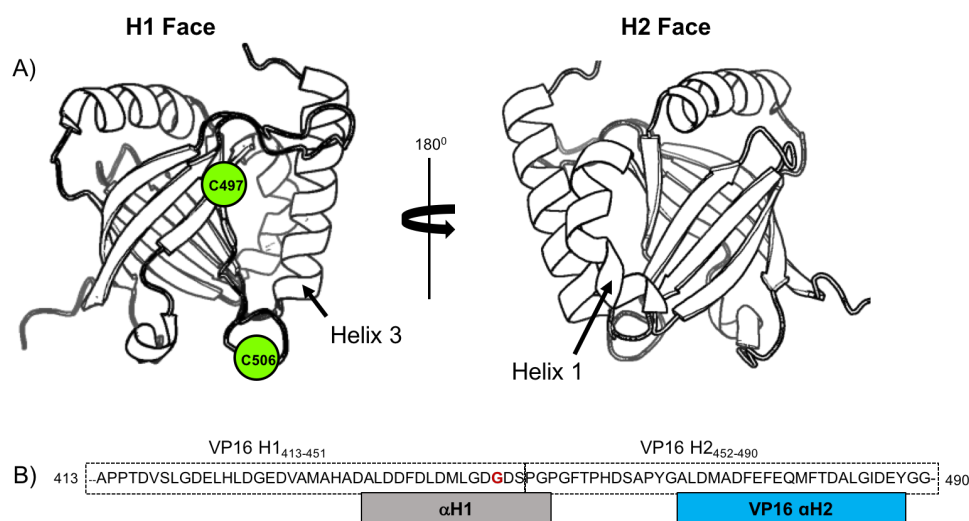
Figure 2.25 Activator tethering at the H2 face of AcID A. The two solvent-exposed cysteines in Med25 are located in the H1 face. Tethering at the H2 face was performed after introducing non-native cysteines at various positions. B. The VP16 αH2 sequence (VP16$_{468-489}$) that was used for tethering studies is homologous to VP16 αH1 (VP16$_{438-454}$).

In initial labeling studies involving cysteine mutations on helix 1 several patterns emerged. As the cysteine was progressively moved down the helix overall labeling dramatically increased (Fig 2.26). This pattern would agree with the model that VP16 binds Med25 H1 in an N-terminal to C-terminal direction wrapping underneath AcID and finally binding the H2 face. The VP16 residue-independent labeling efficiency was quite unusual and suggests that VP16 H2 can bind Med25 AcID in multiple modes or orientations. This runs counter to the much more specific interaction captured in the VP16 αH1 tethering experiments.
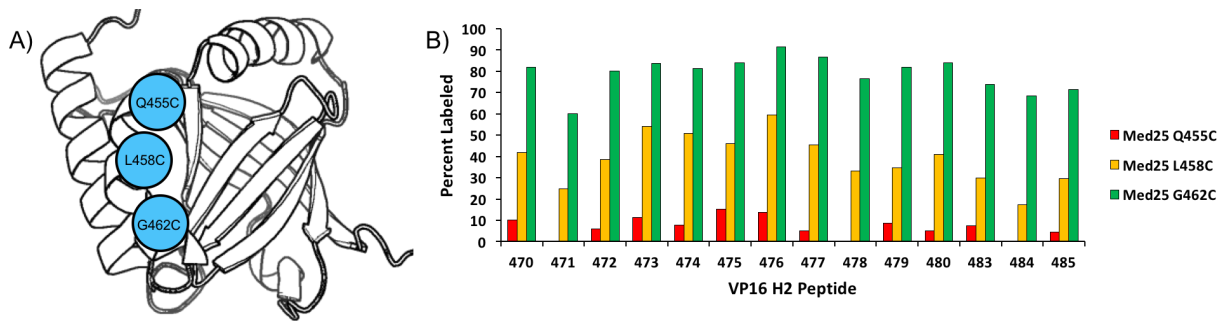
Figure 2.26 Tethering on Helix 1 of the AcID H2 face is location dependent A. Sites of cysteine introduction on helix 1. B. Tethering efficiency of VP16 αH2 for helix 1 cys mutants as measured by mass spectrometry. Four equivalents were incubated with AcID for 4 hrs with 2 equivalents of β-ME.

Tethering efficiency on the β-strands of the H2 binding surface was also site-dependent. Tethering to M512C produced almost no detectable labeling despite the methionine side chain projecting toward solvent and being in close proximity of L458 on helix 1 that displayed moderate tethering. In contrast, VP16 αH2 readily tethered to M470C at the bottom of the β-barrel. In our NMR titration with VP16 L2L3 and in the covalent Med25-VP16 L2L3 complex the residues directly surrounding M470 (Figure 2.27) were heavily perturbed consistent with this being a region that heavily participates in the Med25-VP16 interaction.
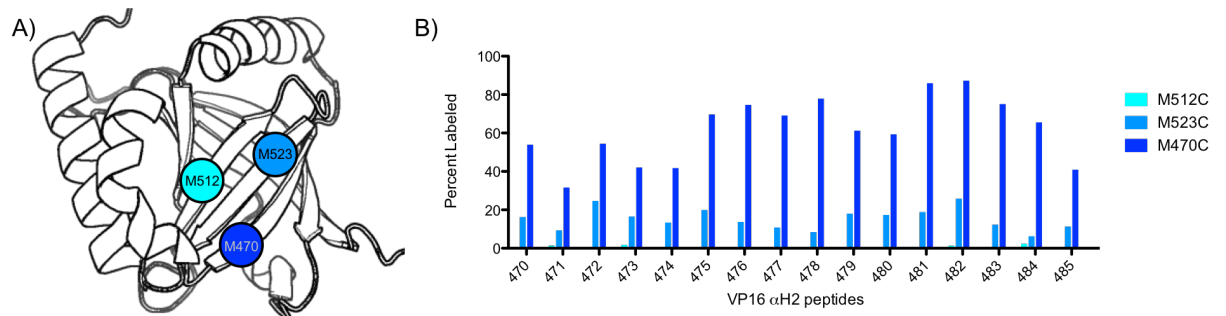
Figure 2.27 Tethering on β-sheets of the AcID H2 face is location dependent A. Sites of cysteine introduction on helix 1. B. Tethering efficiency of VP16 αH2 for helix 1 cys mutants as measured by mass spectrometry. Four equivalents were incubated with AcID for 4 hrs with 2 equivalents of β-ME.

As was observed with the helix h1 mutants, VP16 αH2 binds with seemingly little preferred orientation in contrast to the specific tethering pattern observed with VP16 aH1 peptides at the H1 face. While the H1 and H2 faces are topologically quite similar, homologous VP16 sequences interact with them in divergent manners.

2.4 CONCLUSIONS

Transcriptional coactivators regulate the function of transcriptional activators controlling both healthy and disease-associated gene activity, often simultaneously. Understanding the mechanistic basis of these interactions adds to our understanding of transcriptional activation and assists our efforts to develop small molecules capable of targeting these interactions. The AcID domain of Med25 is a structurally unique fold and prior to beginning this work it was unclear how conserved the mechanisms of activator-coactivator binding were across structurally distinct ABDs. This work has added to our insight of AcID-activator interactions and revealed similarities and differences in the mechanism of complex formation.

Using solution NMR we have demonstrated that there is significant conformational heterogeneity in activator-AcID complex formation. AcID contains two binding sites on opposite faces of the fold that can be targeted by activators of different sequences. The bidentate activator VP16 simultaneously contacts both surfaces of AcID analogous to complexes observed between p53-TAZ1 or p53-KIX.[48,72] Activators can also target single binding surfaces of AcID, as observed with ERM and ATF6α. The N-terminal region of CBP also binds the H2 face of AcID but in a distinct fashion from ATF6α. This heterogeneity suggests that stabilizing individual conformations of AcID via small-molecules may be a way to selectively inhibit individual activator-coactivator interactions while promoting others.

The use of tethered VP16 peptides enabled us to construct individual activator-AcID complexes. Importantly, complexes between VP16 H1 and Med25 suggest that VP16 has a strong orientational preference when binding to AcID lending insight into how VP16 contacts both faces of AcID. This data has guided computational modeling between full length VP16 and AcID. The use of equilibrium binding experiments and these covalent complexes show that activator binding is more promiscuous than previously reported.

The use of transient kinetics reveal that VP16 association with AcID is very fast. Association of activators to the KIX domain are some of the fastest binding events recorded due to electrostatic contributions and VP16-AcID binding is two orders of magnitude faster than those (Fig 2.28). VP16 association to Med15 KIX is similar to the association of pKID and c-Myb to CBP KIX.
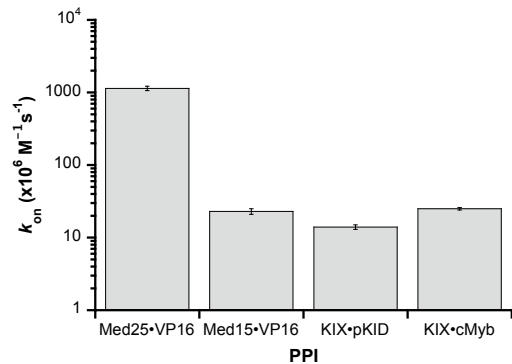
Figure 2.28 Comparison of k_{on} to other activator-coactivator interactions The association rates of VP16 to Med25 compared to the association of activators with the CBP and Med15 KIX domains.

We also demonstrate that tethering VP16 to AcID H1 induces perturbations at both faces of AcID indicating that these two faces are in communication pointing to the possible existence of an allosteric network that links these surfaces. Transient kinetic analysis of activator dissociation from AcID revealed a 20% stabilization of VP16 H2 when in the presence of tethered

VP16 αH1. This is the first demonstration of binding cooperativity in AcID. The KIX allosteric network has been well characterized and we show the existence of allosteric communication in a structurally distinct ABD.

These studies have refined our understanding of activator-AcID complexes and we have used that information to guide our development of small molecule modulators of AcID structure in the next chapter.

2.5 MATERIALS AND METHODS

Plasmids

The Med25 expression plasmid pET21b-Med25(394-543)-His$_6$ (referred to as pAcID) was a gift from Prof. Patrick Cramer.[1] Modified pAcID constructs were prepared using site directed mutagenesis as previously described.[73]

Table 2.1 SDM primers for Med25 mutants

Med25 variant	Primer Sequence
C506A	F: TCCCCCCACGGCGCCCGCCGAGGTGCGCGTGCTCATG
	R: CATGAGCACGCGCACCTCGGCGGGCGCCGTGGGGGGA
C497A	F: GGCCAACGGCTTCGCGGGCGCCGTGCACTTCCCCACACG
	R: CGTGTGGGGAAGTGCACGGCGCCCGCGAAGCCGTTGCC
C429A	F: ACGCGGTCACTGCCCGCCCAGGTCTAC
	R: ATTCACGTAGACCTGGGCGGGCAGTGA
Q455C	F: ATGCAGCTCATCCCCTGCCAGCTGCTGACCACC
	R: GGTGGTCAGCAGCTGGCAGGGGATGAGCTGCAT
L458C	F: ATCCCCCAGCAGCTGTGCACCACCCTGGGCCCT
	R: AGGGCCCAGGGTGGTGCACAGCTGCTGGGGGAT
G462C	F: CTGCTGACCACCCTGTGCCCCTTTGTTCCGGAAC
	R: GTTCCGGAACAAAGGGCACAGGGTGGTCAGCAG
M512C	F: GAGGTGCGCGTGCTCTGCCTCCTGTACTCGTCC
	R: GGACGAGTACAGGAGGCAGAGCACGCGCACCTC
M523C	F: AAGAAGAAGATCTTCTGCGGCCTCATCCCCTAC
	R: GTAGGGGATGAGGCCGCAGAAGATCTTCTTCTT
M470C	F: TTCCGGAACTCAAGGTGTGTCCAGTTCCATTTC
	R: GAAATGGAACTGGACACACCTTGAGTTCCGGAA

Protein expression

pAcID(394-543) was expressed as a C-terminal His$_6$ construct in *E. coli* Rosetta pLysS cells. Overnight starter cultures were grown from Rosetta cells transformed with pLysS cells in LB broth in the presence of 1 mg/mL ampicillin and 0.034 mg/mL chloramphenicol at 37 °C at 150 RPM. Following overnight growth, 1 L of TB supplemented with 1 mg/mL ampicillin and 0.034 mg/mL chloramphenicol was inoculated with 5 mL of the overnight culture and grown at 37 °C to an OD of 0.8. Once the culture reached the correct OD, it was grown overnight at 21 °C in the presence

of 0.5 mM IPTG to induce protein expression. Cells were harvested via centrifugation at 6500

RPM for 20 minutes. Cell pellets were stored at -80 °C until needed for purification.

For isotopically labeled protein used in NMR experiments following overnight growth in LB, TB

media was substituted with M9 minimal media supplemented with Bioexpress (6 mL/L) and 1 g/L

$^{15}NH_4Cl$ or 1 g/L $^{15}NH_4Cl$ and ^{13}C D-glucose for ^{15}N and $^{15}N,^{13}C$ Med25 AcID respectively. Before

inoculation of the 1 L expression flask, the overnight cells were pelleted via centrifugation for 10

minutes at 2500 RPM and the LB was decanted. Cell pellets were resuspended in 20 mL M9 media

followed by centrifugation for 10 mins at 2500 RPM. M9 media was decanted and the washed

pellet resuspended in 10 mL M9 media. 5 mL of cells were then used to inoculate the expression

flask containing M9 media supplemented with the appropriate isotopically labeled reagents.

Protein Purification

Cell pellets were resuspended in lysis buffer(50 mM phosphate, 300 mM NaCl, and 10 mM

imidazole, pH 6.5, 0.7 μL/mL β-ME), lysed by sonication, and centrifuged for 20 mins at 10,000

rpm. Supernatant was filtered and purified by chromatography on an AKTA Pure FPLC first by

Nickle column (HisTrap HP, GE Healthcare) with a gradient that moved from Buffer A (50 mM

phosphate, 300 mM NaCl, and 30 mM imidazole, pH 6.8) to buffer B (50 mM phosphate, 300 mM

NaCl, and 400 mM imidazole, pH 6.8). This was followed by purification via anion exchange

(HiTrap SP HP, GE Healthcare) with a gradient that moved from buffer A (50 mM phosphate, 1

mM DTT, pH 6.8) to buffer B (50 mM phosphate, 1 mM DTT, 1M NaCl, pH 6.8). Pure protein was

dialyzed into the appropriate phosphate storage buffer overnight. Following dialysis, protein was

concentrated via Amicon 5,000 Da cutoff spin concentrator and quantified via a NanoDrop at 280 using an extinction coefficient, ε = 22,460 $M^{-1}cm^{-1}$. Protein identity was confirmed via mass spectrometry (Agilent Q-TOF).

Phosphate Buffers for NMR Experiments:

General AcID storage buffer: 10 mM $NaPO_4$, 50 mM NaCl, pH 6.8

NMR buffer: 20 mM $NaPO_4$, 150 mM NaCl, pH 6.5

Peptide synthesis

Peptide constructs were prepared following standard FMOC solid-phase synthesis methods on a Liberty Blue Microwave synthesizer on Rink Amide Resin. Peptides were cleaved from resin in 95 % TFA, 2.5 % H_2O, 2.5 % TIPS. Peptides in excess cleavage solution were evaporated under N_2, precipitated in diethyl ether, and dissolved in 3:1 100 mM ammonium acetate:acetonitrile with minimal ammonium hydroxide to ensure peptide solubility. Peptides were purified by reverse-phase HPLC on an Agilent 1260 series with a C_{18} column (Agilent) using a gradient between 100 mM ammonium acetate and acetonitrile. Purified peptide fractions were pooled and lyophilized. Dried peptides were dissolved in DMSO and quantification was performed via 1:100 dilution into PBS, pH 7.4 using the peptide-specific extinction coefficient at 280 nm. Peptide identity was confirmed via mass spectrometry (Agilent Q-TOF).

Disulfide capped cysteine peptides

Disulfide-capped cysteine mutant VP16 peptides were cleaved from resin and following ether precipitation were dissolved in 1:1 DMSO:H_2O followed by the addition of 10 equivalents of

cystamine HCl, 30 equivalents of DIPEA, and 1 eq of cysteamine. Reactions were mixed at room temperature for 4-18 hrs. Solvent was removed by lyophilization and peptide was resuspended in 3:1 100 mM ammonium acetate:acetonitrile for HPLC purification. Pure peptides were dissolved in DMSO and stored at -20 °C.

Med25 labeling with VP16 cysteine-capped peptides

Med25 AcID (10 mM NaPO$_4$, 100 mM NaCl, pH 6.8) was incubated with 4 equivalents of each disulfide-capped VP16 peptide and 2 equivalents of β-mercaptoethanol (β-ME) for 4 hrs. Labeling efficiency was determined using an Agilent Q-TOF HPLC-MS. Protein samples were injected onto the instrument and the peptide/protein mixture separated via a Poroshell C$_8$ column using a gradient of 5-100% acetonitrile to water with 0.1% formic acid. Data was analyzed using the Agilent workstation software. Labeling efficiency was determined by comparing the peak heights of mass adducts corresponding to Med25, Med25 + β-ME, and Med25 + peptide using the following equation:

$$Percent\ labeled\ = \frac{Med25_{peptide}}{Med25_{unlabeled} + Med25_{\beta-ME} + Med25_{peptide}}$$

Reported values represent the average of three technical replicates unless otherwise noted.

Preparation of homogenously labeled Med25-VP16 complexes

For larger quantities of fully tethered Med25-VP16 complexes, Med25 was incubated with 2 equivalents of VP16 peptide and 1 equivalent of β-ME for 6 hrs. The complex was then purified on an AKTA Pure FPLC and a HiTrap SP HP column to remove excess peptide. Protein complexes

were then buffer exchanged into the appropriate buffer using passive dialysis followed by concentration with an Amicon Ultra 5,000 Da cutoff spin concentrator.

Direct binding experiments

Direct binding fluorescence polarization assays were performed in triplicate in 384-well black, round bottom plates (Corning 4514) at a final volume of 20 µL. 10 µL of Med25 was added at twice the highest final concentration and serially diluted with AcID storage buffer (10 mM NaPO$_4$, 100 mM NaCl, pH 6.8.) by adding 10 µL of buffer to the well containing protein followed by moving 10 µL of this 2-fold diluted protein to the next sequential well. This dilution was repeated 12 times. In the 13th well only storage buffer is added. FITC (fluorescein isothiocyanate) labeled peptides stocks at 40 µM were prepared in AcID storage buffer and added to wells containing diluted protein or buffer, resulting in a final 2-fold dilution of both peptide (final concentration 20 nM) and protein. The plate was incubated for 30 minutes at room temperature followed by reading on a Pherastar plate reader with polarized excitation at 485 nm and emission intensity was measured through a 535 nM filter. A binding isotherm that accounts for ligand depletion (assuming a 1:1 binding model of peptide to ACID) was fit to the observed anisotropy values as a function of ACID to obtain the apparent equilibrium dissociation K$_d$,

$$y = c + (b - c) \times \frac{[K_d + a + x] - \sqrt{(K_d + a + x)^2 - 4ax}}{2a}$$

Where "a" and "x" are the total concentrations of fluorescent peptide and protein, respectively, "y" is the observed anisotropy at a given protein concentration, "b" is the maximum observed

anisotropy value, and "c" is the maximum observed anisotropy value. Each data point is an average of three independent experiments with the indicated error representing the standard deviation of the three replicated. Data analysis was performed using GraphPad Prism 4.0.

NMR analysis of peptide-AcID complexes

NMR analysis of peptide-AcID complexes were performed via ^{1}H-^{15}N HSQC on a Bruker Avance III 600 Mhz spectrometer equipped with a cryogenic probe at 30 °C. Activator AcID titrations were conducted with Med25 AcID (20 mM NaPO$_4$, 150 mM NaCl, pH 6.5, 5% D$_2$O) at 50 uM and acetylated peptides were added at 0, 0.2, 0.5, 0.8, 1.1, 2, and 3 equivalents with a 2 % final DMSO concentration. Control spectra were obtained with Med25 and DMSO only. Tethered activator-AcID complexes were prepared and purified as described above and spectra were obtained in the absence of DMSO. Data Processing and visualization was performed using NMR Pipe and Sparky.[74]

Stopped-Flow Fluorescence Spectroscopy

Stopped-flow kinetic assays were performed on a Kintek SF-2001 stopped-flow apparatus equipped with a 100-W Xe arc lamp in two-syringe mode. The 4-DMN fluorophore was excited at 440 nm and its emission was monitored at wavelengths >510 nm, using a long-pass filter (Corion). All solutions were allowed to equilibrate in the instrument for at least 5 min before experiments were performed. Concentrations reported are after mixing.

All kinetic traces reported are an average of either ~80 (association experiments), or ~40 (dissociation experiments) individual traces. A double exponential was fitted to the transient

kinetic time courses, $F(t)$ as in Eq. 1, to obtain the fluorescence amplitudes (F_n) and the observed

rate constants (k_{obs}) for each exponential phase, where $F(0)$ is the initial fluorescence intensity

and t is time. The possibility of traces fitting to more exponential phases was also explored, but

no improvements in fits were observed.

$$F(t) = F(0) + F_1 \times (1 - e^{-k_{obs,1} \times t}) + F_2 \times (1 - e^{-k_{obs,2} \times t})$$

Analysis of the time courses was performed using Kaleidagraph 4.5 software. The dependence of

the observed rate constants on Med25 (association experiments) or unlabeled peptide

(dissociation experiments) concentration was analyzed using Kaleidagraph 4.5 software. All

reported values for observed rate constants are the average of two separate biological replicates

with different peptide and protein stocks, and the errors are the standard deviation. In calculating

microscopic rate constants, this error was propagated through standard methods.

Association Experiments

A total of 50 nM 4-DMN-VP16(438-490) was rapidly mixed with various concentrations (80-240

nM, final concentrations after mixing) of Med25 in stopped-flow buffer at 10 ºC. The measured

time domains (0.03 and 0.2 s) were selected to enhance data analysis as they were closest to the

predicted best time frame by preliminary fits in the Kintek software. An "inverted" series of

experiments was also explored, where the fluorescent peptide (80-240 nM) was varied and

Med25 was kept constant (50 nM), and gave similar kinetics but with somewhat lower S/N. We

note that the concentration ranges for the association experiments are not quite in the range of

what is considered "pseudo-first order," however, global fitting of all the association fluorescence traces in Kintek Explorer 6.2 software with microscopic rate constants restrained to their calculated values did not reveal any significant deviations.

To obtain well constrained value for $k_{obs,2,max}$ for calculating microscopic rate constants, we performed an experiment with [Med25] well above the apparent K_d and an increased concentration of labeled VP16(438-490) to increase S/N. Here, 500 nM 4-DMN-VP16(438-490) was rapidly mixed with 20 μM Med25 in stopped-flow buffer at 10 ºC, and the resultant kinetic trace was fitted to a single exponential to obtain a value for $k_{obs,2,max}$. A similar experiment with VP16(467-490) did not reveal any observable change in fluorescence, which likely indicates that the fluorescence value of the second conformation is not sufficiently different from the first conformation to detect in association experiments. This is also consistent with the idea that the equilibrium constant between the two bound states is much lower for VP16(467-488)

Dissociation Experiments

Med25•VP16(438-490): A total of 50 nM 4-DMN-VP16(438-490) was preequilibrated with 100 nM Med25 in stopped-flow buffer, and then rapidly mixed with 10 μM unlabeled VP16(438-490) at 10 ºC.

Med25•VP16(467-488): A total of 250 nM 4-DMN-VP16(467-488) was preequilibrated with 1.5 μM Med25 or the Med25-αH1$_{G450C}$ tethered construct in stopped-flow buffer, and then rapidly mixed with 5-100 μM unlabeled competitor VP16(455-490). The longer unlabeled construct was used instead of the shorter (467-488) construct because it displaced a higher proportion of the

labeled peptide at lower concentrations, increasing signal-to-noise. To obtain a well constrained value, the concentration dependence of the fast k_{obs} was fit to either equation 2, below, or to a constant if no obvious curvature was observed. In this equation, k_{on} is set to the value of the VP16(438-490) construct, [Unlabeled] refers to the concentration of the competitor peptide, and $K_{d,unlabeled}$ is the unlabeled peptide's apparent dissociation constant. The slower k_{obs} was fit to a constant.

$$k_{obs} = k_{off} + \frac{k_{on} \times [Med25]}{1 + \dfrac{[Unlabeled]}{K_{d,unlabeled}}}$$

Calculation of Microscopic Rate Constants

In previous work, we have used a Taylor series approximation of the exact equation for a two-step association mechanism, however here the kinetics did not meet the requirements to use this approximation (i.e., sufficient time separation of the two phases at the limit of zero Med25). Instead, because we observed two phases in dissociation experiments, we were able to utilize the exact expression for a dissociation experiment (Equation 3) to calculate all first-order microscopic rate constants.

$$k_{obs,off,1,2} = \frac{k_{off} + k_f + k_r \pm \sqrt{(k_{off} + k_f + k_r)^2 - 4 \times k_{off} \times k_r}}{2}$$

Because $k_{obs,2,max}$ is the sum of k_f and k_r, k_{off} is simply the sum of the two observed off-rate constants minus $k_{obs,2,max}$ (Equation 4).

$$k_{off} = k_{obs,off,1} + k_{obs,off,2} - k_{obs,2,max}$$

A value for k_r can also be easily resolved from this expression, by first subtracting the two observed off-rate constants and then substituting observable parameters and rearranging (Equation 5):

$$k_{obs,off,1} - k_{obs,off,2} = \sqrt{(k_{off} + k_f + k_r)^2 - 4 \times k_{off} \times k_r}$$

$$= \sqrt{(k_{obs,off,1} + k_{obs,off,2})^2 - 4 \times (k_{obs,off,1} + k_{obs,off,2} - k_{obs,2,max}) \times k_r}$$

$$k_r = \frac{(k_{obs,off,1} + k_{obs,off,2})^2 - (k_{obs,off,1} - k_{obs,off,2})^2}{4 \times (k_{obs,off,1} + k_{obs,off,2} - k_{obs,2,max})}$$

Then, k_f is simply obtained by subtracting the calculated value of k_r from $k_{obs,2,max}$.

We could not obtain data from association experiments with the short VP16(467-488) construct due to the dead time of the stopped-flow instrument (3-4 ms), so we applied the fast-equilibrium approximation to calculate microscopic rate constants for k_{off} and k_r. Under this approximation, the faster k_{obs} value is assigned to k_{off}, and the slower k_{obs} is assigned to k_r. We are confident in the values obtained from this approximation because when it is applied to calculate k_{off} and k_r for the Med25•VP16(438-490) interaction, the values are misestimated by ≤ 10% of the values calculated from the exact mechanism. This small discrepancy is expected to be even smaller for this system, as the primary determinant of the appropriate-ness of the approximation, the difference between k_f and k_{off}, is much larger.

2.6 REFERENCES

1   Vojnic, E. *et al.* Structure and VP16 binding of the Mediator Med25 activator interaction domain. *Nature structural & molecular biology* **18**, 404-409, doi:10.1038/nsmb.1997 (2011).

2   Milbradt, A. G. *et al.* Structure of the VP16 transactivator target in the Mediator. *Nature structural & molecular biology* **18**, 410-415, doi:10.1038/nsmb.1999 (2011).

3   Ptashne, M. Regulation of transcription: from lambda to eukaryotes. *Trends in biochemical sciences* **30**, 275-279, doi:10.1016/j.tibs.2005.04.003 (2005).

4   Ptashne, M. 1997 Albert Lasker Award for Basic Medical Research. Control of gene transcription: an outline. *Nature medicine* **3**, 1069-1072 (1997).

5   Ptashne, M. & Gann, A. Transcription initiation: imposing specificity by localization. *Essays Biochem* **37**, 1-15 (2001).

6   Zaman, Z., Ansari, A. Z., Gaudreau, L., Nevado, J. & Ptashne, M. Gene transcription by recruitment. *Cold Spring Harb Symp Quant Biol* **63**, 167-171 (1998).

7   Naar, A. L., B.; Tjian, R. Transcriptional Coactivator Complexes. *Annu Rev Biochem* **70**, 465-501 (2001).

8   Goodman, R. H. & Smolik, S. CBP/p300 in cell growth, transformation, and development. *Genes & development* **14**, 1553-1577 (2000).

9   Vo, N. & Goodman, R. H. CREB-binding protein and p300 in transcriptional regulation. *The Journal of biological chemistry* **276**, 13505-13508, doi:10.1074/jbc.R000025200 (2001).

10   The UniProt, C. UniProt: the universal protein knowledgebase. *Nucleic acids research* **45**, D158-D169, doi:10.1093/nar/gkw1099 (2017).

11   Poss, Z. C., Ebmeier, C. C. & Taatjes, D. J. The Mediator complex and transcription regulation. *Critical reviews in biochemistry and molecular biology* **48**, 575-608, doi:10.3109/10409238.2013.840259 (2013).

12   Allen, B. L. & Taatjes, D. J. The Mediator complex: a central integrator of transcription. *Nature reviews. Molecular cell biology* **16**, 155-166, doi:10.1038/nrm3951 (2015).

13   D'Alessio, J. A., Ng, R., Willenbring, H. & Tjian, R. Core promoter recognition complex changes accompany liver development. *Proceedings of the National Academy of Sciences of the United States of America* **108**, 3906-3911, doi:10.1073/pnas.1100640108 (2011).

14   Deato, M. D. *et al.* MyoD targets TAF3/TRF3 to activate myogenin transcription. *Molecular cell* **32**, 96-105, doi:10.1016/j.molcel.2008.09.009 (2008).

15   Asturias, F. J., Jiang, Y. W., Myers, L. C., Gustafsson, C. M. & Kornberg, R. D. Conserved structures of mediator and RNA polymerase II holoenzyme. *Science* **283**, 985-987 (1999).

16   Bernecky, C., Grob, P., Ebmeier, C. C., Nogales, E. & Taatjes, D. J. Molecular architecture of the human Mediator-RNA polymerase II-TFIIF assembly. *PLoS biology* **9**, e1000603, doi:10.1371/journal.pbio.1000603 (2011).

17   Davis, J. A., Takagi, Y., Kornberg, R. D. & Asturias, F. A. Structure of the yeast RNA polymerase II holoenzyme: Mediator conformation and polymerase interaction. *Molecular cell* **10**, 409-415 (2002).

18   Malik, S. & Roeder, R. G. Dynamic regulation of pol II transcription by the mammalian Mediator complex. *Trends in biochemical sciences* **30**, 256-263, doi:10.1016/j.tibs.2005.03.009 (2005).

19   Ren, Y. B., E.; Ren, Z.; Zhang, J.; Wang, Q.; Fondell, J. Specific Structural Motifs Determine TRAP220 Interactions with Nuclear Hormone Receptors. *Molecular and cellular biology* **20**, 5433–5446 (2000).

20   Malik, S. *et al.* Structural and functional organization of TRAP220, the TRAP/mediator subunit that is targeted by nuclear receptors. *Molecular and cellular biology* **24**, 8244-8254, doi:10.1128/MCB.24.18.8244-8254.2004 (2004).

21   Brzovic, P. S. *et al.* The acidic transcription activator Gcn4 binds the mediator subunit Gal11/Med15 using a simple protein interface forming a fuzzy complex. *Molecular cell* **44**, 942-953, doi:10.1016/j.molcel.2011.11.008 (2011).

22   Piskacek, M., Vasku, A., Hajek, R. & Knight, A. Shared structural features of the 9aaTAD family in complex with CBP. *Mol Biosyst* **11**, 844-851, doi:10.1039/c4mb00672k (2015).

23   Nozawa, K., Schneider, T. R. & Cramer, P. Core Mediator structure at 3.4 A extends model of transcription initiation complex. *Nature* **545**, 248-251, doi:10.1038/nature22328 (2017).

24   Robinson, P. J. *et al.* Structure of a Complete Mediator-RNA Polymerase II Pre-Initiation Complex. *Cell* **166**, 1411-1422 e1416, doi:10.1016/j.cell.2016.08.050 (2016).

25   Tsai, K. L. *et al.* Subunit architecture and functional modular rearrangements of the transcriptional mediator complex. *Cell* **157**, 1430-1444, doi:10.1016/j.cell.2014.05.015 (2014).

26   Plaschka, C. *et al.* Architecture of the RNA polymerase II-Mediator core initiation complex. *Nature* **518**, 376-380, doi:10.1038/nature14229 (2015).

27   Phillips, A. J. & Taatjes, D. J. Small molecule probes to target the human Mediator complex. *Isr J Chem* **53**, 588-595, doi:10.1002/ijch.201300039 (2013).

28   Nishikawa, J. L. *et al.* Inhibiting fungal multidrug resistance by disrupting an activator-Mediator interaction. *Nature* **530**, 485-489, doi:10.1038/nature16963 (2016).

29   Mallinger, A. *et al.* Discovery of Potent, Selective, and Orally Bioavailable Small-Molecule Modulators of the Mediator Complex-Associated Kinases CDK8 and CDK19. *J Med Chem* **59**, 1078-1101, doi:10.1021/acs.jmedchem.5b01685 (2016).

30   Yang, F., DeBeaumont, R., Zhou, S. & Naar, A. M. The activator-recruited cofactor/Mediator coactivator subunit ARC92 is a functionally important target of the VP16 transcriptional activator. *Proceedings of the National Academy of Sciences of the United States of America* **101**, 2339-2344 (2004).

31   Sela, D. *et al.* Role for human mediator subunit MED25 in recruitment of mediator to promoters by endoplasmic reticulum stress-responsive transcription factor ATF6alpha. *The Journal of biological chemistry* **288**, 26179-26187, doi:10.1074/jbc.M113.496968 (2013).

32   Aguilar, X. *et al.* Interaction studies of the human and Arabidopsis thaliana Med25-ACID proteins with the herpes simplex virus VP16- and plant-specific Dreb2a transcription factors. *PloS one* **9**, e98575, doi:10.1371/journal.pone.0098575 (2014).

33   Landrieu, I. *et al.* Characterization of ERM transactivation domain binding to the ACID/PTOV domain of the Mediator subunit MED25. *Nucleic acids research* **43**, 7110-7121, doi:10.1093/nar/gkv650 (2015).

34   Verger, A. *et al.* The Mediator complex subunit MED25 is targeted by the N-terminal transactivation domain of the PEA3 group members. *Nucleic acids research* **41**, 4847-4859, doi:10.1093/nar/gkt199 (2013).

35   Lee, H. K., Park, U. H., Kim, E. J. & Um, S. J. MED25 is distinct from TRAP220/MED1 in cooperating with CBP for retinoid receptor activation. *The EMBO journal* **26**, 3545-3557, doi:10.1038/sj.emboj.7601797 (2007).

36   Whittaker, C. H., R. Distribution and Evolution of von Willebrand/Integrin A Domains: Widely Dispersed DOmains with Roles in Cell Adhesion and Elsewhere. *Mol Biol Cell* **13**, 3369-3387, doi:10.1091/mbc.E02- (2002).

37   Youn, H. S., Park, U. H., Kim, E. J. & Um, S. J. PTOV1 antagonizes MED25 in RAR transcriptional activation. *Biochemical and biophysical research communications* **404**, 239-244, doi:10.1016/j.bbrc.2010.11.100 (2011).

38   Bieche, I. *et al.* Expression of PEA3/E1AF/ETV4, an Ets-related transcription factor, in breast tumors: positive links to MMP2, NRG1 and CGB expression. *Carcinogenesis* **25**, 405-411, doi:10.1093/carcin/bgh024 (2004).

39   Bojovic, B. B. & Hassell, J. A. The PEA3 Ets transcription factor comprises multiple domains that regulate transactivation and DNA binding. *The Journal of biological chemistry* **276**, 4509-4521, doi:10.1074/jbc.M005509200 (2001).

40   Hirai, H., Tani, T. & Kikyo, N. Structure and functions of powerful transactivators: VP16, MyoD and FoxA. *Int J Dev Biol* **54**, 1589-1596, doi:10.1387/ijdb.103194hh (2010).

41   Bontems, F. *et al.* NMR structure of the human Mediator MED25 ACID domain. *Journal of structural biology* **174**, 245-251, doi:10.1016/j.jsb.2010.10.011 (2011).

42   Eletsky, A. *et al.* Solution NMR structure of MED25(391-543) comprising the activator-interacting domain (ACID) of human mediator subunit 25. *Journal of structural and functional genomics* **12**, 159-166, doi:10.1007/s10969-011-9115-1 (2011).

43   Chasman, D. I., Leatherwood, J., Carey, M., Ptashne, M. & Kornberg, R. D. Activation of yeast polymerase II transcription by herpesvirus VP16 and GAL4 derivatives in vitro. *Molecular and cellular biology* **9**, 4746-4749 (1989).

44   Li, L. *et al.* Herpes Simplex Virus 1 Infection of Tree Shrews Differs from That of Mice in the Severity of Acute Infection and Viral Transcription in the Peripheral Nervous System. *J Virol* **90**, 790-804, doi:10.1128/JVI.02258-15 (2015).

45   Roizman, B. & Zhou, G. The 3 facets of regulation of herpes simplex virus gene expression: A critical inquiry. *Virology* **479-480**, 562-567, doi:10.1016/j.virol.2015.02.036 (2015).

46   Brutscher, B. *et al.* NMR Methods for the Study of Instrinsically Disordered Proteins Structure, Dynamics, and Interactions: General Overview and Practical Guidelines. *Advances in experimental medicine and biology* **870**, 49-122, doi:10.1007/978-3-319-20164-1_3 (2015).

47   De Guzman, R. N., Wojciak, J. M., Martinez-Yamout, M. A., Dyson, H. J. & Wright, P. E. CBP/p300 TAZ1 domain forms a structured scaffold for ligand binding. *Biochemistry* **44**, 490-497, doi:10.1021/bi048161t (2005).

48   Lee, C. W., Arai, M., Martinez-Yamout, M. A., Dyson, H. J. & Wright, P. E. Mapping the interactions of the p53 transactivation domain with the KIX domain of CBP. *Biochemistry* **48**, 2115-2124, doi:10.1021/bi802055v (2009).

49   Thakur, J. K., Yadav, A. & Yadav, G. Molecular recognition by the KIX domain and its role in gene regulation. *Nucleic acids research* **42**, 2112-2125, doi:10.1093/nar/gkt1147 (2014).

50   Feng, H. *et al.* Structural basis for p300 Taz2-p53 TAD1 binding and modulation by phosphorylation. *Structure* **17**, 202-210, doi:10.1016/j.str.2008.12.009 (2009).

51   Wang, N., Lodge, J. M., Fierke, C. A. & Mapp, A. K. Dissecting allosteric effects of activator-coactivator complexes using a covalent small molecule ligand. *Proceedings of the National Academy of Sciences of the United States of America* **111**, 12061-12066, doi:10.1073/pnas.1406033111 (2014).

52   Law, S. M., Gagnon, J. K., Mapp, A. K. & Brooks, C. L., III. Prepaying the entropic cost for allosteric regulation in KIX. *Proceedings of the National Academy of Sciences of the United States of America*, doi:10.1073/pnas.1405831111 (2014).

53   Scholes, N. S. & Weinzierl, R. O. Molecular Dynamics of "Fuzzy" Transcriptional Activator-Coactivator Interactions. *PLoS Comput Biol* **12**, e1004935, doi:10.1371/journal.pcbi.1004935 (2016).

54   Warfield, L., Tuttle, L. M., Pacheco, D., Klevit, R. E. & Hahn, S. A sequence-specific transcription activator motif and powerful synthetic variants that bind Mediator using a fuzzy protein interface. *Proceedings of the National Academy of Sciences of the United States of America* **111**, E3506-3513, doi:10.1073/pnas.1412088111 (2014).

55   Sadowsky, J. D. *et al.* Turning a protein kinase on or off from a single allosteric site via disulfide trapping. *Proceedings of the National Academy of Sciences of the United States of America* **108**, 6056-6061, doi:10.1073/pnas.1102376108 (2011).

56   Arkin, M. R. *et al.* Binding of small molecules to an adaptive protein-protein interface. *Proceedings of the National Academy of Sciences of the United States of America* **100**, 1603-1608, doi:10.1073/pnas.252756299 (2003).

57   Erlanson, D. A. *et al.* Site-directed ligand discovery. *Proceedings of the National Academy of Sciences of the United States of America* **97**, 9367-9372 (2000).

58   Erlanson, D. A., Wells, J. A. & Braisted, A. C. Tethering: fragment-based drug discovery. *Annu Rev Biophys Biomol Struct* **33**, 199-223, doi:10.1146/annurev.biophys.33.110502.140409 (2004).

59   Wysocka, J. & Herr, W. The herpes simplex virus VP16-induced complex: the makings of a regulatory switch. *Trends in biochemical sciences* **28**, 294-304, doi:10.1016/S0968-0004(03)00088-4 (2003).

60   Uesugi, M., Nyanguile, O., Lu, H., Levine, A. J. & Verdine, G. L. Induced alpha helix in the VP16 activation domain upon binding to a human TAF. *Science* **277**, 1310-1313, doi:Doi 10.1126/Science.277.5330.1310 (1997).

61   Pearson, W. R., Wood, T., Zhang, Z. & Miller, W. Comparison of DNA sequences with protein sequences. *Genomics* **46**, 24-36, doi:10.1006/geno.1997.4995 (1997).

62   Ferreon, J. C. *et al.* Cooperative regulation of p53 by modulation of ternary complex formation with CBP/p300 and HDM2. *Proceedings of the National Academy of Sciences of the United States of America* **106**, 6591-6596, doi:10.1073/pnas.0811023106 (2009).

63   Krois, A. S., Ferreon, J. C., Martinez-Yamout, M. A., Dyson, H. J. & Wright, P. E. Recognition of the disordered p53 transactivation domain by the transcriptional adapter zinc finger domains of CREB-binding protein. *Proceedings of the National Academy of Sciences of the United States of America* **113**, E1853-1862, doi:10.1073/pnas.1602487113 (2016).

64   Schreiber, G. & Fersht, A. R. Rapid, electrostatically assisted association of proteins. *Nat Struct Biol* **3**, 427-431 (1996).

65   Schreiber, G., Haran, G. & Zhou, H. X. Fundamental aspects of protein-protein association kinetics. *Chemical reviews* **109**, 839-860, doi:10.1021/cr800373w (2009).

66   Fuller, A. A., Seidl, F. J., Bruno, P. A., Plescia, M. A. & Palla, K. S. Use of the environmentally sensitive fluorophore 4-N,N-dimethylamino-1,8-naphthalimide to study peptoid helix structures. *Biopolymers* **96**, 627-638 (2011).

67   Loving, G. & Imperiali, B. Thiol-reactive derivatives of the solvatochromic 4-N,N-dimethylamino-1,8-naphthalimide fluorophore: a highly sensitive toolset for the detection of biomolecular interactions. *Bioconjug Chem* **20**, 2133-2141, doi:10.1021/bc900319z (2009).

68   Loving, G. & Imperiali, B. A versatile amino acid analogue of the solvatochromic fluorophore 4-N,N-dimethylamino-1,8-naphthalimide: a powerful tool for the study of dynamic protein interactions. *Journal of the American Chemical Society* **130**, 13630-13638, doi:10.1021/ja804754y (2008).

69   Shammas, S. L., Travis, A. J. & Clarke, J. Remarkably fast coupled folding and binding of the intrinsically disordered transactivation domain of cMyb to CBP KIX. *J Phys Chem B* **117**, 13346-13356, doi:10.1021/jp404267e (2013).

70   Johnson, K. A. Rapid kinetic analysis of mechanochemical adenosinetriphosphatases. *Methods in enzymology* **134**, 677-705 (1986).

71   Shammas, S. L., Travis, A. J. & Clarke, J. Allostery within a transcription coactivator is predominantly mediated through dissociation rate constants. *Proceedings of the National Academy of Sciences of the United States of America* **111**, 12055-12060, doi:10.1073/pnas.1405815111 (2014).

72   Teufel, D. P., Freund, S. M., Bycroft, M. & Fersht, A. R. Four domains of p300 each bind tightly to a sequence spanning both transactivation subdomains of p53. *Proceedings of the National Academy of Sciences of the United States of America* **104**, 7009-7014, doi:10.1073/pnas.0702010104 (2007).

73   Pomerantz, W. C. *et al.* Profiling the dynamic interfaces of fluorinated transcription complexes for ligand discovery and characterization. *ACS chemical biology* **7**, 1345-1350, doi:10.1021/cb3002733 (2012).

74   Delaglio, F. *et al.* NMRPipe: a multidimensional spectral processing system based on UNIX pipes. *Journal of biomolecular NMR* **6**, 277-293 (1995).

Chapter 3

SITE-SELECTIVE SMALL MOLECULE MODULATORS OF ACID-ACTIVATOR INTERACTIONS[1]

3.1 ABSTRACT

The AcID activator binding domain in Med25 interacts with multiple transcriptional activators that regulate transcriptional programs involved in both healthy and diseased-related cellular processes. As a result, small molecule modulators of these activator-AcID protein-protein interactions would be useful both as probe molecules to dissect Med25-dependent transcriptional pathways and as potential therapeutic agents. Here we show that two native cysteines within the AcID domain can be targeted by small molecules and in doing so modulate activator-AcID binding events. We screened these two native cysteines using the site-directed Tethering strategy to identify small molecules that covalently target AcID and inhibit ERM binding. A molecule, A6, identified from this screen engages a conformational change network in AcID and induces perturbations at both binding sites of AcID. This molecule induces allosteric changes in AcID and stabilizes binding at the opposite AcID binding surface. This molecule can be converted into a cell active irreversible alkylator capable of inhibiting ATF6α-mediated gene expression in HeLa cells.

---

[1] The research described in chapter 3 is a collaborative effort. A.R. Henderson synthesized and purified ERM peptides, expressed Med25 for the Tethering screen, performed protein alkylation experiments, and performed direct binding experiments. Dr. Zachary Hill performed the Tethering screen in the lab of Prof. James Wells at UCSF. HSQC NMR was performed in collaboration with Prof. Tomasz Cierpicki and Brian Linhares. Matthew Henley performed kinetics experiment. Matthew Beyersdorf performed PrOF NMR. Manuscript in progress. Dr. Clint Regan synthesized small molecule analogs. Contributions are indicated in figure captions.

3.2 BACKGROUND

DISEASE-ASSOCIATED MED25-ACTIVATOR INTERACTIONS

Med25 is a key binding partner of several different transcriptional activators, and, as detailed in Chapters 1 and 2, the Activator Interaction Domain (AcID) is the motif responsible for forming direct interactions. One such set of activators is the ETV/PEA3 subfamily of Ets transcription factors, comprised of ETV1, ETV4 and ERM. ERM, and likely the other ETS PEA3 subfamily members ETV1 and ETV4, form direct contacts with AcID and regulate cellular differentiation and cell cycle progression. The ETV/PEA3 (polyomavirus enhancer activator 3) subfamily is expressed ubiquitously in adult tissue, but is thought to play a specific role in morphological branching of developing embryonic tissues.[1-3] Endoplasmic reticulum (ER) stress response genes are governed by the transcriptional activator ATF6α. In unstressed cells ATF6α exists as a latent transmembrane ER protein transitioning to an active DNA-binding transcription factor following the induction of cellular stress resulting in proteolytic cleavage and nuclear translocation.[4-7] And, as discussed in Chapter 2, the viral transcriptional activator VP16 uses complexation with Med25 to turn on genes associated with viral replication. While these transcription factors and the contacts they make through Med25 are essential for basic cellular function and development they are also implicated in the transition to certain disease phenotypes.

Med25 in cancer metastasis and progression

The ETV/PEA3 subfamily of ETS activators play a significant role in maintaining context-dependent cellular phenotypes.[8] ETV/PEA3 members (ERM (ETV5), ETV1, and ETV4) are overexpressed in HER2/Neu-associated breast cancers.[9-11] Additionally, ETV/PEA3 members

mediate the conversion of breast cancer cells to a metastatic phenotype through the regulation of matrix metalloproteinase (MMP) expression.[12-14] This metastatic breast cancer phenotype can be diminished through knockdown of *pea3* expression with shRNA. This observation is strong evidence that inhibiting ETV/PEA3 activity by targeting ETV/PEA3-coactivator complexes, such as the ERM-Med25 interaction, with small molecules is a way to treat ETV-mediated diseases.

The observation that downregulation of ETV/PEA3 family members, including ERM, results in a reversion to a healthy phenotype or an abrogation of metastatic character across both breast and prostate cancer cells is evidence of the role played by these transcription factors in promoting disease progression. The existence of Med25 as a key binding partner of ERM and regulator of its transcription makes this protein-protein interaction a compelling potential point of therapeutic intervention. Several cellular experiments involving activator-AcID interactions also point to the potential utility in disturbing these complexes. A mutation on the H1 face of AcID, Q451E, has been shown to disrupt pull-down by ERM and VP16 from cellular lysate.[15,16] The ability of a single mutation in AcID to disrupt activator interactions in the cellular environment is promising evidence that this interface can be perturbed by well-designed chemical probes.

The role of ETV/PEA3 activators in metastatic cancers and the demonstration that genetically inhibiting the AcID-ETV interaction blocks the expression of oncogenes such as MMP underscore the value of this protein-protein interface as a therapeutic target.

SMALL MOLECULE MODULATORS

While we ultimately hope to identify bioactive molecules capable of modulating Med25-activator complexes that drive aberrant transcription in different disease states, the development of selective and effective chemical probes that aid the mechanistic dissection of

Med25-activator complexes *in vitro* and *in vivo* will be necessary first steps. Site-selective

covalent molecules are particularly attractive as mechanistic probes and as potential

therapeutics because they offer the ability to identify molecules that bind specific areas on a

target protein thereby making it easier to link experimental observations to specific small

molecule-protein interactions.[17,18]

Disulfide Tethering is a site-selective small molecule screening strategy
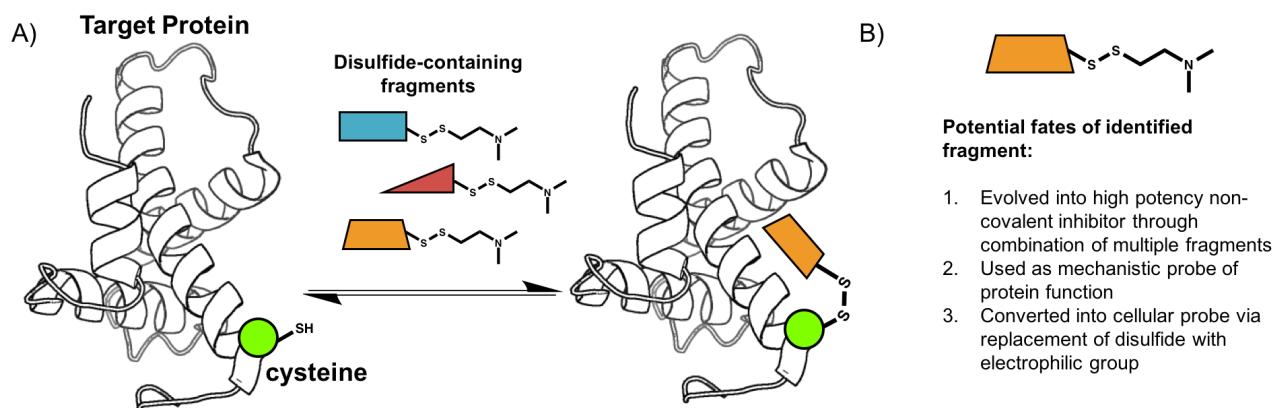
Figure 3.1 Tethering is a site-selective small molecule screening strategy A. Disulfide tethering enables discovery of site-selective small molecules through covalent stabilization of low molecular weight fragments via reversible disulfide bond formation between molecule and protein. B. Application of identified fragments.
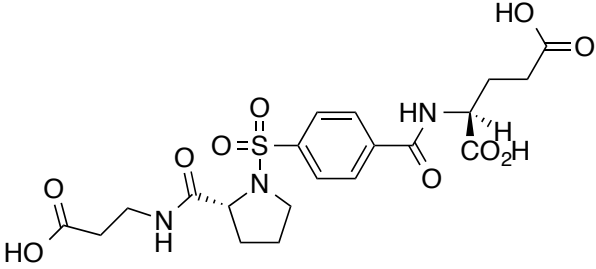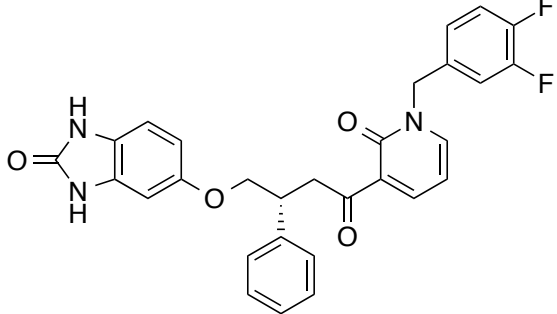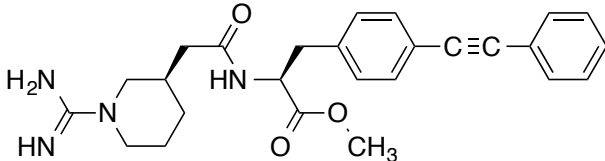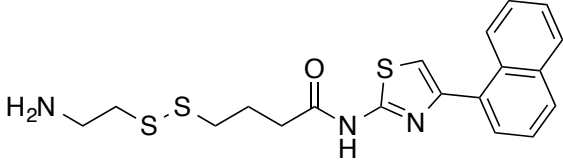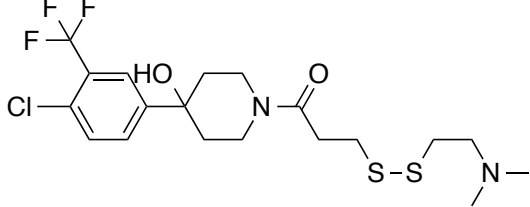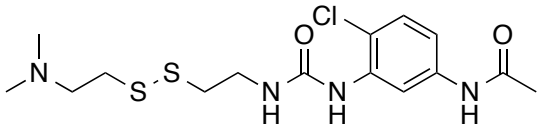
A site-selective small molecule screening strategy of particularly wide application and

utility is disulfide Tethering. Develop by Jim Wells and coworkers at Sunesis Pharamceuticals in

2000, Tethering has been used to identify molecules targeting a wide array of protein targets

including enzyme active sites, allosteric sites on enzymes, and protein-protein interactions.[19-22]

Tethering involves screening a library of disulfide-containing fragments against a protein target

bearing a cysteine in proximity to the desired molecule binding site under reversible conditions

(Fig 3.1). This allows the identification of molecular fragments possessing even modest affinity

for their binding site due to the presence of the disulfide bond between the fragment and protein that stabilizes them sufficiently to enable detection via MS or another readout.[23] Historically, Tethering was designed to enable rapid sampling of multiple regions of a protein target of interest resulting in several fragments that could then be combined to produce a non-covalent molecule of high affinity and specificity.[24] Recently, our lab and others have found great utility in the use of molecules as covalent mechanistic tools to dissect protein function.[25-27]

An excellent example of targeting an activator-coactivator complex was the use of Tethering to screen the MLL binding surface of KIX, leading to the molecule 1-10 (Table 3.1).[25] This molecule acts as an inhibitor of MLL binding, a molecular co-chaperone capable of stabilizing the KIX domain, and stabilized the fold sufficiently for the first crystal structure of the KIX coactivation domain to be obtained. Additionally, it has been a useful probe in studying the allosteric network linking the pKID and MLL binding sites on KIX.[26] 1-10 engages the KIX allosteric network in a similar fashion to MLL and enhances binding of pKID through a 25% reduction in dissociation constant.

We hypothesized that a Tethering screen would be useful for identifying small molecule modulators of AcID-activator complexes based upon the mechanistic similarities between the AcID and KIX domains shown in the previous chapter. These have the potential to be extraordinarily useful mechanistic probes and eventually, possibly novel therapeutics. Beyond just inhibitors of activator binding to AcID, these site-selective tools can facilitate the mechanistic dissection of activator-Med25 binary and ternary complex formation. Because AcID can interact with many diverse activators using an overlapping set of amino acids on a shared binding surface,

Table 3.1 Molecules identified by Tethering and their targets

Molecule	Protein Target	Class	Notes	Citation
	Thymidilate Synthase	Enzyme Inhibitor		Erlanson et al. *PNAS*, **2000**, 97, 9367-9372.[19]
	PDK1 kinase	Allosteric inhibitor		Erlanson et al. *PNAS*, **2011**, 21, 3078-3083.[28]
	IL-2α-IL-2 interface	PPI inhibitor		Arkin et al. *PNAS*, **2003**, 100, 1603-1608.[20]
	Caspase-5	Allosteric inhibitor		Gao et al. *Chem. Biol. Drug. Des.*, **2012**, 79, 209-215.[29]
1-10	KIX-MLL	PPI inhibitor		Wang et al. *J. Am. Chem. Soc.*, **2013**, 135, 3363-3366.[25]
	KIX-pKID	PPI inhibitor		Lodge et al. *Medchemcomm.*, **2014**, 5, 370-375.[23]

one potentially exciting application of Tethering would be to identify stabilizers of specific AcID conformations more suitable to binding one set of activators over another. These chemical co-chaperones could hypothetically be used to promote productive activator-AcID interactions in cells while inhibiting or preventing AcID interactions with disease-associated activators. This approach offers the chance to be less disruptive to transcriptional regulation at large, with only the desired activator-AcID complexes being inhibited. This can only be achieved through enhanced mechanistic understanding of activator-Med25 complexes that will be facilitated through the development of high quality chemical probes.

Cell active small molecules

While Tethering is an efficient and effective method of identifying high quality site-selective modulators of activator-coactivator interactions, the disulfide moiety is not suitable for use in the reducing cellular environment. To translate molecules identified via Tethering into cell active probes, one may exchange the disulfide for any number of irreversible cysteine-reactive electrophilic groups. Judicious selection of an appropriate electrophile will enable the mechanistic dissection of activator-Med25 complexes in cells. A key advantage of Med25 is the presence of solvent-exposed native cysteines in the AcID domain that can be both targeted in a Tethering screen and used as cellular targets for covalent probes. This contrasts with our previous Tethering work with KIX which lacks native cysteines making the site-specific study of KIX in cells more onerous. The presence of native cysteines in Med25 expedites the process of moving identified in vitro modulators of a given activator-Med25 complex into cell-active chemical probes.

3.3 RESULTS

Covalent, site-specific probes of Med25 AcID would be essential tools to add to our understanding of activator-Med25 complexes. Because of the fortuitous presence of three native cysteines in Med25 AcID, one, or all, of these cysteines would be useful handles for the discovery of covalent probes. Recently, the Cravatt and Weerapana labs have developed proteome wide methods for identifying and assesing the nucleophilicity and reactivity of functionally relevant cysteines through alkylation with iodoacetamide probes.[30,31] Before initiating a screening campaign for molecules targeting these cysteines it is necessary to determine both the accessibility of each AcID cysteine and to ensure that they are located in functionally relevant positions within the domain.

ASSESSING REACTIVITY OF NATIVE MED25 ACID CYSTEINES

Med25 AcID contains two solvent exposed cysteines

Med25 AcID contains three native cysteines, two of which are located within the H1 binding surface of AcID (Figure 3.2). Based on published NMR structures, the thiol side chains of C497 and C506 project outwards towards solvent. Cysteine 429 projects inwards towards the center of the beta-barrel making it less likely to be accessible to a covalent small molecule. A suitable cysteine would be both reactive with small molecules and positioned such that when labeled with a small molecule, functional changes to AcID structure or binding activity are modulated.
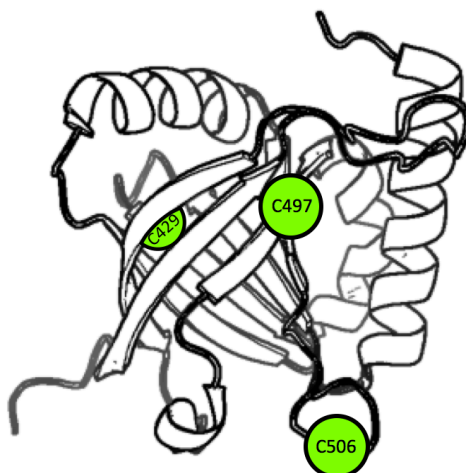
Figure 3.2 Native cysteines in Med25 AcID The AcID domain contains three native cysteines. C497 and C506 are within the H1 face of AcID. C429 project inwards towards the center of the β-barrel.

To assess the degree to which each AcID cysteine was predisposed to alkylation via small molecules, Med25 AcID was incubated with several iodoacetamide bearing compounds. Following incubation, the degree of alkylation was measured via mass spectrometry (Figure 3.3). After incubation with iodoacetamide, all Med25 AcID was consumed resulting in predominantly monoalkylated Med25 AcID. The presence of some bisalkylated product indicated that at least two cysteines were reactive with this molecule. The increased hydrophobic surface area of IAdimethylbenzene resulted in a larger percentage of bisalkylated AcID. 4-iodoacetamidosalicylic acid (IAsalicylic acid) very potently bisalkylated AcID. The ability to alkylate two cysteines within AcID provides evidence that this domain can be covalently targeted by small molecules provided they are of suitable chemical composition. The alkylating efficiencies of the dimethylbenzene and salicylic acid moieties suggest that labeling is greatly improved by molecules with significant hydrophobic surface areas and a carboxylic acid or related functional group.
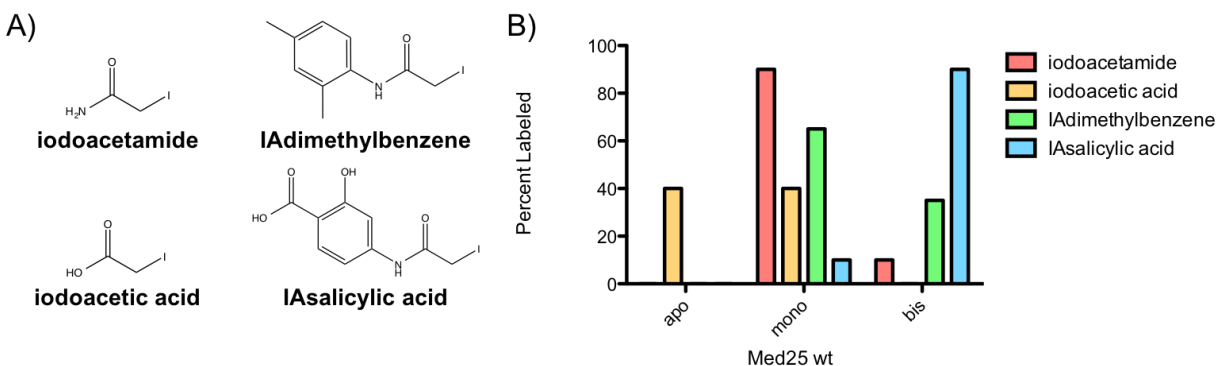
Figure 3.3 Solvent accessibility of native Med25 cysteines A. Iodoacetamide-bearing compounds used to test AcID alkylation. B. Labeling efficiency of each iodoacetamide compound as measured by mass spectrometry.

To determine which of the three native cysteines were small molecule-reactive, cysteine to alanine mutations were prepared via SDM for C497 and C506. Following incubation with 4-iodoacetamidosalicylic acid, Med25 C497A and C506A were monoalkylated as opposed to the bisalkylation observed with wt Med25. Thus, C497 and C506 are both small-molecule reactive, while C429 appears unreactive. Both C497 and C506 are within the H1 binding face of AcID and thus favorably situated to be inhibitors of Activator-AcID complexes.

Covalent targeting of native Med25 AcID cysteines inhibits activator binding

While AcID C497 and C506 are small molecule-reactive, we next assessed whether covalent modification of either cysteine with a small molecule could inhibit activator binding to Med25. When AcID labeled at C497 and C506 with IAdimethylbenzene was used in FP binding experiments no inhibition of activator binding was observed (Fig 3.4.C). However, when Med25 AcID was labeled at C497 and C506 with 4-iodoacetamidosalicylic acid, inhibition of activators ranged from 2.7 to nearly 10-fold. (Fig 3.4.B). 4-Iodoacetamidosalicylic acid is a low molecular weight fragment (193 Da) and its ability inhibit activator binding when alkylated to Med25 AcID show that C497 and C506 are suitable targets for covalent small-molecule modulators of Med25

AcID. Mere alkylation with IAdimethylbenzene alone does not induce inhibition suggesting that effective modulators of AcID-activator binding must target key mechanistic drivers of activator binding.
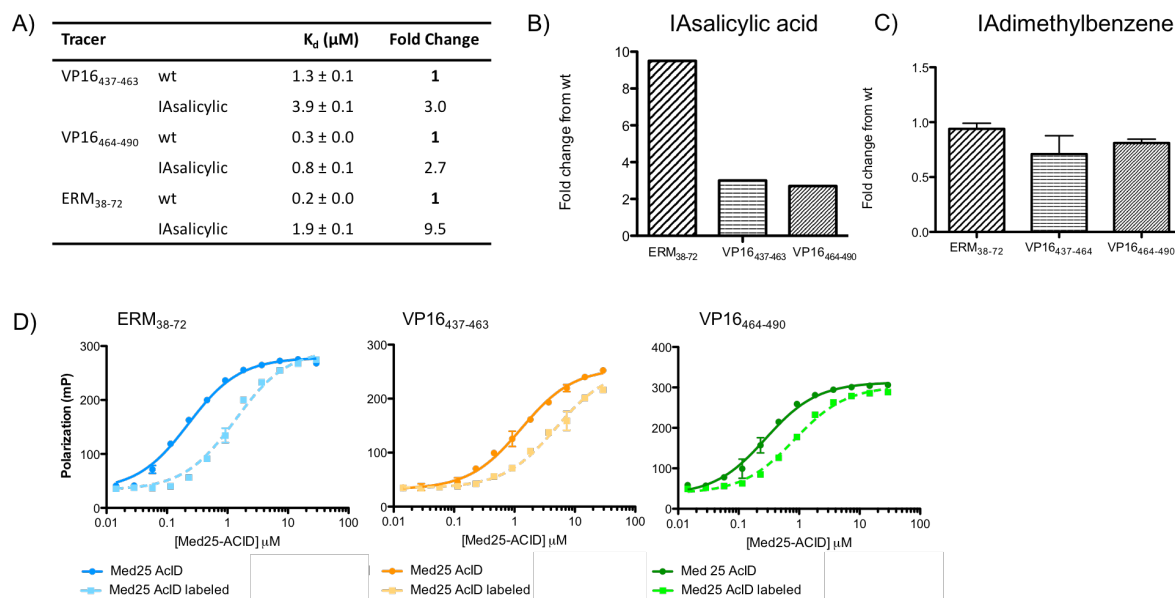
Figure 3.4 4-Iodoacetamidosalicylic acid inhibits activator binding A. Changes in dissociation constant for fluorescent activator peptides. B. Fold-change in binding between wild type Med25 AcID and AcID bisalkylated with 4-iodoacetamidosalicylic acid. C. Fold-change in binding between wild type Med25 AcID and AcID bisalkylated with 4-iodoacetamidosalicylic acid. D. FP binding curves of activator peptides to wt Med25 AcID and AcID bisalklyated with 4-iodoacetamidosalicylic acid. All data points are represented as the mean and standard deviation of conditions performed in triplicate.

Because 4-iodoacetamidosalicylic acid reacts with both AcID C497 and C506, we sought to define the contribution of each individual alkylation in inhibiting activator binding. Samples of Med25 C497A and C506A were monoalkylated with 4-iodoacetamidosalicylic acid and binding of activators was assessed by FP (Fig 3.5). Alkylation of C497 with 4-iodoacetamidosalicylic acid produced the most pronounced inhibition. While this would point to C497 being the preferred cysteine to target with covalent molecules, it is important to note that this conclusion stems from

examining one molecule. A different molecular scaffold targeting C506 may produce significant inhibition or otherwise perturb AcID-activator complex formation. In addition to finding inhibitors of activator-AcID complexes, compounds capable of stabilizing or inducing discrete conformations of AcID would be highly useful molecular probes with potentially significant biological effects.

A)

Med25 C497A
- ERM$_{38-72}$
- ERM$_{38-72}$ labeled
- VP16$_{437-463}$
- VP16$_{437-463}$ labeled
- VP16$_{464-490}$
- VP16$_{464-490}$ labeled

Med25 C506A
- ERM$_{38-72}$
- ERM$_{38-72}$ labeled
- VP16$_{437-463}$
- VP16$_{437-463}$ labeled
- VP16$_{464-490}$
- VP16$_{464-490}$ labeled

B)

	Tracer		K_d (µM)	Fold Change
Med25 C497A	VP16$_{437-463}$	apo	1.66 ± 0.08	**1.3**
		IAsalicylic	2.20 ± 0.08	
	VP16$_{464-490}$	apo	0.17 ± 0.01	**1.8**
		IAsalicylic	0.30 ± 0.02	
	ERM$_{38-72}$	apo	0.25 ± 0.02	**1.4**
		IAsalicylic	0.35 ± 0.02	
Med25 C506A	VP16$_{437-463}$	apo	1.95 ± 0.07	**3.2**
		IAsalicylic	6.18 ± 0.29	
	VP16$_{464-490}$	apo	0.35 ± 0.14	**2.65**
		IAsalicylic	0.93 ± 0.03	
	ERM$_{38-72}$	apo	0.49 ± 0.02	**4.0**
		IAsalicylic	1.95 ± 0.08	

Figure 3.5 Contribution of C497 and C506 alkylation to activator binding inhibition A. FP binding curves of activator peptides to C497A and C506A mutant Med25 AcID with 4-iodoacetamidosalicylic acid. B. Fold-change in binding between mutant Med25 AcID and mutant AcID monoalkylated with 4-iodoacetamidosalicylic acid. All data points are represented as the mean and standard deviation of conditions performed in triplicate.

A TETHERING SCREEN IDENTIFIES MODULATORS OF ACID FUNCTION

The successful alkylation of C497 and C506 demonstrated that these residues are reactive and positioned in functionally relevant locations. To identify covalent molecules capable of targeting these cysteines we performed a Tethering screen in collaboration with the laboratory of Prof. Jim Wells and UCSF.

FP Tethering screen of a Med25 AcID-activator complex

Traditional Tethering screening utilizes mass spectrometry to detect interacting fragments. While this gives important information about fragment binding, it does not give information about the inhibitory activity of each fragment. Fluorescence polarization (FP) Tethering screens first measure the ability of each fragment to inhibit binding of a fluorescently-labeled peptide followed by assessment of the degree to which active fragments labeled the target protein.
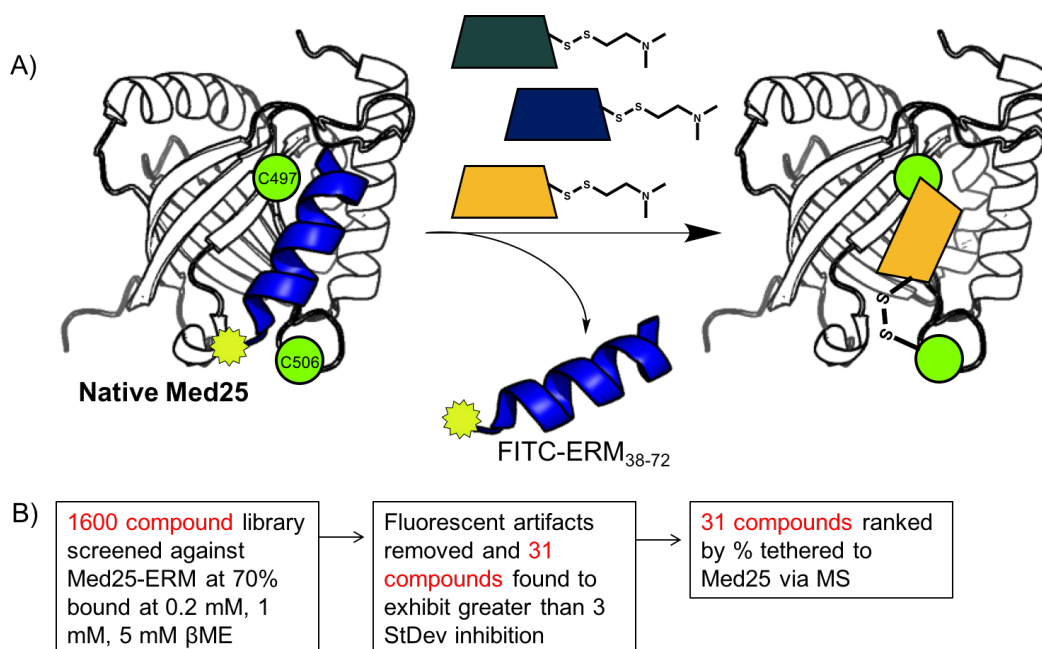
Figure 3.6 FP Tethering screen of a Med25-ERM complex A. ERM in complex with Med25 AcID was screened against 1600 disulfide-bearing fragments at three different concentrations of β-ME and percent inhibition was determined. The most potent inhibitors (>3 standard deviations) were assessed by MS to determine the degree to which they were covalent. B. Schematic illustrating screen order. Performed with Dr. Zachary Hill, UCSF.

Because ERM was inhibited by 4-iodoacetamidosalicylic acid to the largest degree (Fig 3.4) and because of the role PEA3 family members play in metastasis, it was used as the fluorescent tracer in the screen. The screen was conducted such that ERM was 70% bound to

AcID making it easy to assess inhibition of ERM and also provided a sufficiently large dynamic range to potentially identify fragments that enhanced ERM binding to AcID. Screening at three different β-ME concentrations acted as a stringency filter by outcompeting fragments only weakly captured by Med25 (Fig 3.6).

After screening the 1600 compound Wells library, the 31 most effective inhibitors (% inhibition > 3 standard deviations above the mean) were carried forward to determine their extent of covalent labeling. Both the FP screen and the MS analysis were performed at three β-ME concentrations. Because disulfide bond formation is reversible, increasing β-ME concentration serves as a stringency filter. At the highest β-ME concentrations only the fragments with true affinity for the protein binding site will retain activity. Figures 3.7 and 3.8 rank the top 31 hits first by inhibition percentage followed by labeling percentage in the presence of 0.2 mM β-ME.

Perhaps unexpectedly, the most effective inhibitors were not the most effective labelers of AcID and vice-versa. Some of the top inhibitors (> 40 %) displayed low protein labeling while some of the most effective labelers of AcID were comparatively weak inhibitors (Figure 3.8). Although fluorescent artifacts were removed, some of the best inhibitors (A2 and A3) barely labeled Med25 and it is possible that these either function as aggregators of Med25 or otherwise interfere with the FP assay.

| Fragment	Inhibition 0.2mM BME	Inhibition 1mM BME	Inhibition 5mM BME	% Single Labeled 0.2mM BME	% Single Labeled 1mM BME	% Single Labeled 5mM BME	% Double Labeled 0.2mM BME	% Double Labeled 1mM BME	% Double Labeled 5mM BME
A2	50.3	8.03	8.82	0	6	6	1	0	0
A3	43.9	24.6	9.89	5	5	7	1	0	0
A4	34.3	19	4.51	0	0	5	16	13	7
A5	32.6	24.8	46.8	33	9	17	8	0	4
A6	24.5	16.8	33.3	33	24	5	5	0	11
A7	24.3	27.1	32.9	22	21	3	9	17	9
A8	24	23.9	25	35	35	17	2	2	1
A9	20.4	18.3	23.1	44	32	18	15	22	16
A10	18.8	15.7	22.3	49	57	15	7	4	1
A11	18.6	16.9	17.1	11	18	5	5	0	1
B2	16.6	15.6	13.8	0	0	1	0	0	0
B3	16	10.2	17.7	24	13	9	0	0	1
B4	14.5	16.3	17.9	41	52	16	0	0	6
B5	12.8	12.2	19	16	14	10	0	12	10
B6	11.5	12.9	13.8	48	35	24	0	6	2
B7	11.1	12.3	10.3	26	33	17	0	7	5
B8	10.9	16.1	16.6	40	37	30	23	16	14
B9	10.5	30.9	3.84	54	46	19	0	0	1
B11	10.2	2.66	19.1	22	13	9	0	1	3
B10	10.2	12.7	15.9	6	7	8	8	7	8
C2	9.29	8.17	17.2	0	0	16	0	0	3
C3	9.17	10.2	17.6	0	6	0	0	6	14
C4	8.64	12.9	11.3	0	17	11	0	0	0
C5	7.45	4.68	14.6	19	5	14	45	31	6
C6	4.72	5.35	15.9	50	29	19	0	1	0
C7	4.4	8.8	14.4	8	11	7	0	0	12
C9	4.04	7.49	14.3	42	45	26	0	0	5
C8	4.04	9.37	15.3	31	25	7	9	6	4
C10	3.36	4.68	17.2	11	8	3	8	5	0
C11	-0.0426	12.1	15.3	61	46	29	0	0	3
D2	-3.67	13.6	1.7	9	9	13	0	7	8

Figure 3.7 FP Tethering Results ranked by inhibition percentage Top compounds from screen ranked by percent inhibition at 0.2 mM β-ME. Highest inhibition is indicated in green progressively turning to red (lowest inhibition). Highest % labeled is indicated in green progressively turning to red (lowest % labeling).

Fragment	Inhibition 0.2mM BME	Inhibition 1mM BME	Inhibition 5mM BME	% Single Labeled 0.2mM BME	% Single Labeled 1mM BME	% Single Labeled 5mM BME	% Double Labeled 0.2mM BME	% Double Labeled 1mM BME	% Double Labeled 5mM BME
C11	-0.0426	12.1	15.3	61	46	29	0	0	3
B9	10.5	30.9	3.84	54	46	19	0	0	1
C6	4.72	5.35	15.9	50	29	19	0	1	0
A10	18.8	15.7	22.3	49	57	15	7	4	1
B6	11.5	12.9	13.8	48	35	24	0	6	2
A9	20.4	18.3	23.1	44	32	18	15	22	16
C9	4.04	7.49	14.3	42	45	26	0	0	5
B4	14.5	16.3	17.9	41	52	16	0	0	6
B8	10.9	16.1	16.6	40	37	30	23	16	14
A8	24	23.9	25	35	35	17	2	2	1
A5	32.6	24.8	46.8	33	9	17	8	0	4
A6	24.5	16.8	33.3	33	24	5	5	0	11
C8	4.04	9.37	15.3	31	25	7	9	6	4
B7	11.1	12.3	10.3	26	33	17	0	7	5
B3	16	10.2	17.7	24	13	9	0	0	1
B11	10.2	2.66	19.1	22	13	9	0	1	3
A7	24.3	27.1	32.9	22	21	3	9	17	9
C5	7.45	4.68	14.6	19	5	14	45	31	6
B5	12.8	12.2	19	16	14	10	0	12	10
C10	3.36	4.68	17.2	11	8	3	8	5	0
A11	18.6	16.9	17.1	11	18	5	5	0	1
D2	-3.67	13.6	1.7	9	9	13	0	7	8
C7	4.4	8.8	14.4	8	11	7	0	0	12
B10	10.2	12.7	15.9	6	7	8	8	7	8
A3	43.9	24.6	9.89	5	5	7	1	0	0
A2	50.3	8.03	8.82	0	6	6	1	0	0
A4	34.3	19	4.51	0	0	5	16	13	7
B2	16.6	15.6	13.8	0	0	1	0	0	0
C2	9.29	8.17	17.2	0	0	16	0	0	3
C3	9.17	10.2	17.6	0	6	0	0	6	14
C4	8.64	12.9	11.3	0	17	11	0	0	0

Figure 3.8 FP Tethering Results ranked by labeling efficiency Top compounds from screen ranked by highest single labeling percentage at 0.2 mM β-ME. Highest inhibition is indicated in green progressively turning to red (lowest inhibition). Highest % labeled is indicated in green progressively turning to red (lowest % labeling).

The presence of effective labelers of AcID that nonetheless did not inhibit ERM binding (B9 and C6) was also notable because they may modulate AcID structure and function beyond inhibiting direct binding. These results highlight a relative weakness of the FP Tethering format. Because all molecules are first assessed and filtered by a change in fluorescence polarization and thus the labeling-efficiency of the entire library is not assessed, there is not direct information about interactions of each fragment in the library with the protein. Additionally, this FP-first method will include molecules that induce protein aggregation and precipitation leading to false positives. In addition to inhibitors, we are also interested in molecules that act as stabilizers of AcID or molecules that induce and capture unique conformations of AcID. A traditional MS-based Tethering screen may more effectively uncover fragments possessing these qualities.
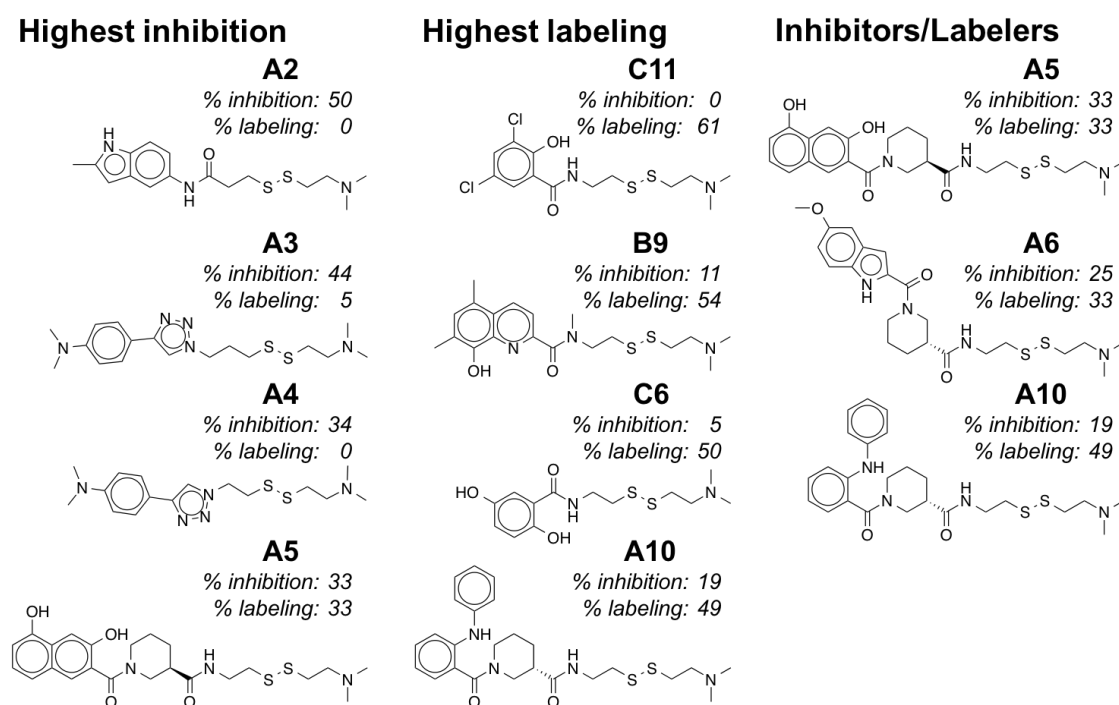
Figure 3.9 Tethering screen identifies fragments with unique properties and diverse structure FP Tethering screen of AcID identified certain fragments that were potent inhibitors of ERM binding yet weakly covalent, fragments that were covalent yet poor inhibitors, and compounds that were both potent inhibitors and labelers of AcID.

Despite the low molecular weight (~400 Da), several distinct molecular scaffolds were identified (Fig 3.9). The molecules that possessed high levels of both labeling and inhibition all contained a nipecotic acid moiety appended to some other variable chemical moiety indicating that there are privileged chemical scaffolds with enhanced AcID-binding capabilities and inhibitory strength.

Fragment A6

The fragment A6 interested us because of its ability to both label AcID and inhibit ERM binding. To effectively study the effect A6 had on activator binding and AcID structure it is necessary to isolate AcID fully labeled with small molecule at either of the reactive cysteines. Despite incubating Med25 with a large excess of A6 and low β-ME concentrations, it was not possible to achieve 100 % labeled AcID (Fig 3.10). Because disulfide bond formation is reversible, for the equilibrium to shift entirely towards a molecule-protein complex the molecule must be stabilized through non-covalent contacts with amino acids in and next to the protein binding site. If the molecule is not sufficiently stabilized due to low affinity binding of AcID it may be difficult to shift the equilibrium all the way to the fully bound state under conditions in which the protein remain stable.
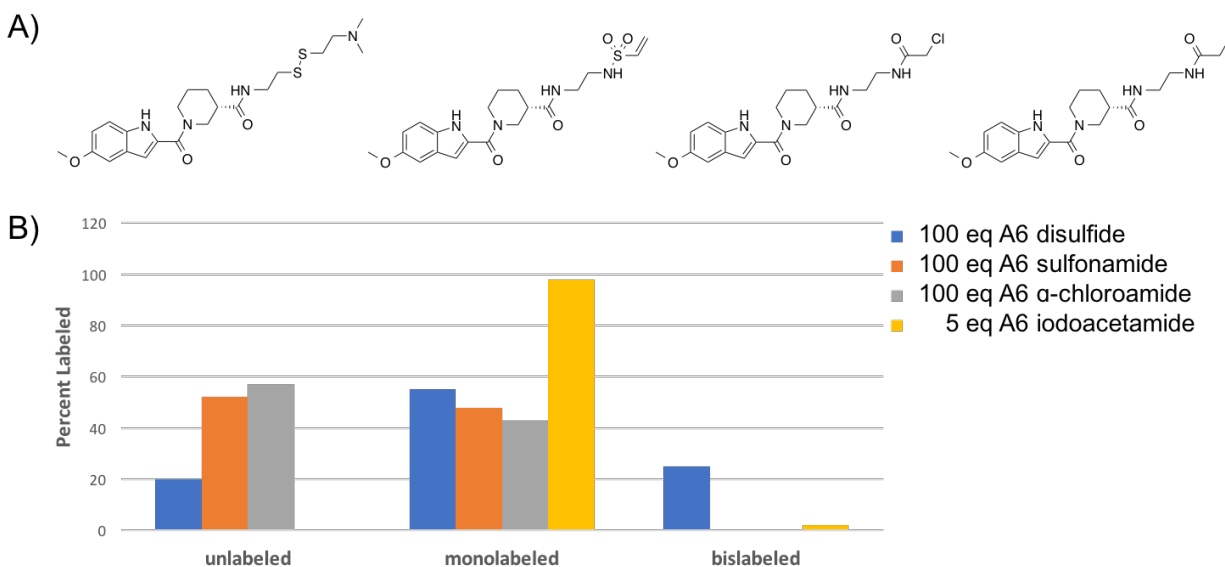
Figure 3.10 Labeling studies with A6 analogs A. A6 disulfide was converted into an irreversible molecule through replacement of the disulfide moiety with electrophilic alkylating groups including a sulfonamide, α-chloroamide, and iodoacetamide. B. Labeling of AcID with each A6 analog measure by mass spectrometry. Each analog was incubated with AcID for 18 hrs at the indicated stoichiometry. With Dr. Clint Regan.

IRREVERSIBLE ANALOGS OF A6

Disulfide bonds are readily reduced in the reducing environment of the cell. Thus, molecules identified via Tethering must be modified before they can be utilized as cellular probes. Replacement of the disulfide moiety with an electrophilic alkylating group enables these fragments to be turned into irreversible probes that can be used as cellular probes.

The disulfide in A6 was replaced with several electrophilic moieties (Fig 3.10) Initially sulfonamide and α-chloroamide analogs of A6 were prepared and their AcID labeling tested. Even in vast excess (100 eq) both the sulfonamide and α-chloroamide variants of A6 did not fully label Med25. Conversely, an iodoacetamide variant of A6 was prepared and it rapidly and efficiently labeled Med25 AcID at much more reasonable stoichiometries (5 eq) (Fig 3.10).

A6 iodoacetamide was surprising in is selectivity. As we have demonstrated, C497 and C506 are readily labeled by 4-iodoacetamidosalicylic acid. Conversely, A6 iodoacetamide only labels Med25 C506 indicating that A6 iodoacetamide must bind AcID in a fairly specific manner that precludes it from alkylating C497.

A6 iodoacetamide induces local and distal conformational change of AcID structure

In Chapter 2 we showed that Med25 AcID displays significant heterogeneity in the complexes it forms with different activators. We also observed that when VP16 αH1 was covalently tethered to AcID we observed perturbations in both the H1 and H2 binding faces of AcID indicating some network of amino acids capable of propagating binding events across large distance of the protein. To see how A6 iodoacetamide perturbed AcID structure it was reacted with C506 of ^{15}N labeled protein and HSQC NMR experiments performed (Fig 3.11). HSQC analysis of this complex revealed significant perturbations both in regions surrounding C506 and the H1 face of AcID, but also at the opposite H2 face of AcID (Fig 3.12). Like tethered VP16 αH1, A6 iodoacetamide can engage the network of amino acids linking the two binding surfaces.
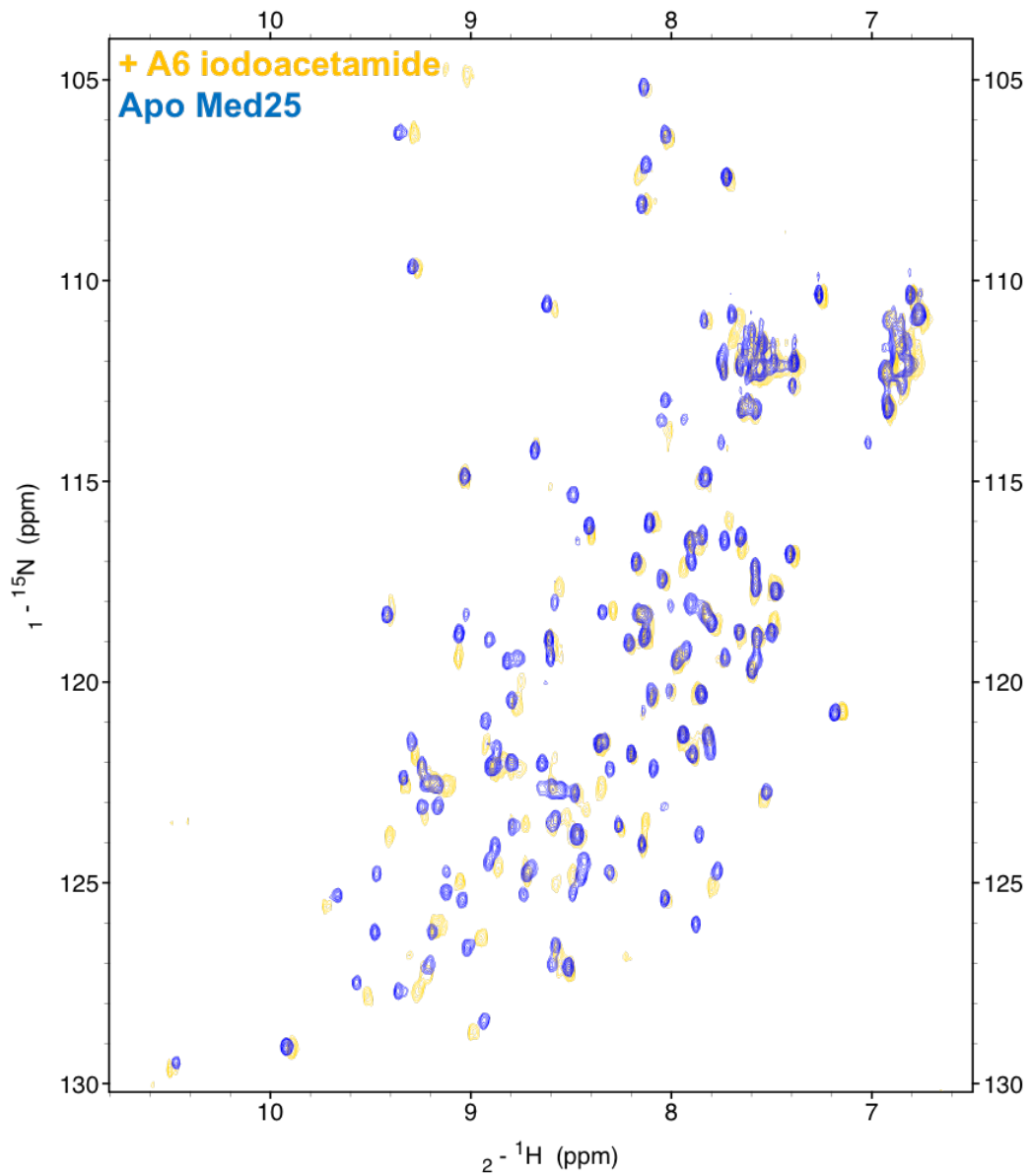
Figure 3.11 HSQC of A6 iodoacetamide reveals significant perturbations Overlay of HSQC spectra of wt Med25 (Blue) and Med25 + A6 iodoacetamide labeled at C506 (Gold).
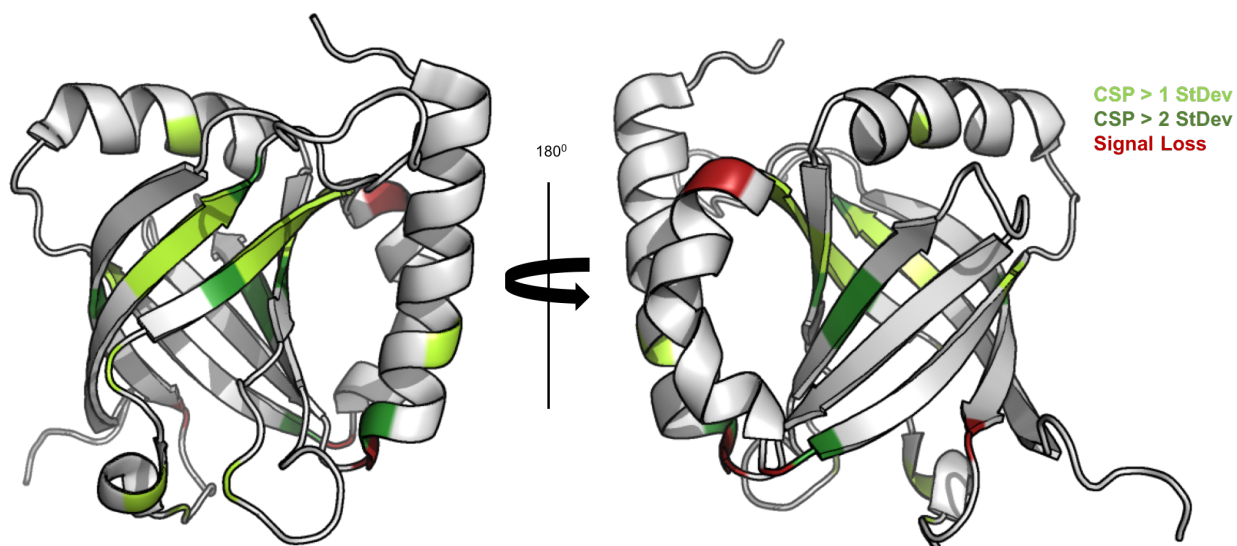
Figure 3.12 Chemical shifts are induced in both faces of AcID by A6 iodoacetamide Perturbations of A6 iodoacetamide plotted onto surface of Med25 AcID. Residues that experiences significant broadening are colored red.

To gain a better understanding of the A6-Med25 interaction we utilized Protein-Observed Fluorine NMR (PrOF).[32,33] PrOF monitors ^{19}F which is essentially absent in biological systems but can be readily incorporated into proteins through the use of the unnatural ^{19}F-containing amino acid 3-fluorotyrosine.[34] An advantage of PrOF NMR is that one is monitoring side chain perturbations rather than perturbations to the amide backbone as is done in HSQC experiments with ^{15}N-modified protein. This makes PrOF exquisitely sensitive to small changes in protein structure induced by ligand binding.

Med25 AcID was prepared with 3FY incorporated at all four native AcID tyrosines: Y432, Y487, Y515, and Y528 (Fig 3.13.B). A PrOF experiment with A6 iodoacetamide labeled at C506 of 3FY Med25 produced a specific perturbation pattern (Fig 3.13.C). Small shifts were observed in residues Y487 and Y515 which are found at the opposite H2 face of AcID quite removed from the cite of A6 labeling. A striking loss of signal was observed for Y528 which is found at the bottom

of the β-barrel and near C506. This could be indicative of a direct interaction between A6 and Y528 or could be attributed to more general A6-induced perturbations in this region of the protein. Fig 3.13.B highlights the close proximity between C506 and Y528.
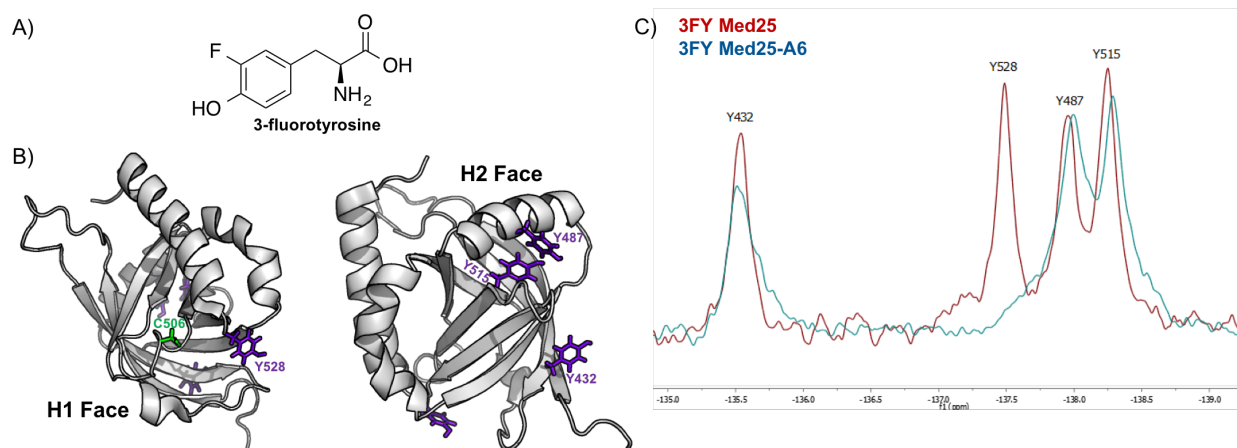
Figure 3.13 PrOF NMR of the AcID-A6 iodoacetamide complex A. 3-fluorotyrosine (3FY) can be incorporated into Med25 AcID at all 4 native tyrosine locations. B. Sites of 3FY incorporation into Med25 AcID at both the H1 and H2 face. C506 is in close proximity to Y528. C. PrOF spectra of wt 3FY Med25 (red) and 3FY Med25 tethered to A6 iodoacetamide. Significant peak broadening was observed for Y528 in the presence of A6 iodoacetamide. Performed by Matthew Beyersdorf.

A small molecule acts as an allosteric modulator of AcID

In Chapter 2 we demonstrated the presence of allosteric positive cooperativity in activator binding. Binding of VP16 αH2 was stabilized in the presence of tethered VP16 αH1. This stabilization was driven through a 20 % reduction in k_{off} and 35 % reduction in k_r. Because A6 iodoacetamide can also engage a conformational change network accessed by VP16 αH1 G450C leading to perturbations in both faces of AcID, we wondered if A6 might also serve as an allosteric stabilizer of AcID-activator complexes. As in chapter 2, a 4-DMN labeled VP16 αH2 peptide was competed with acetylated VP16 H2 but in the presence of A6 iodoacetamide rather than tethered VP16 αH1 G450C. In contrast to tethered VP16 αH1, the k_{off} value describing VP16 dissociation from AcID, was not impacted by A6. However, the rate corresponding to the conformational

change phase, k_r, was reduced by 20% suggesting that A6 reorders the AcID H2 face binding landscape resulting in a more favored binding interaction between VP16 αH2 and AcID (Fig 3.14).

$$\text{Med25} + \text{VP16} \underset{k_{off}}{\overset{k_{on}}{\rightleftharpoons}} \text{Med25•VP16} \underset{k_r}{\overset{k_f}{\rightleftharpoons}} \text{Med25•VP16*}$$
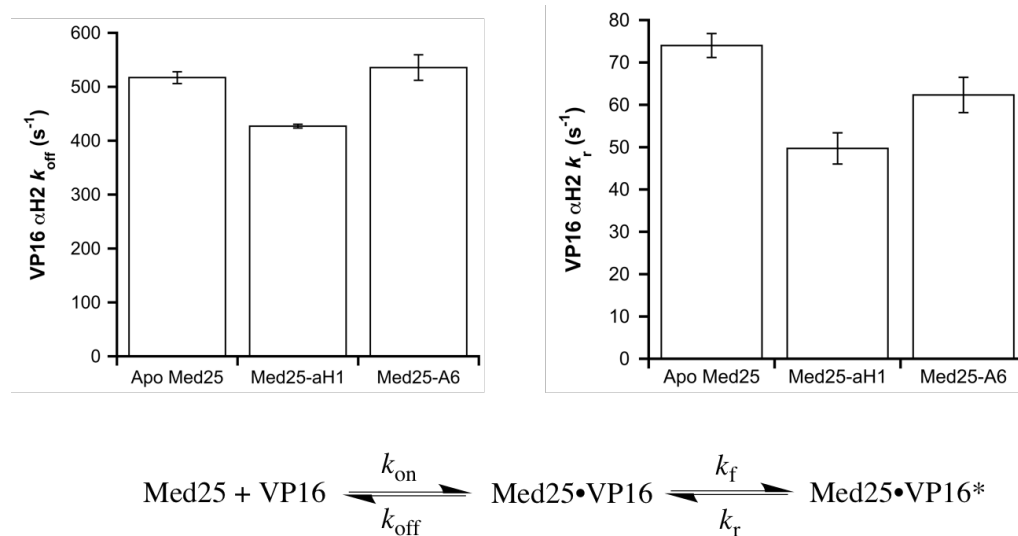
Figure 3.14 A6 acts as an allosteric stabilizer of a Med25-VP16 complex Dissociation of VP16 αH2 from Med25 in the presence of covalent ligands. 4-DMN labeled VP16 αH2 bound to AcID was competed with acetylated VP16 H2 and monitored by stopped flow fluorescence.

A6 IODOACETAMIDE INHIBITS ATF6α MEDIATED GENE EXPRESSION

A6 acts as a structural modulator of AcID structure and as an inhibitor of ERM binding. Linking these in vitro observations to biological activity is an important step in validating Med25 as a therapeutic target. The transcriptional activator ATF6α is an endoplasmic reticulum (ER) associated activator that is activated by cellular stress and the accumulation of misfolded proteins at the ER. Under stress conditions ATF6α translocates to the nucleus and activates transcription of ER chaperones. One such chaperone is HSPA5, the expression of which is regulated by ATF6α under cellular stress (Fig 3.15.A).[6,35] Because ATF6α interacts with Med25 AcID, we examined whether treatment of cells with A6 iodoacetamide can inhibit expression of ATF6α-responsive genes including HSPA5.[4,36]

HeLa cells were pretreated with A6 iodoacetamide followed by the induction of stress via treatment with thapsigargin leading to elevated HSPA5 expression and gene expression was measured by RT-qPCR.[37] Treatment with A6 iodoacetamide resulted in dose-dependent inhibition of HSPA5 demonstrating that targeting the ATF6α-Med25 interaction with covalent molecules is a viable method of altering Med25 mediated transcription (Fig 3.15.B).
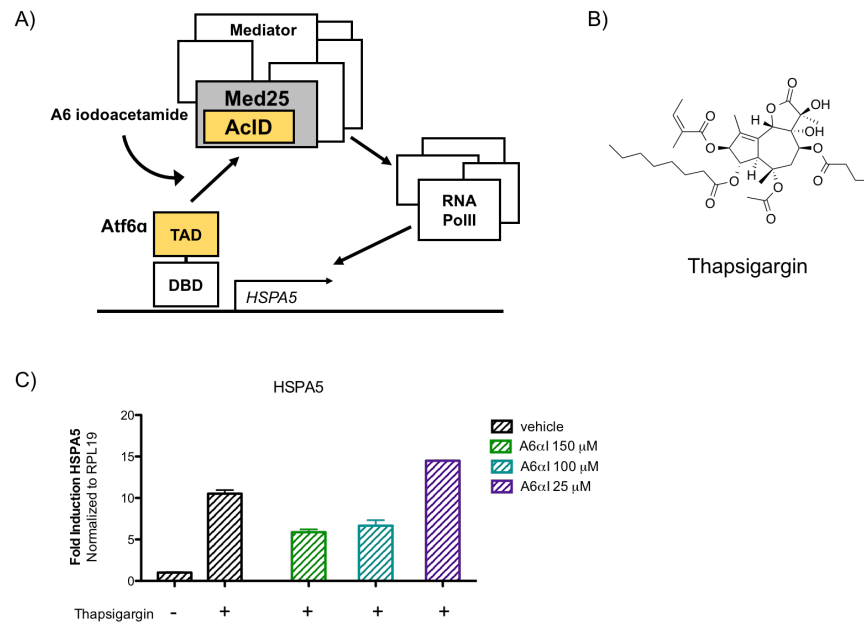
Figure 3.15 Inhibiton of ATF6α-Med25 mediated gene expression by A6 iodoacetamide A. HSPA5 expression is mediated by an ATF6α interaction with Med25 via the AcID domain. B. Thapsigargin induces ER-associated stress leading to the activation and translocation of ATF6α to the nucleus. C. HeLa cells were treated with DMSO (vehicle) and A6 iodoacetamide at the indicated concentrations for two hours followed by incubation with thapsigargin for 3 hrs. mRNA was isolated and converted to cDNA and HSPA5 levels determined by RT-qPCR. HSPA5 expression levels were normalized to RPL19. All signals are the mean and standard deviation of two technical replicates.

3.4 CONCLUSIONS

Med25 plays an important role in the both normal and disease-associated transcriptional programs through interactions with a diverse group of transcriptional activators. The AcID activator binding domain of Med25 has been observed in only one other protein, PTOV1, in humans. Thus, as a rare protein fold and structurally divergent ABD, AcID is an exciting therapeutic target. Adding to its significance, AcID contains native cysteines that can be used as handles for covalent small molecules.

We have shown that two of the three native cysteines within the AcID domain can be targeted by covalent small molecules. Further these two cysteines are within the H1 face of AcID and when alkylated by 4-iodoacetamidosalicylic acid, activator binding is inhibited which demonstrates that these cysteines are positioned in functionally relevant locations.

These results motivated us to use the site-specific Tethering screening strategy to identify covalent small molecule modulators of AcID. In a screen of 1600 molecules, we identified molecules that inhibited ERM binding and covalently labeled AcID. Conversion of one of these hits, A6, from a disulfide to an irreversible iodoacetamide alkylator enabled homogenous labeling of AcID. A6 iodoacetamide induced perturbations in AcID at the site of alkylation and at the opposite H2 binding face of AcID suggesting that it can engage the same conformational change network that the covalent VP16 peptides could access in Chapter 2. Further, A6 iodoacetamide induced allosteric changes when bound to AcID. VP16 binding at the H2 face of AcID was enhanced through a reduction in dissociation rate constants.

The conversion of the A6 disulfide into an irreversible A6 iodoacetamide also meant that it could be used as a cellular probe of Med25-regulated transcription. A6 iodoacetamide inhibited

ATF6α-dependent expression of HSPA5 suggesting that cellular targeting of native cysteines within AcID can alter transcriptional output.

3.5 MATERIALS AND METHODS

Plasmids

The Med25 expression plasmid pET21b-Med25(394-543)-His$_6$ (referred to as pAcID) was a gift from Prof. Patrick Cramer.[38] Modified pAcID constructs were prepared using site directed mutagenesis as previously described.[32]

Protein expression

pAcID(394-543) was expressed as a C-terminal His$_6$ construct in *E. coli* Rosetta pLysS cells. Overnight starter cultures were grown from Rosetta cells transformed with pLysS cells in LB broth in the presence of 1 mg/mL ampicillin and 0.034 mg/mL chloramphenicol at 37 °C at 150 RPM. Following overnight growth, 1 L of TB supplemented with 1 mg/mL ampicillin and 0.034 mg/mL chloramphenicol was inoculated with 5 mL of the overnight culture and grown at 37 °C to an OD of 0.8. Once the culture reached the correct OD, it was grown overnight at 21 °C in the presence of 0.5 mM IPTG to induce protein expression. Cells were harvested via centrifugation at 6500 RPM for 20 minutes. Cell pellets were stored at -80 °C until needed for purification.

For isotopically labeled protein used in NMR experiments following overnight growth in LB, TB media was substituted with M9 minimal media supplemented with Bioexpress (6 mL/L) and 1 g/L ^{15}NH$_4$Cl or 1 g/L ^{15}NH$_4$Cl and ^{13}C D-glucose for ^{15}N and ^{15}N,^{13}C Med25 AcID respectively. Before inoculation of the 1 L expression flask, the overnight cells were pelleted via centrifugation for 10 minutes at 2500 RPM and the LB was decanted. Cell pellets were resuspended in 20 mL M9 media followed by centrifugation for 10 mins at 2500 RPM. M9 media was decanted and the washed

pellet resuspended in 10 mL M9 media. 5 mL of cells were then used to inoculate the expression flask containing M9 media supplemented with the appropriate isotopically labeled reagents.

Protein Purification

Cell pellets were resuspended in lysis buffer(50 mM phosphate, 300 mM NaCl, and 10 mM imidazole, pH 6.5, 0.7 μL/mL β-ME), lysed by sonication, and centrifuged for 20 mins at 10,000 rpm. Supernatant was filtered and purified by chromatography on an AKTA Pure FPLC first by Nickle column (HisTrap HP, GE Healthcare) with a gradient that moved from Buffer A (50 mM phosphate, 300 mM NaCl, and 30 mM imidazole, pH 6.8) to buffer B (50 mM phosphate, 300 mM NaCl, and 400 mM imidazole, pH 6.8). This was followed by purification via anion exchange (HiTrap SP HP, GE Healthcare) with a gradient that moved from buffer A (50 mM phosphate, 1 mM DTT, pH 6.8) to buffer B (50 mM phosphate, 1 mM DTT, 1M NaCl, pH 6.8). Pure protein was dialyzed into the appropriate phosphate storage buffer overnight. Following dialysis, protein was concentrated via Amicon 5,000 Da cutoff spin concentrator and quantified via a NanoDrop at 280 using an extinction coefficient, ε = 22,460 $M^{-1}cm^{-1}$. Protein identity was confirmed via mass spectrometry (Agilent Q-TOF).

Phosphate Buffers for NMR Experiments:

General AcID storage buffer: 10 mM $NaPO_4$, 50 mM NaCl, pH 6.8

NMR buffer: 20 mM $NaPO_4$, 150 mM NaCl, pH 6.5

Peptide synthesis

Peptide constructs were prepared following standard FMOC solid-phase synthesis methods on a Liberty Blue Microwave synthesizer on Rink Amide Resin. Peptides were cleaved from resin in 95 % TFA, 2.5 % H_2O, 2.5 % TIPS. Peptides in excess cleavage solution were evaporated under N_2, precipitated in diethyl ether, and dissolved in 3:1 100 mM ammonium acetate:acetonitrile with minimal ammonium hydroxide to ensure peptide solubility. Peptides were purified by reverse-phase HPLC on an Agilent 1260 series with a C_{18} column (Agilent) using a gradient between 100 mM ammonium acetate and acetonitrile. Purified peptide fractions were pooled and lyophilized. Peptide identity was confirmed via mass spectrometry (Agilent Q-TOF).

Med25 labeling with alkylating small molecules

Med25 AcID (10 mM $NaPO_4$, 100 mM NaCl, pH 6.8) was incubated with 10 equivalents of each alkylator for 12 hrs. Labeling efficiency was determined using an Agilent Q-TOF HPLC-MS. Protein samples were injected onto the instrument and the molecule/protein mixture separated via a Poroshell C_8 column using a gradient of 5-100% acetonitrile to water with 0.1% formic acid. Data was analyzed using the Agilent workstation software. Labeling efficiency was determined by comparing the peak heights of mass adducts corresponding to Med25, Med25 + 1 alkylation, and Med25 + 2 alkylation using the following equation:

$$Percent\ labeled\ = \frac{Med25_{1\ or\ 2\ alkylations}}{Med25_{unlabeled} + Med25_{1\ alkylation} + Med25_{peptide2\ alkylations}}$$

Tethering Screen

An FP-Tethering screen of AcID in complex with ERM 70% bound was performed in collaboration with the Wells Laboratory at UCSF in an analogous manner to a previously reported method. [23] 1600 compounds were screened at three different β-ME concentrations (0.1 mM, 1 mM and 5 mM). Mass spectrometry analysis was performed on the 31 most potent inhibitors (>3 standard deviations from average % inhibition) as previously reported.[23]

Direct binding experiments

Direct binding fluorescence polarization assays were performed in triplicate in 384-well black, round bottom plates (Corning 4514) at a final volume of 20 μL. 10 μL of Med25 was added at twice the highest final concentration and serially diluted with AcID storage buffer (10 mM NaPO$_4$, 100 mM NaCl, pH 6.8.) by adding 10 μL of buffer to the well containing protein followed by moving 10 μL of this 2-fold diluted protein to the next sequential well. This dilution was repeated 12 times. In the 13th well only storage buffer is added. FITC (fluorescein isothiocyanate) labeled peptides stocks at 40 μM were prepared in AcID storage buffer and added to wells containing diluted protein or buffer, resulting in a final 2-fold dilution of both peptide (final concentration 20 nM) and protein. The plate was incubated for 30 minutes at room temperature followed by reading on a Pherastar plate reader with polarized excitation at 485 nm and emission intensity was measured through a 535 nM filter. A binding isotherm that accounts for ligand depletion (assuming a 1:1 binding model of peptide to ACID) was fit to the observed anisotropy values as a function of ACID to obtain the apparent equilibrium dissociation K_d,

$$y = c + (b - c) \times \frac{[K_d + a + x] - \sqrt{(K_d + a + x)^2 - 4ax}}{2a}$$

Where "a" and "x" are the total concentrations of fluorescent peptide and protein, respectively, "y" is the observed anisotropy at a given protein concentration, "b" is the maximum observed anisotropy value, and "c" is the maximum observed anisotropy value. Each data point is an average of three independent experiments with the indicated error representing the standard deviation of the three replicated. Data analysis was performed using GraphPad Prism 4.0.

NMR analysis of the A6-AcID complex

NMR analysis of A6-AcID complexes were performed via ^{1}H-^{15}N HSQC on a Bruker Avance III 600 Mhz spectrometer equipped with a cryogenic probe at 30 °C. Alkylated-AcID complexes were prepared and purified as described above and spectra were obtained in the absence of DMSO. Data Processing and visualization was performed using NMR Pipe and Sparky.[39]

Assaying inhibitory effects of A6 iodoacetamide against ERM endogenous gene expression

For endogenous gene expression analysis, 1×10^5 HeLa cells were seeded into a 24-well plate and allowed to adhere overnight. Media was removed and replaced with Opti-Mem media containing vehicle of A6 iodoacetamide delivered in DMSO (1% v/v) at the indicated concentrations. After cells were incubated with either vehicle or compound for 2h, cells were stimulated with thapsigargin at a final concentration of 500 nM. After 4h, the media was removed and total RNA was isolated using RNeasy Plus RNA isolation kits (Qiagen) according to manufacturer's protocol.

Each RNA sample was used to synthesize cDNA using iScript cDNA synthesis kits (Bio-Rad). Real-Time Quantitative PCR (RT-qPCR) analysis was carried out in an Applied Biosystems StepPlusOne using SYBR green master mix and primers for human genes:

Gene	Primer Sequence
RPL19	F: 5'-ATGTATCACAGCCTGTACCTG-3' R: 5'-TTCTTGGTCTCTCTTCCTCCTTG-3'
HSPA5	F: 5': CTGGGTACATTTGATCTGACTGG:3 R: 5': CTTACCGACCTTTCGGTGGTCCTACG:3'

RT-qPCR analysis was carried out using the comparative C_T Method ($\Delta\Delta C_T$ Method) as previously described to estimate HSPA5 mRNA levels relative to the reference RPL19 mRNA levels. The reported mean and standard deviation for HSPA5 expression were determined using two technical replicates from one representative biological replicate.

3.6 REFERENCES

1   Chotteau-Lelievre, A. *et al.* Expression patterns of the Ets transcription factors from the PEA3 group during early stages of mouse development. *Mechanisms of development* **108**, 191-195 (2001).
2   Chotteau-Lelievre, A. *et al.* PEA3 transcription factors are expressed in tissues undergoing branching morphogenesis and promote formation of duct-like structures by mammary epithelial cells in vitro. *Developmental biology* **259**, 241-257 (2003).
3   Chotteau-Lelievre, A., Desbiens, X., Pelczar, H., Defossez, P. A. & de Launoit, Y. Differential expression patterns of the PEA3 group transcription factors through murine embryonic development. *Oncogene* **15**, 937-952, doi:10.1038/sj.onc.1201261 (1997).
4   Sela, D. *et al.* Role for human mediator subunit MED25 in recruitment of mediator to promoters by endoplasmic reticulum stress-responsive transcription factor ATF6alpha. *The Journal of biological chemistry* **288**, 26179-26187, doi:10.1074/jbc.M113.496968 (2013).
5   Chen, X., Shen, J. & Prywes, R. The luminal domain of ATF6 senses endoplasmic reticulum (ER) stress and causes translocation of ATF6 from the ER to the Golgi. *The Journal of biological chemistry* **277**, 13045-13052, doi:10.1074/jbc.M110636200 (2002).
6   Haze, K., Yoshida, H., Yanagi, H., Yura, T. & Mori, K. Mammalian transcription factor ATF6 is synthesized as a transmembrane protein and activated by proteolysis in response to endoplasmic reticulum stress. *Mol Biol Cell* **10**, 3787-3799 (1999).
7   Ye, J. *et al.* ER stress induces cleavage of membrane-bound ATF6 by the same proteases that process SREBPs. *Molecular cell* **6**, 1355-1364 (2000).
8   Feng, F. Y., Brenner, J. C., Hussain, M. & Chinnaiyan, A. M. Molecular pathways: targeting ETS gene fusions in cancer. *Clinical cancer research : an official journal of the American Association for Cancer Research* **20**, 4442-4448, doi:10.1158/1078-0432.CCR-13-0275 (2014).
9   Benz, C. C. *et al.* HER2/Neu and the Ets transcription activator PEA3 are coordinately upregulated in human breast cancer. *Oncogene* **15**, 1513-1525, doi:10.1038/sj.onc.1201331 (1997).
10   Wang, Y. *et al.* ER81 Expression in Breast Cancers and Hyperplasia. *Patholog Res Int* **2011**, 980513, doi:10.4061/2011/980513 (2011).
11   Chotteau-Lelievre, A. *et al.* Prognostic value of ERM gene expression in human primary breast cancers. *Clinical cancer research : an official journal of the American Association for Cancer Research* **10**, 7297-7303, doi:10.1158/1078-0432.CCR-04-0593 (2004).
12   Bieche, I. *et al.* Expression of PEA3/E1AF/ETV4, an Ets-related transcription factor, in breast tumors: positive links to MMP2, NRG1 and CGB expression. *Carcinogenesis* **25**, 405-411, doi:10.1093/carcin/bgh024 (2004).
13   Davidson, B. *et al.* The clinical role of the PEA3 transcription factor in ovarian and breast carcinoma in effusions. *Clinical & experimental metastasis* **21**, 191-199 (2004).
14   de Launoit, Y. *et al.* [PEA3 family of transcription factors and the regulation of oncogenesis]. *Bulletin du cancer* **93**, 985-989 (2006).

15   Verger, A. *et al.* The Mediator complex subunit MED25 is targeted by the N-terminal transactivation domain of the PEA3 group members. *Nucleic acids research* **41**, 4847-4859, doi:10.1093/nar/gkt199 (2013).

16   Milbradt, A. G. *et al.* Structure of the VP16 transactivator target in the Mediator. *Nature structural & molecular biology* **18**, 410-415, doi:10.1038/nsmb.1999 (2011).

17   Arkin, M. R., Tang, Y. & Wells, J. A. Small-molecule inhibitors of protein-protein interactions: progressing toward the reality. *Chemistry & biology* **21**, 1102-1114, doi:10.1016/j.chembiol.2014.09.001 (2014).

18   Arkin, M. R. & Wells, J. A. Small-molecule inhibitors of protein-protein interactions: progressing towards the dream. *Nat Rev Drug Discov* **3**, 301-317, doi:10.1038/nrd1343 (2004).

19   Erlanson, D. A. *et al.* Site-directed ligand discovery. *Proceedings of the National Academy of Sciences of the United States of America* **97**, 9367-9372 (2000).

20   Arkin, M. R. *et al.* Binding of small molecules to an adaptive protein-protein interface. *Proceedings of the National Academy of Sciences of the United States of America* **100**, 1603-1608, doi:10.1073/pnas.252756299 (2003).

21   Wells, J. *et al.* Drug discovery at signaling interfaces. *Ernst Schering Res Found Workshop*, 19-27 (2003).

22   Ostrem, J. M., Peters, U., Sos, M. L., Wells, J. A. & Shokat, K. M. K-Ras(G12C) inhibitors allosterically control GTP affinity and effector interactions. *Nature* **503**, 548-551, doi:10.1038/nature12796 (2013).

23   Lodge, J. M., Rettenmaier, T. J., Wells, J. A., Pomerantz, W. C. & Mapp, A. K. FP Tethering: a screening technique to rapidly identify compounds that disrupt protein-protein interactions. *MedChemComm* **5**, 370-375, doi:10.1039/C3MD00356F (2014).

24   Erlanson, D. A., Wells, J. A. & Braisted, A. C. Tethering: fragment-based drug discovery. *Annu Rev Biophys Biomol Struct* **33**, 199-223, doi:10.1146/annurev.biophys.33.110502.140409 (2004).

25   Wang, N. *et al.* Ordering a dynamic protein via a small-molecule stabilizer. *Journal of the American Chemical Society* **135**, 3363-3366, doi:10.1021/ja3122334 (2013).

26   Wang, N., Lodge, J. M., Fierke, C. A. & Mapp, A. K. Dissecting allosteric effects of activator-coactivator complexes using a covalent small molecule ligand. *Proceedings of the National Academy of Sciences of the United States of America* **111**, 12061-12066, doi:10.1073/pnas.1406033111 (2014).

27   Hardy, J. A., Lam, J., Nguyen, J. T., O'Brien, T. & Wells, J. A. Discovery of an allosteric site in the caspases. *Proceedings of the National Academy of Sciences of the United States of America* **101**, 12461-12466, doi:10.1073/pnas.0404781101 (2004).

28   Erlanson, D. A. *et al.* Discovery of a potent and highly selective PDK1 inhibitor via fragment-based drug discovery. *Bioorganic & medicinal chemistry letters* **21**, 3078-3083, doi:10.1016/j.bmcl.2011.03.032 (2011).

29   Gao, J. & Wells, J. A. Identification of specific tethered inhibitors for caspase-5. *Chem Biol Drug Des* **79**, 209-215, doi:10.1111/j.1747-0285.2011.01261.x (2012).

30   Shannon, D. A. & Weerapana, E. Covalent protein modification: the current landscape of residue-specific electrophiles. *Current opinion in chemical biology* **24**, 18-26, doi:10.1016/j.cbpa.2014.10.021 (2015).

31   Weerapana, E. *et al.* Quantitative reactivity profiling predicts functional cysteines in proteomes. *Nature* **468**, 790-795, doi:10.1038/nature09472 (2010).

32   Pomerantz, W. C. *et al.* Profiling the dynamic interfaces of fluorinated transcription complexes for ligand discovery and characterization. *ACS chemical biology* **7**, 1345-1350, doi:10.1021/cb3002733 (2012).

33   Urick, A. K., Calle, L. P., Espinosa, J. F., Hu, H. & Pomerantz, W. C. Protein-Observed Fluorine NMR Is a Complementary Ligand Discovery Method to 1H CPMG Ligand-Observed NMR. *ACS chemical biology* **11**, 3154-3164, doi:10.1021/acschembio.6b00730 (2016).

34   Gee, C. T. *et al.* Protein-observed (19)F-NMR for fragment screening, affinity quantification and druggability assessment. *Nat Protoc* **11**, 1414-1427, doi:10.1038/nprot.2016.079 (2016).

35   Yamamoto, K. *et al.* Transcriptional induction of mammalian ER quality control proteins is mediated by single or combined action of ATF6alpha and XBP1. *Dev Cell* **13**, 365-376, doi:10.1016/j.devcel.2007.07.018 (2007).

36   Sela, D. *et al.* Endoplasmic reticulum stress-responsive transcription factor ATF6alpha directs recruitment of the Mediator of RNA polymerase II transcription and multiple histone acetyltransferase complexes. *The Journal of biological chemistry* **287**, 23035-23045, doi:10.1074/jbc.M112.369504 (2012).

37   Oslowski, C. M. & Urano, F. Measuring ER stress and the unfolded protein response using mammalian tissue culture system. *Methods in enzymology* **490**, 71-92, doi:10.1016/B978-0-12-385114-7.00004-0 (2011).

38   Vojnic, E. *et al.* Structure and VP16 binding of the Mediator Med25 activator interaction domain. *Nature structural & molecular biology* **18**, 404-409, doi:10.1038/nsmb.1997 (2011).

39   Delaglio, F. *et al.* NMRPipe: a multidimensional spectral processing system based on UNIX pipes. *Journal of biomolecular NMR* **6**, 277-293 (1995).

Chapter 4

Small Molecule Targeting of NF-κB Regulatory Proteins[1]

4.1 ABSTRACT

In addition to activator-coactivator interactions, PPIs regulate many other facets of transcriptional signaling pathways essential for transcriptional activation. Targeting PPIs outside of activator-coactivator interactions offer alternate points for therapeutic intervention. The NF-κB signaling cascade is a challenging therapeutic target because of the extensive cross-talk of individual NF-κB subunits in alternate signaling pathways. We have employed a novel peptide stabilization strategy to produce a cell permeable peptide capable of inhibiting the IKK complex essential for NF-κB activation. This peptide selectively inhibits canonical NF-κB signaling in cells while leaving the non-canonical pathway unperturbed. We also mechanistically define the activity of the recently reported ketogibberellic acid methyl ester small molecule that displays activity against NF-κB. Both of these molecules represent alternate means of targeting transcriptional activation beyond activator-coactivator interactions.

---

[1] The research described in chapter 4 is a collaborative effort. A.R. Henderson synthesized and purified NBD peptides, performed RT-qPCR experiments, performed pull-downs and western blots, and looked at nuclear translocation of NF-κB subunits. Dr. Paul Bruno designed, synthesized and purified NBD2 peptides, validated their efficacy in NF-κB luciferase reporter assays, performed RT-qPCR experiments, and performed proteolytic stability assays . James Annand synthesized and purified gibberellic acid analogs and performed confocal microscopy experiments. Contributions are indicated in figure captions. Contents of this article and adapted and reproduced from a published article: Bruno PA, Morriss-Andrews A, Henderson AR, Brooks CL, 3rd, Mapp AK. A Synthetic Loop Replacement Peptide That Blocks Canonical NF-kappaB Signaling. *Angewandte Chemie*. 2016;55(48):14997-5001.

4.2 BACKGROUND

Transcriptional activation is the end result of upstream signaling pathways comprising a complex network of protein-protein interactions. While activator-coactivator protein-protein interactions are critical mediators of gene expression, targeting upstream protein-protein interactions with small molecules offer alternate means to control transcription in diseased cells. The NF-κB signaling pathway is illustrative of a transcriptional pathway with multiple points of potential therapeutic intervention.

Nuclear factor kappa-light-chain enhancer of B cells (NF-κB) is a group of inducible transcription factors that participate in a broad array of cellular responses in many different cell types.[1] Beyond the set of five core transcription factors, there is a large network of regulatory proteins that govern NF-κB induction. Given the complexity of NF-κB regulation and its central role in many cellular processes, aberrant NF-κB activity is implicated in a variety of human diseases including inflammatory disorders, autoimmune diseases, and cancers.[2] As a result, NF-κB has been the subject of many drug discovery efforts aimed the pathway's core components. Efforts to target this pathway have been complicated by the central role of NF-κB in many cellular processes, highlighting the need for molecules with enhanced specificity or novel targets within the regulatory cascade.

NF-κB FAMILY MEMBERS

The core NF-κB family is a group of 5 transcription factors (RelA (p65), RelB, c-Rel, p50(p105), p52(p100)) that control cell growth and proliferation, response to stress, and multiple facets of the immune system(Fig 4.1).[3] Each member contains an N-terminal 300 amino acid Rel

homology domain (RHD) that is composed of a DNA-binding sequence, a region for association with other NF-κB subunits, and a nuclear localization sequence (NLS). RelA, RelB, and c-Rel all contain at least one transcriptional activation domain (TAD) consistent with their overall function as activators of gene expression.[4] p50 and p52 lack TADs and instead have a large c-terminal region composed of ankyrin repeats that is proteolytically cleaved to form active p50 and p52. The lack of a TAD in either p50 or p52 is consistent with their role as repressors of transcription.[5] The five family members are capable of forming 15 possible homo- and heterodimers that produce distinct transcriptional outputs. Homo- and heterodimers composed of at least one TAD-containing subunit function as activators while p50:p50, p50:p52, and p52:p52 act as suppressors.
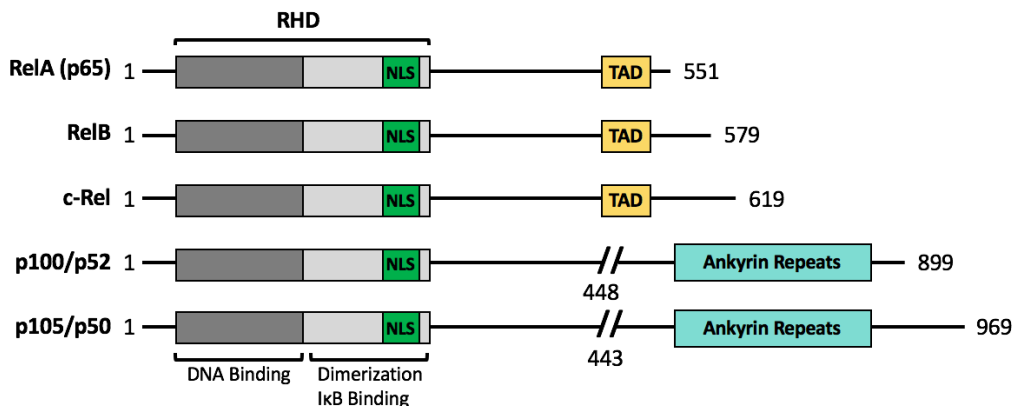
Figure 4.1 NF-κB Family Members NF-κB transcription factors possess Rel Homology Domains (RHD) responsible for DNA binding and dimerization. The Rel proteins, p65, RelB, and c-Rel all contain transcriptional activation domains, which p100/p52 and p105/p50 lack. Instead, p100/p52 and p105/p50 contain auto-inhibitory Ankyrin repeats that can be proteolytically cleaved.

In the absence of an inducing signal, NF-κBs exist as inactive, cytosolic proteins. In the cytosol NF-κBs are sequestered by Inhibitor of κB (IκBs) which block the nuclear localization sequences of RelA, RelB, and c-Rel.[6] Uncleaved p50 and p52 (p105 and p100, respectively)

contain an inhibitory ankyrin repeat in their C-terminal domains and thus self-inhibit nuclear translocation. Activation of NF-kB occurs through two pathways, canonical and non-canonical, each induced by a different set of cellular stimuli (Fig 4.2). The canonical pathway is induced by a variety of signals including cytokines (IL-1β, TNFα) and genotoxic stress at membrane-bound receptors which activate the IKK complex. The IKK complex is composed of two IκB kinases, IKKα and IKKβ, and a regulatory domain NEMO (NF-κB essential modifier). The IKK complex phosphorylates IκB leading to IκB release from the p65:p50 heterodimer. IκB undergoes polyubiquitination and subsequent proteasomal degradation. This allows nuclear translocation of the NF-κB heterodimer leading to expression of target genes. While both IKKs are present in the IKK-NEMO holoenzyme, phosphorylation of downstream targets seems to be accomplished predominantly by IKKβ.[7,8] In non-canonical activation, a different set of cellular stimuli activate NF-κB inducing kinase (NIK) leading to phosphorylation of an IKKα homodimer. The IKKα dimer phosphorylates p100 leading to polyubiquitination and proteolytic cleavage of its C-terminal inhibitory domain exposing the nuclear localization sequence of a p52:RelB heterodimer enabling nuclear translocation and subsequent expression of target genes.[9,10]

In NF-κB signaling, the molecular and structural basis activator-coactivator interactions remain poorly characterized. This has made the discovery and development of small molecule inhibitors targeting these interfaces challenging. [11,12]   NF-κB activation is dependent on the coordinated interplay of many protein-protein interactions. Targeting these PPI offer a means of selectively inhibiting discrete signaling pathways within NF-κB. We describe two distinct approaches to disrupting alternative parts of this pathway.
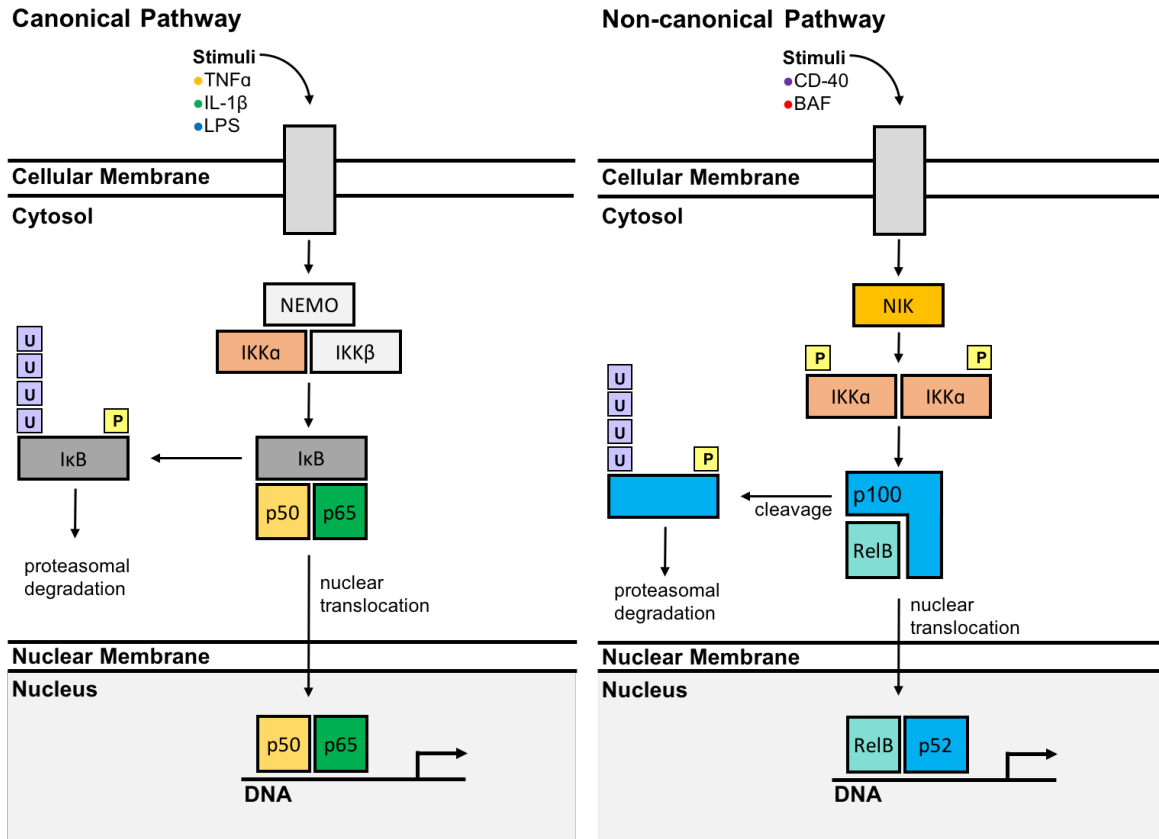
Figure 4.2 Canonical and non-canonical NF-κB signaling pathways Canonical and non-canonical NF-κB are induced via different signaling mechanisms leading to activation of different subsets of NF-κB dimers through alternate protein-protein interaction cascades.

RESULTS

Targeting the IKK Complex

As an integrator of many cellular signals and regulator of multiple genes across many cell types, NF-κB is an enticing yet challenging therapeutic target. Despite this broad activity, certain components of the pathway assemble and operate only in specific-contexts making them valuable targets for inhibitor development. The inhibitor of κB kinase (IKK) complex solely regulates the canonical NF-κB activation pathway which is the pathway most often dysregulated in cancer and inflammatory diseases.[2,13]   The IKK complex is a heterotetramer composed of IKKβ and IKKα associated with two NEMO scaffold proteins.[14,15] NEMO is unique to the IKK complex,

116

while IKKα and IKKβ function in non-canonical NF-κB signaling and other cellular pathways.[16] In response to stimulation by TNFα, NEMO associates with polyubiquitinilated RIP1 kinase and the rest of the TNF receptor complex enabling phosphorylation of IKKs via TAK1 kinase.[9] Phosphorylation activates IKKα and IKKβ enabling them to phosphorylate and inactivate IκBs sequestering NF-κB dimers in the cytosol thus freeing them to translocate to the nucleus.

Structural analysis of the complex revealed that NEMO dimerizes as a coiled-coiled to which IKK helices assemble forming a 4-helix bundle (Fig 4.3).[17] The crux of this interaction is the six amino acid NEMO binding domain (NBD), [737]LDWSWL[742], on both IKKα and IKKβ that directly contacts the core NEMO dimer. Mutational analysis revealed that two tryptophans critical for IKK association to NEMO are stabilized by an intramolecular hydrogen bond between D738 and S740 forming a short loop. Canonical NF-kB activation is inhibited when this 6 residue peptide is conjugated to a cell-penetrating peptide (CPP) with an IC_{50} of approximately 100 μM.[18-21]
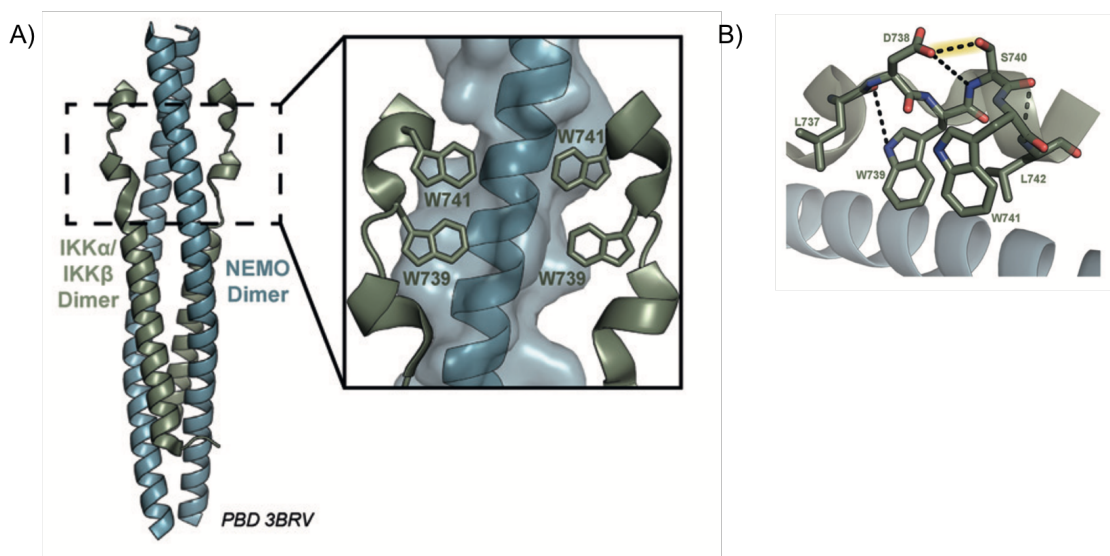
**Figure 4.3 IKK complex assembly is mediated by a 4-helix bundle** A. X-ray crystal structure of the core IKK complex assembly. IKKs form critical contacts with two tryptophans. B. The NBD sequence of IKK positions W739 and W741 on an unstructured loop stabilized by an intramolecular hydrogen bond between D738 and S740. Modified from Bruno et al. *Angew. Chem. Int. Ed.* **2016**. 55, 14997-15001.

IKK NBD is stabilized by an intramolecular hydrogen bond

Work by Rushe and colleagues revealed that the IKK-NEMO interaction is mediated by a 6 amino acid sequence containing two hot spot tryptophans that are positioned by an intramolecular hydrogen bond between D738 and S740 (Fig 4.3.b) forming a loop lacking α-helicity or β-sheet character.[17] Given the importance of these tryptophans in mediating this PPI, we hypothesized that further stabilization of this loop by replacement of the hydrogen bond bridge with a non-labile connection may increase potency and stability of this NBD peptide as a cellular inhibitor of the IKK-NEMO interaction.

Substitution of D738 and D740 with allylglycine enabled replacement of the hydrogen bond loop with a 4-carbon synthetic loop via ring closing metathesis (Fig 4.4).[22] Molecular dynamics simulations of wild type NBD and NBD stabilized by a c-c bond (NBD2, Fig 4.5.a) reveal similar key dihedral angles indicating that this modification preserves key NBD loop geometry.[23] This modification did not significantly alter the secondary structure of the peptide as circular dichroism spectra of the modified peptide compare favorably to wild type NBD. Significantly, NBD2 displayed dramatic proteolytic stability to chmyotrypsin compared to NBD$_{WT}$ or unmetathesized NBD1.

IKK NBD$_{WT}$
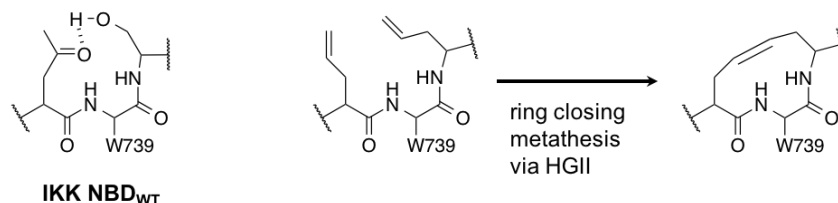
Figure 4.4 Synthetic loop replacement of NBD hydrogen bond The tryptophan-bearing loop that contacts NEMO is stabilized by an intramolecular hydrogen bond. Replacement of this hydrogen bond with allylglycine enables ring closing metathesis via Hoveyda-Grubbs generation II catalyst.

Consistent with its enhanced proteolytic stability, NBD2 was a potent inhibitor of NF-κB activity in cells. IL-1β potently activates NF-κB signaling (Fig 4.2) and drives luciferase activity in an NF-κB driven reporter assay. While NBD$_{WT}$ produced 50% inhibition at approximately 100 μM, NBD2 was 10 times as potent displaying 50 % inhibition at 10 μM (Fig 4.5). A variant of NBD2 with both tryptophans replaced by alanine, NBD3, did not inhibit NF-κB activation.
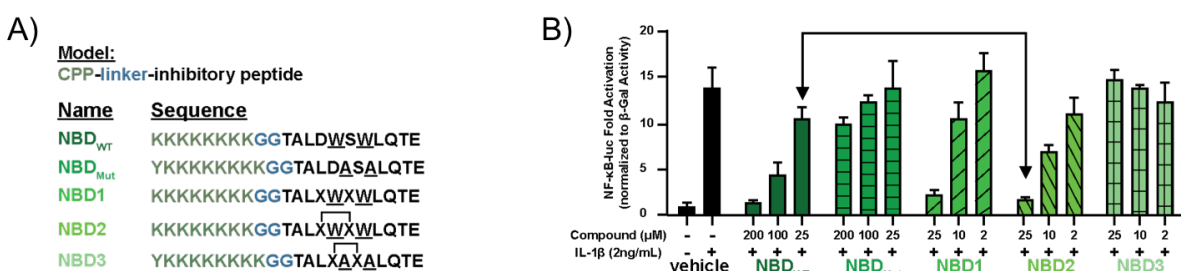
Figure 4.5 Cellular activity of modified NBD peptides A. NBD peptides were composed of a octalysine cell penetrating peptide (CPP), a diglycine linker (GG), and variations of the NBD sequence. B. Inhibition of IL-1β induced NF-κB-driven luciferase activity by NBD constructs in HeLa cells. Performed by Paul Bruno. Modified from Bruno et al. *Angew. Chem. Int. Ed.* **2016**. 55, 14997-15001.

Also consistent with direct NBD2 engagement of the IKK-NEMO interface, inhibition of canonical NF-κB driven genes MIP3α and IL-8 were observed (Fig 4.6).[24,25] MIP3α expression is associated with inflammatory bowel diseases and the canonical p50:p65 heterodimer is found at the MIP3α promoter following induction by IL-1β. Expression of IL-8, a driver of metastasis, has been shown to be contingent on p65.[25,26] Because of the dependence of these genes on the intact IKK holoenzyme, the corresponding downregulation of IL-8 and MIP3α can be explained by the ability of NBD2 to disrupt this protein-protein interaction.
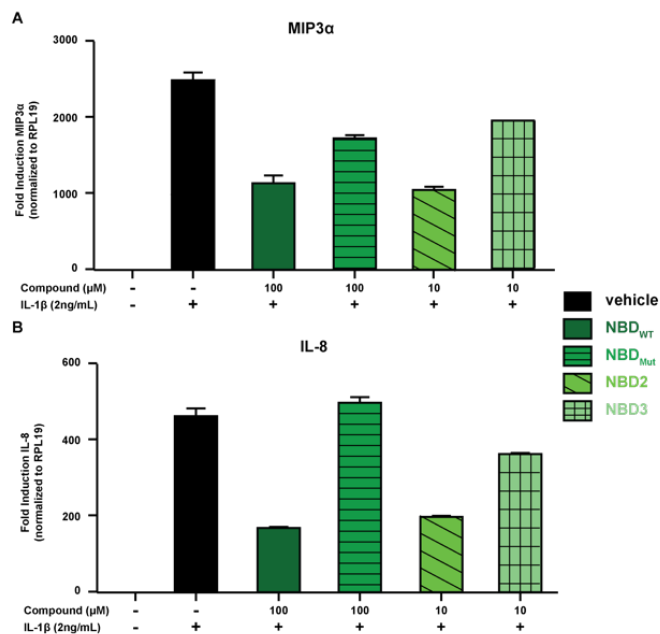
Figure 4.6 NBD inhibits canonical NF-κB regulated genes Effects of NBD analogs on MIP3α and IL-8 expression as measured by RT-qPCR. Performed by Paul Bruno. Modified from Bruno et al. *Angew. Chem. Int. Ed.* **2016**. 55, 14997-15001.

The apparent context specificity of the IKK-NEMO interaction is enticing in that it offers the potential to selectively inhibit one major signaling pathway in NF-κB, while leaving the other unperturbed. Unlike the canonical pathway, non-canonical NF-κB activation is driven through IKKα homodimerization. The IKKα homodimer is phosphorylated by NIK in response to a cellular signal leading to phosphorylation of cytosol-sequestered NF-κB dimers (Fig 4.7). Critically, this pathway is NEMO-independent and although NBD2 is derived from a sequence of IKKα, this sequence has solely been characterized as a NEMO interaction domain. To assess this specificity, NBD2 was tested for its ability to inhibit genes regulated through non-canonical NF-κB signaling. CyclinD1 is required for progress through the G1 stage of the cell cycle and its expression has been linked to NFκB.[27] Cyclin D1 expression is specifically linked to activity of IKKα and p65, both predominately active in non-canonical signaling.[8] NBD2 had no effect on CyclinD1 expression as

measured by RT-qPCR after treatment in HeLa cells offering strong evidence that NBD2 is a specific modulator of canonical NF-κB signaling.
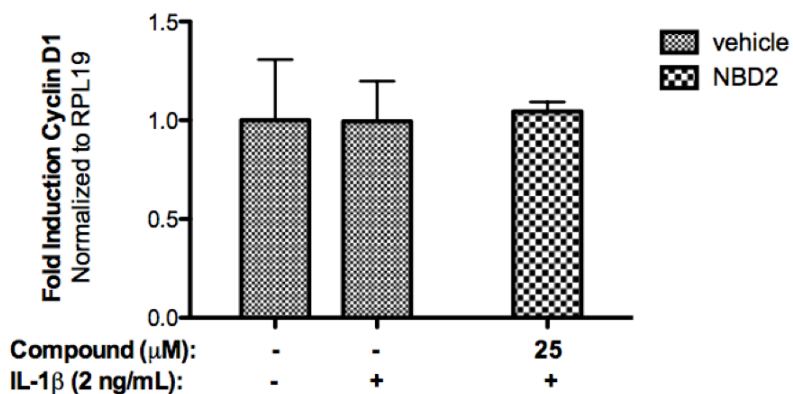
Figure 4.7 NBD2 does not inhibit non-canonical NF-κB regulated genes CyclinD1 expression is not inhibited by NBD2. Performed by Andrew Henderson. Modified from Bruno et al. *Angew. Chem. Int. Ed.* **2016**. 55, 14997-15001.

Thus, NBD2 is a selective inhibitor of canonical NF-κB signaling. Because of the considerable cross-talk in NF-κB and the function of individual subunits in different signaling pathways, a chemical probe capable of acting specifically on an individual pathway is valuable. The use of this synthetic loop replacement strategy increased the potency and stability of the NBD peptide by a factor of 10. The success of this peptide points to the utility in targeting transcriptional PPI beyond activator-coactivator interactions.

While the IKK complex is critical for the activation of canonical NF-κB activation, components of this complex also have alternate functions in the NF-κB pathway. Targeting these alternate functions provides an additional method of controlling this pathway. To that end we have investigated a recently reported inhibitor of NF-κB activity, a derivative of gibberellic acid, and sought to mechanistically define its method of action.

Determining the Mechanism of Gibberelin-induced NF-κB Activity

Therapeutic potential of gibberellins

Gibberellins are plant hormones that regulate a number of developmental processes in including flowering, stem elongation, and seed germination.[28] A subset of these hormones, the tetracyclic diterpenoid Gibberellic acids, have been investigated for their therapeutic utility and have shown anti-tumor, anti-inflammatory, and analgesic activity (Fig 4.8).[29,30] Pharbinilic acid, an allogibberic acid, displayed anticancer cytotoxicity against a panel of cancer cell lines.[31] Further, gibberellic acid and allogibberic acid modulate NF-κB signaling activity.[32,33]

pharbinilicic acid   allogibberic acid   gibberellic acid
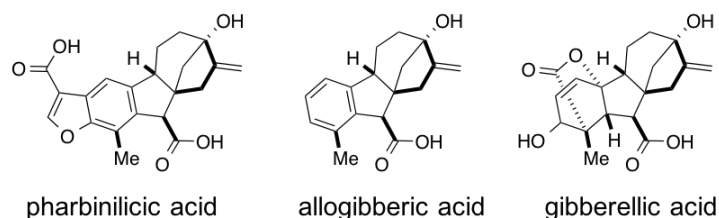
Figure 4.8 Gibberellins with biological activity in human cells Gibberelins are plant hormones that have been identified to have anti-tumor, anti-inflammatory, and analgesic activity in human cells.

Gibberellic acid activity against NF-κB

Annand and colleagues demonstrated that derivatives of gibberellic acid potently inhibited an NF-κB-driven luciferase reporter assay (Fig 4.9)[34]. While pharbinilic acid was inactive in this assay, the conversion of free carboxylic acids to methyl esters increased its activity. Alternatively, converting the carboxylic acid of gibberellic acid to a methyl ester did not enhance activity. Oxidation of the secondary alcohol on gibberellic acid methyl ester (GAme) to form

ketogibberelic acid methyl ester (kGAme) dramatically enhanced activity (Figure 4.9).[34]

Expression of MIP3α was also inhibited by treatment with kGAme.
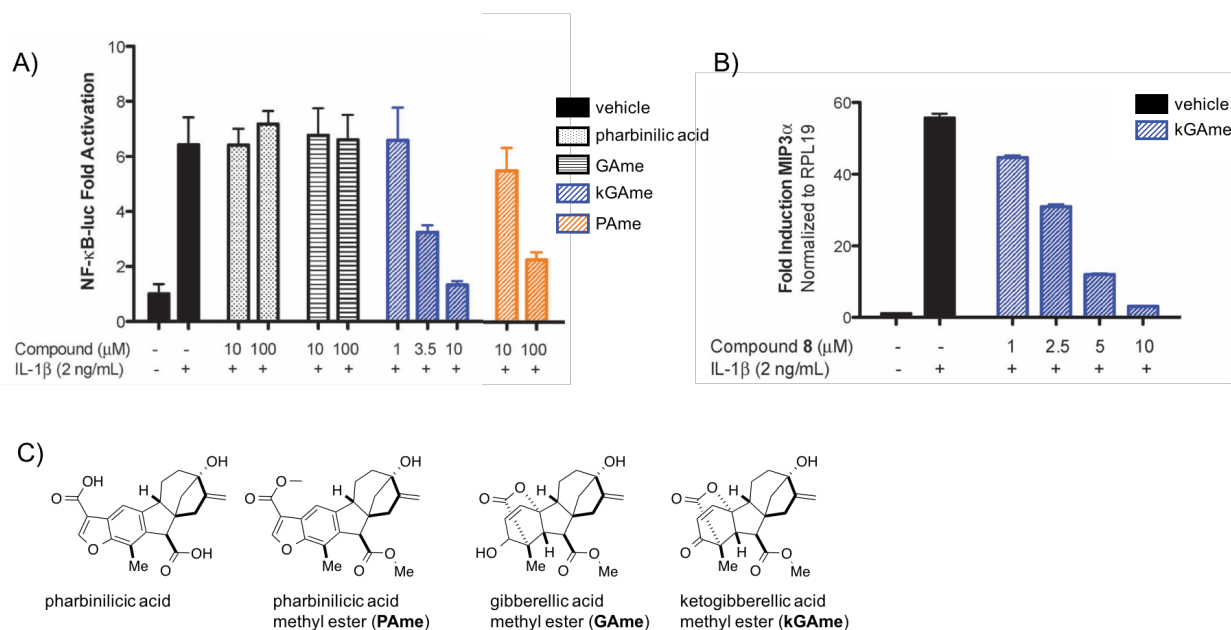
Figure 4.9 Ketogibberellic acid methyl ester inhibits NF-κB activity in cells A. The enone variant of gibberellic acid, kGAme, potently inhibits NF-κB driven luciferase activity. B. kGAme also potently inhibits the expression of NF-κB regulated MIP3α. C. Compounds tested. Modified from Annand et al., *Chem. Commun.* **2015**, 51, 8990-8993.[34]

Target Identification of ketogibberellic acid

Because of the potency with which kGAme inhibited NF-κB signaling, we were interested in uncovering the mechanism by which it acted on the NF-κB pathway and in identifying its protein binding partners. The oxidation of the secondary alcohol to the ketone formed an α,β unsaturated carbonyl which are known cysteine-targeting electrophiles. Thus, the enhanced activity of kGAme could be due to it now acting through a covalent mechanism. To identify protein binding partners, a biotinylated variant of kGAme was prepared (Fig 4.10). This

compound (kGAB) retained activity in an NF-κB driven luciferase reporter assay in HeLa cells, whereas the reduced biotinylated gibberellic acid (GAB) was not active.
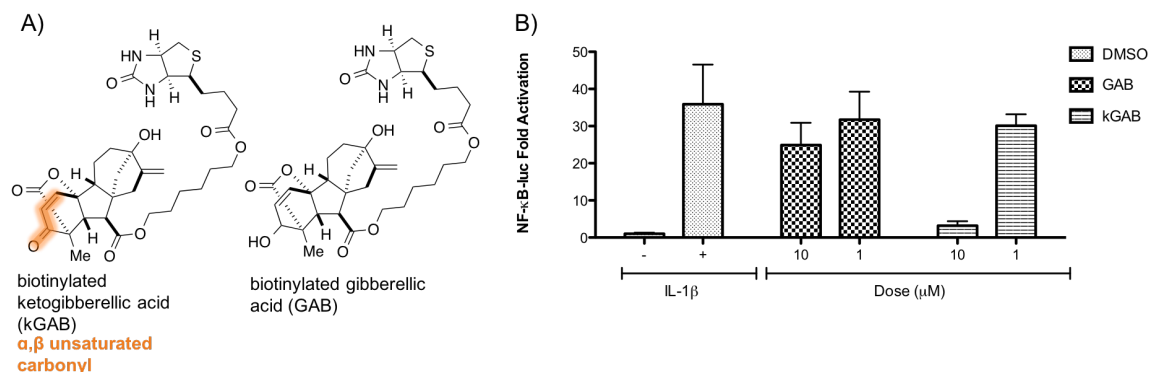
Figure 4.10 Biotinylated ketogibberelic acid methyl ester retains activity A. A biotinylated variant of ketogibberelic acid methyl ester (kGAB) was prepared via attachment of biotin at the carboxylic acid. Biotinylated gibberellic acid methyl ester (GAB) is inactive. B. Use of this molecule in an NF-κB reporter assay showed activity, whereas the reduced form GAB lacked activity. The error is SDOM, determined from three technical replicates. Performed by Andrew Henderson.

Biotin is a naturally occurring small-molecule with extremely high affinity for the protein, neutravidin.[35,36] This tight interaction enables pull-down of biotinylated proteins from cellular lysate via beads coated in immobilized neutravidin. Neutravidin will also pull down biotinylated small molecules and, by extension, proteins that have affinity for the active moiety of the biotinylated compound.[37] Our pull-down involved treatment of HeLa lysate pre-stimulated with IL-1β to induce NF-κB activity followed by exposure to magnetic neutravidin-beads. Following incubation of kGAB-treated lysate with neutravidin beads, beads are pelleted and washed to remove proteins not captured by kGAB. Captured proteins are then eluted from the beads via boiling where they can then be run on a gel and probed for NF-κB subunits via western blot (Fig 4.11).
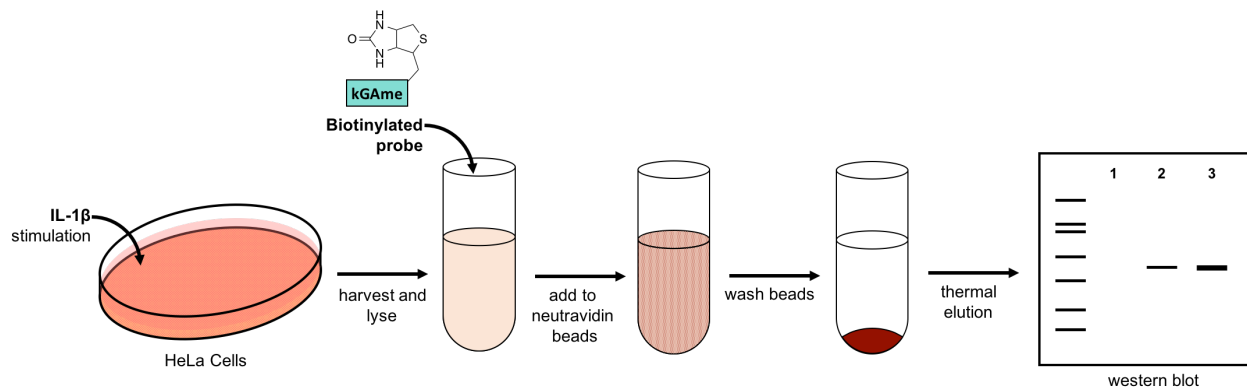
Figure 4.11 Schematic of pull-down with biotinylated kGAme HeLa lysates were stimulated with IL-1β followed by lysis to which the biotinylated probe was added. After incubation to allow molecule engagement with cellular targets, lysate was incubated with neutravidin-coated beads. Bead were washed post-incubation to remove non-interacting proteins followed by thermal elution. Eluted proteins were run on a gel and probed via western blot.

Pull-down with biotinylated ketogibberelic acid methyl ester (kGAB) showed interaction with several components of NF-κB signaling (Fig 4.12). Three of the core transcription factors: p65, RelB, and c-Rel were detected while p50 and p52 were not (Fig 4.12.b). p50 and p52, and their unprocessed forms (p105 and p100), differ from the other core NF-κB transcription factors in their lack of transcriptional activation domains offering a potential explanation for the absence of pull-down. Because all 5 proteins contain a nearly homologous Rel homology domain, this result would indicate that kGAme is targeting a location outside of this sequence. It is also possible that p65, RelB and c-Rel are being pulled down as part of a larger protein complex and thus are not true binding targets of kGAme. Efforts to probe pulled-down lysate with a streptavidin-HRP conjugate to detect the presence of the biotinylated molecule bound to p65, RelB, or c-Rel were inconclusive due to the large number of naturally occurring biotinylated proteins in cells.
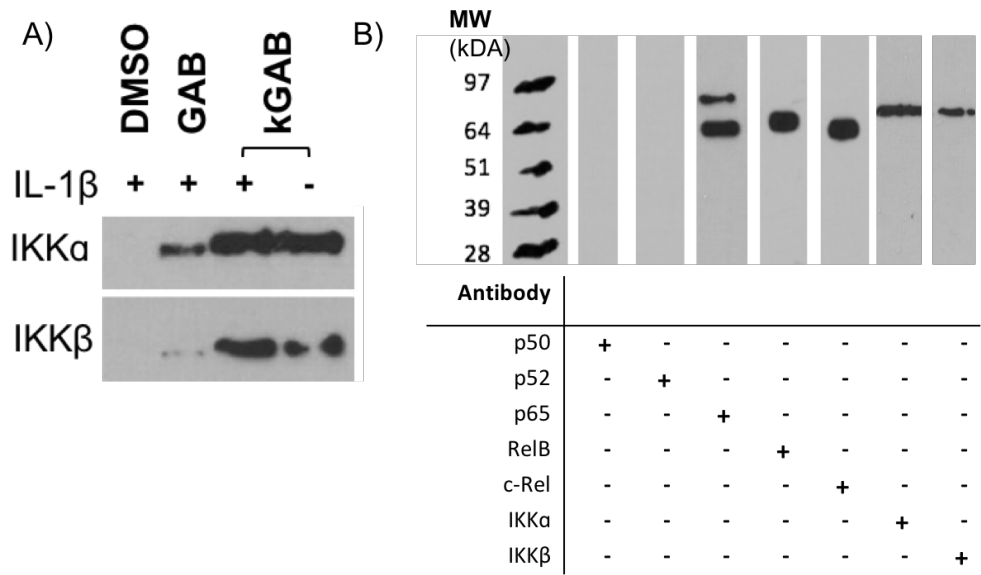
Figure 4.12 Biotinylated kGAme interacts with NF-κB components A. western blot of proteins pulled out of HeLa lysate by kGAB. Blot was probed by rabbit anti-IKKα or rabbit anti-IKKβ followed by anti-rabbit HRP. B. Summary of all pulled-down NF-κB proteins identified by western blot. Performed by Andrew Henderson.

To assess the possibility that kGAme did not directly target the core NF-kB transcription factors or simply interacted with multiple NF-κB components, we probed for NF-κB subunits in the upstream signaling pathway (Fig 4.12.a). Pull-down of IKKα and IKKβ, kinases involved in inactivating IκB proteins thus liberating NF-κB dimers and allowing nuclear translocation, was observed. Interestingly, the inactive compound, GAB, the reduced form of kGAB, which lacked cellular activity in luciferase reporter assays was able to pull-down IKKα and IKKβ albeit at much lower levels. Pull-down of proteins from DMSO-treated lysate was not observed.

Nuclear translocation of IKKα is inhibited by kGAme

Because of the detected pull-down of IKKα and IKKβ, both upstream partners of NF-κB signaling, we wondered if kGAme might target the IKK-NEMO complex, inactivate the kinase

activity of the IKKs, or inhibit NF-κB activity in some fashion that would otherwise disrupt nuclear translocation of the core NF-κB transcription factors. Nuclear translocation was assessed by treating HeLa cells with DMSO, GAme (inactive), and kGAme (active) followed by nuclear and cytosolic fractionation. These fractions were run on a gel and then probed for NF-κB components via western blot (Figure 4.13). IL-1β serves as a very useful control in this experiment as cells not stimulated with IL-1β showed very low levels of nuclear p65 and c-Rel whereas stimulated cells see a large increase in nuclear protein. In the absence of an activating signal, NF-κB transcription factors are sequestered in the cytosol, but there is low-level basal cycling of IκB phosphorylation allowing for NF-kβ translocation to the nucleus whereupon it is then rapidly shuttled out and bound again by IκB.[6,38] Nuclear translocation of p65 and c-Rel were not inhibited by kGAme, but translocation of IKKα was significantly attenuated. These results were confirmed by immunofluorescence microscopy. IL-1β stimulated nuclear transclocation of p65 of and IKKα whereas treatment with kGAme inhibited translocation of IKKα, but not p65 (Fig 4.14).

IKKα is largely considered a cytosolic protein so this result was surprising. However, studies have examined alternative nuclear roles of IKKα.[39] Nuclear accumulation of IKKα has been observed upon induction by TNFα, another stimulator of canonical NF-κB activity.[40,41] IKKα also contributes to tumor progression via phosphorylating CBP, switching CBP's binding preference from p53 to p65.[42]
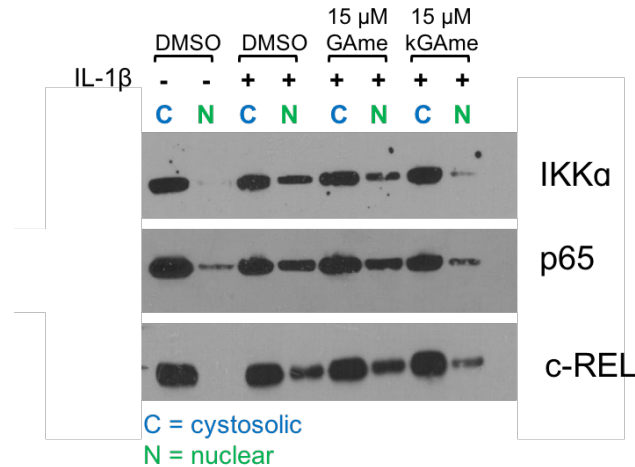
Figure 4.13 kGAme inhibits nuclear translocation HeLa cells treated with DMSO, GAme (inactive), and kGAme (active) followed by stimulation via IL-1β. Cell lysate was fractionated into nuclear and cystosolic components and probed with the indicated antibodies. Performed by Andrew Henderson.
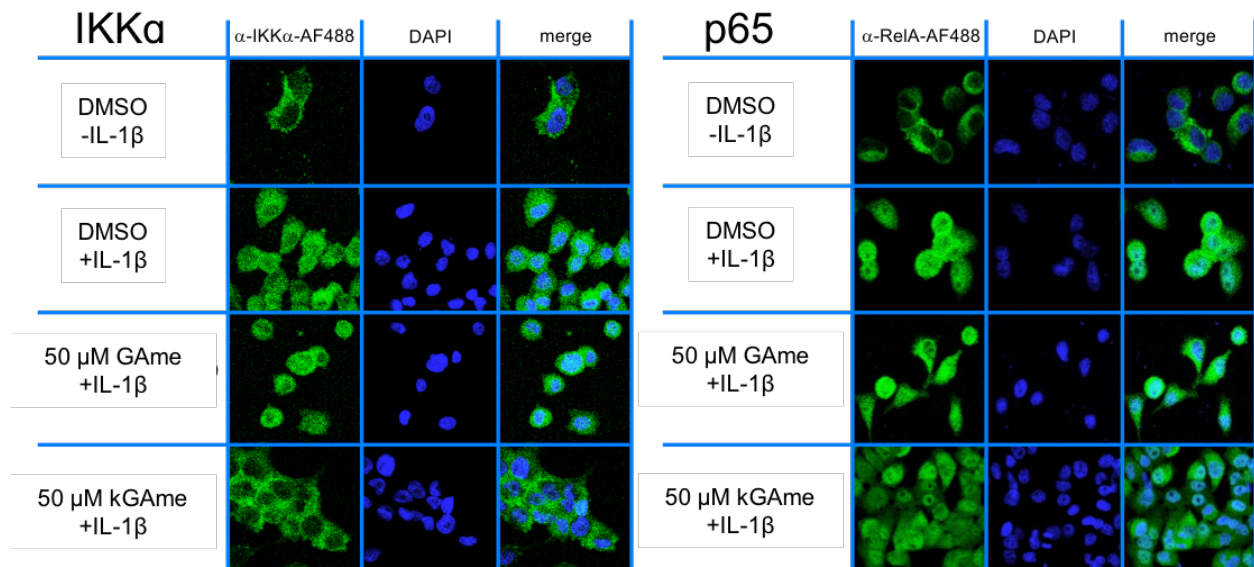
Figure 4.14 kGAme inhibits nuclear translocation via fluorescence microscopy HeLa cells treated with DMSO, GAme (inactive), and kGAme (active) followed by stimulation via IL-1β, as well as DMSO treated unstimulated cells, were permeabilized, fixed, and treated with antibodies against either IKKα or RelA (p65) followed by green fluorescent secondary antibodies were visualized by confocal microscopy. DAPI was used to stain for the nucleus to help identify the nuclear localization of IKKα and RelA (p65). Performed by James Annand.

Further efforts to determine the direct, covalent binding partners of kGAme are being assisted by the proteomics expertise of the Weerapana Lab at Boston College. Experiments with their lab are focused on determining the proteome-wide binding partners of kGAme. These efforts will enable further mechanistic studies to determine how kGAme inhibits NF-κB activity.

4.4 CONCLUSIONS

The NF-κB signaling cascade is reliant on multiple protein-protein interactions to regulate its function. We have demonstrated that targeting a protein-protein interaction essential for the activation of NF-κB transcription can specifically and potently inhibit NF-κB signaling. The synthetic loop replacement strategy employed to stabilize the hydrogen bond stabilized turn in the NBD peptide dramatically increased its stability and potency. Canonical NF-κB signaling is the pathway most often dysregulated in cancer and inflammatory diseases. The ability of NBD2 to selectively inhibit this pathway has therapeutic utility against these diseases while leaving the non-canonical and other alternate functions of NF-κB intact. An analysis of protein-protein interactions revealed that over 1400 PPIs are mediated by hot spots on loop-like structures distinct from α-helices or β-sheets.[43] Thus, this stabilization strategy may have applicability at other interfaces beyond the IKK complex.

Ketogibberellic acid methyl ester (kGAme) is a potent inhibitor of NF-kB transcriptional activity. We have shown that it does interact with core NF-κB transcription factors and the upstream IKKα and IKKβ kinases. These interactions occur either through direct covalent targeting of these proteins or the result of targeting a protein complex to which these proteins are associated. Refined proteomics methods will facilitate the identification of the direct protein

targets of kGAme. We also showed that kGAme inhibits nuclear translocation of the IKKα kinase while leaving the translocating ability of the core NF-κB subunits intact.

MATERIALS AND METHODS

Peptide Synthesis

Peptides used in this study All peptides were synthesized on CLEAR amide resin (Peptides International) using standard HBTU/HOBT/DIEA solid phase peptide synthesis protocols as previously described.[44] The TFA- cleaved peptides were precipitated with chilled diethyl ether, purified by reverse-phased HPLC using a 0.1% TFA/CH3CN solvent system and verified by electrospray mass spectrometry. Peptides containing allylglycine were incorporated using FMOC-L-allylglycine (AnaSpec) using the methods described above.

Ring closing metathesis (RCM) reaction

Metathesis reactions were carried out using a Biotage Initiator Microwave Reactor. Metathesis reaction of the dried bis-olefin resin bound FMOC-TALX(W/A)X(W/A)LQTE peptide of **NBD2** and **NBD3** were performed in a nitrogen atmosphere in a glass 10 mL microwave reaction vessel. The microwave vessel containing the dried bis-olefin resin bound peptide was charged with 2 mL of a dry, degassed solution of 0.4 M LiCl in DMF. The resin was allowed to swell with the DMF solution for 1 hour at which point a solution of Hoveyda-Grubbs Generation II catalyst (20 mol%) in dry dichloromethane (0.5 mL) was added to the swollen resin. The vessel containing the resin and catalyst was inserted in the microwave reactor (Biotage Initiator) and radiated (varying power) for 15 minutes at a constant temperature of 100 °C. After the resin had been subjected to microwave irradiation, the reaction mixture was transferred to a manual peptide synthesizer vessel and washed 3x with dichloromethane and 3x with dimethylformamide to remove any residual catalyst. The octalysine cell-penetrating peptide (8K) and diglycine linker (GG) were

added to the resin bound, metathesized peptide using the peptide synthesis methods described above.

NF-κB luciferase reporter assay

The NF-κB luciferase reporter plasmid carrying 6 tandem κB-sites (NF-κB-luc), CMV-β-Gal, and pBSSK were generously provided by Dr. Jorge Iñigues-Lluhí (The University of Michigan Pharmacology Department).[45] HeLa cells were grown in Dulbecco's Modified Eagle Medium (DMEM, Invitrogen) supplemented with 10% Fetal Bovine Serum (FBS). Cells were maintained in 5% CO_2 at 37 °C. For luciferase assays, $4x10^5$ cells were seeded in a 6-well dish and allowed to adhere for 16h. The media was removed and cells were transfected with 400 ng NF-κB-luc, 200 ng CMV- β-Gal, and 1,400 ng pBSSK using Lipofectamine 2000 (Life Technologies) according to manufacturer's instructions. After 4.5h, transfection solution was removed and replaced with DMEM containing 10% FBS. After 24h, cells were trysinized and resuspended in DMEM supplemented with 10% FBS and seeded into a 96-well plate at a density of $8x10^3$ cells per well. After 16h, media was removed and supplemented with Opti-Mem containing vehicle, SLR peptides, or biotinylated ketogibberellic acid delivered in DMSO (1% v/v) at the indicated concentrations. After transfected cells incubated with either vehicle or compound for 1h, cells were stimulated with either PBS or IL-1β at a final concentration of 2 ng/mL. After an additional 3h incubation time, media was removed and cells were lysed with 60 μL of passive lysis buffer (Promega). Luciferase and β- Galactosidase activities were determined as previously described.[46] NF-κB luciferase activity and response curve analysis was performed using GraphPad software. The mean and standard deviation were determined using three independent experiments.

Assaying inhibitory effects of SLR peptides against NF-κB endogenous gene expression

For endogenous gene expression analysis, 1×10^5 HeLa cells were seeded into a 24-well plate and allowed to adhere overnight. Media was removed and replaced with Opti-Mem media containing vehicle of SLR peptide delivered in DMSO (1% v/v) at the indicated concentrations. After cells were incubated with either vehicle of peptide for 1h, cells were stimulated with either PBS or IL-1β at a final concentration of 2 ng/mL. After 2h, the media was removed and total RNA was isolated using RNeasy Plus RNA isolation kits (Qiagen) according to manufacturer's protocol. Each RNA sample was used to synthesize cDNA using iScript cDNA synthesis kits (Bio-Rad). Real-Time Quantitative PCR (RT-qPCR) analysis was carried out in an Applied Biosystems StepPlusOne using SYBR green master mix and primers for human genes:

Gene	Primer Sequence
RPL19	F: 5'-ATGTATCACAGCCTGTACCTG-3'
	R: 5'-TTCTTGGTCTCTCTTCCTCCTTG-3'
MIP3α	F: 5'-TACTCCACCTCTGCGGCGAATCAGAA-3'
	R: 5'-GTGAAACCTCCAACCCCAGCAAGGTT-3'
IL-8	F: 5'-ATGACTTCCAAGCTGGCCGTGGCT-3'
	R: 5'- CTCAGCCCTCTTCAAAAACTTCT-3'
CyclinD1	F: 5'- ACAAACAGATCATCCGCAAACAC-3'
	R: 5'-TGTTGGGGGCTCCTCAGGTTC-3'

RT-qPCR analysis was carried out using the comparative C_T Method ($\Delta\Delta C_T$ Method) as previously described to estimate MIP3α mRNA levels relative to the reference RPL19 mRNA levels. The reported mean and standard deviation for MIP3α and IL-8 expression were determined using three technical replicates from one representative biological replicate.[47,48] Three biological replicates were performed. The reported mean and standard deviation for Cyclin D1 were determined using two technical replicates from one representative biological replicate. Two

biological replicates were performed.

Pull-downs with biotinylated ketogibberellic acid (kGAB)

HeLa cells were grown in Dulbecco's Modified Eagle Medium (DMEM, Invitrogen) supplemented with 10% Fetal Bovine Serum (FBS). Cells were maintained in 5% CO_2 at 37 °C. $2x10^6$ cells were plated into 2 wells of a 6-well plate and allowed to adhere for 16h. The media was then removed and cells were stimulated for 3 hrs in Opti-Mem containing either PBS or 2ng/mL IL-1β. Following stimulation, media was removed and cells were lysed with1 mL NP-40 lysis buffer (150 mM NaCl, 1% NP-40, 50 mM Tris pH 8.0 + 10 uL HALT (100X protease inhibitor)) at 4^0C on an orbital shaker for 15 mins. Lysate was moved to 1.5 mL Eppendorf tubes and centrifuged at 14,000 RPMs for at 4 °C for 20 minutes. Next, 100 μL lysate was treated with DMSO, kGAB, or inactive reduced biotinylated gibberellic acid (GAB) to a final concentration of 15 μM and allowed to mix in 1.5 mL Eppendorf tubes via end-over-end mixing for 2 hrs at room temperature. Meanwhile, 50 μL magnetic SpeedBead Neutravidin beads were washed 6 times with 1 mL of wash buffer (10 mM $NaPO_4$, 150 mM NaCl, 0.1% NP-40, 10% glycerol, pH 7.2) with the help of a magnetic rack to pellet beads between each wash. After 2 hrs, lysate was added to neutravidin beads and mixed by end over end tumbling for 16 hrs at 4 °C. Neutravidin beads were pelleted and lysate removed. The beads were next washed 6 x 1 mL with wash buffer. Next, 18.75 μL of 4X NuPAGE LDS sample buffer (Invitrogen) and 6.25 μL of 1 mM DTT was added to beads and beads were boiled at 95 °C for 10 minutes with vortexing every 3 minutes. Samples were then centrifuged for 1 minute at 14,000 RPM. Protein concentration was quantified via Pierce BCA assay and equal amounts of

protein loaded onto a 10% Bis-Tris SDS-PAGE gel. Western blotting was performed with the indicated NF-κB antibodies (Abcam; 1:10,000 dilution, biotin free).

Nuclear Translocation

HeLa cells were grown in Dulbecco's Modified Eagle Medium (DMEM, Invitrogen) supplemented with 10% Fetal Bovine Serum (FBS). Cells were maintained in 5% CO_2 at 37 °C. 5×10^7 cells were plated into 10 cm dishes and allowed to adhere for 16h. The media was removed and cells were treated with DMSO, 15 μM kGAme, or 15 μM GAme in Opti-mem for 1 hr. Cells were then stimulated for 3 hrs with either PBS or 2ng/mL IL-1β final concentration. Media was then removed and cells scraped off of plate with 5 mL cold PBS and pelleted via centrifugation at 2500 RPM for 5 minutes. The pellet was then washed with 2 mL cold buffer A (make fresh: 10 mM HEPES, 1. 5 mM $MgCl_2$, 10 mM KCl, 0.5 mM PMSF, 05 mM DTT). The pellet was then resuspended in 1 mL buffer A and pelleted via centrifugation in Eppendorf tubes at 1000 RPM. Supernatant was removed, and the pellet resuspended in Buffer B (15 μL/million cells; 10 mM HEPES, 1. 5 mM $MgCl_2$, 10 mM KCl, 0.5 mM PMSF, 05 mM DTT, 0.1 % NP-40) and incubated at 4 °C for 5 minutes on an orbital shaker. The tubes were then spun for 15 minutes at 13,000 RPM at 4 °C. The resulting supernatant is the cytosolic extract while the pellet is the nuclear fractions. The nuclear pellet was then resuspended in buffer C (10 μL/million cells; 20 mM HEPES, 0.42 NaCl, 1.5 mM $MgCl_2$, 0.2 mM EDTA, 25 % glycerol, 0.5 mM DTT, 0.5 mM PMSF) and incubated for 15 minutes at 4 °C with occasional vortexing. Samples were next spun for 15 minutes at 13,000 RPM at 4 °C. The supernatant (nuclear fraction) was transferred to a new tube and diluted with 60 μL/ million

cells with buffer D (20 mM HEPES, 50 mM Kcl, 0.2 mM EDTA, 20 % glycerol, 0.5 mM DTT, 0.5 mM

PMSF). Cytosolic and nuclear fractions were then quantified using a Pierce BCA assay and equal

protein concentrations were loaded onto an SDS-PAGE gel. Western blotting analysis was

completed with IKKα, IKKβ, and p65 antibodies (Abcam).

4.6 REFERENCES

1   Sen, R. & Baltimore, D. Multiple nuclear factors interact with the immunoglobulin enhancer sequences. *Cell* **46**, 705-716 (1986).
2   Hoesel, B. & Schmid, J. A. The complexity of NF-kappaB signaling in inflammation and cancer. *Molecular cancer* **12**, 86, doi:10.1186/1476-4598-12-86 (2013).
3   Ghosh, S., May, M. J. & Kopp, E. B. NF-kappa B and Rel proteins: evolutionarily conserved mediators of immune responses. *Annu Rev Immunol* **16**, 225-260, doi:10.1146/annurev.immunol.16.1.225 (1998).
4   Hansen, S. K., Baeuerle, P. A. & Blasi, F. Purification, reconstitution, and I kappa B association of the c-Rel-p65 (RelA) complex, a strong activator of transcription. *Molecular and cellular biology* **14**, 2593-2603 (1994).
5   Plaksin, D., Baeuerle, P. A. & Eisenbach, L. KBF1 (p50 NF-kappa B homodimer) acts as a repressor of H-2Kb gene expression in metastatic tumor cells. *J Exp Med* **177**, 1651-1662 (1993).
6   Hayden, M. S. & Ghosh, S. Shared principles in NF-kappaB signaling. *Cell* **132**, 344-362, doi:10.1016/j.cell.2008.01.020 (2008).
7   Pasparakis, M., Luedde, T. & Schmidt-Supprian, M. Dissection of the NF-kappaB signalling cascade in transgenic and knockout mice. *Cell Death Differ* **13**, 861-872, doi:10.1038/sj.cdd.4401870 (2006).
8   Perkins, N. D. Integrating cell-signalling pathways with NF-kappaB and IKK function. *Nature reviews. Molecular cell biology* **8**, 49-62, doi:10.1038/nrm2083 (2007).
9   Israel, A. The IKK complex, a central regulator of NF-kappaB activation. *Cold Spring Harb Perspect Biol* **2**, a000158, doi:10.1101/cshperspect.a000158 (2010).
10   Xiao, G., Fong, A. & Sun, S. C. Induction of p100 processing by NF-kappaB-inducing kinase involves docking IkappaB kinase alpha (IKKalpha) to p100 and IKKalpha-mediated phosphorylation. *The Journal of biological chemistry* **279**, 30099-30105, doi:10.1074/jbc.M401428200 (2004).
11   Gilmore, T. D. & Herscovitch, M. Inhibitors of NF-kappaB signaling: 785 and counting. *Oncogene* **25**, 6887-6899, doi:10.1038/sj.onc.1209982 (2006).
12   Miller, S. C. *et al.* Identification of known drugs that act as inhibitors of NF-kappaB signaling and their mechanism of action. *Biochem Pharmacol* **79**, 1272-1280, doi:10.1016/j.bcp.2009.12.021 (2010).
13   Zhang, Q., Lenardo, M. J. & Baltimore, D. 30 Years of NF-kappaB: A Blossoming of Relevance to Human Pathobiology. *Cell* **168**, 37-57, doi:10.1016/j.cell.2016.12.012 (2017).
14   Zandi, E., Rothwarf, D. M., Delhase, M., Hayakawa, M. & Karin, M. The IkappaB kinase complex (IKK) contains two kinase subunits, IKKalpha and IKKbeta, necessary for IkappaB phosphorylation and NF-kappaB activation. *Cell* **91**, 243-252 (1997).
15   Yamaoka, S. *et al.* Complementation cloning of NEMO, a component of the IkappaB kinase complex essential for NF-kappaB activation. *Cell* **93**, 1231-1240 (1998).

16   Hinz, M. & Scheidereit, C. The IkappaB kinase complex in NF-kappaB regulation and beyond. *EMBO Rep* **15**, 46-61, doi:10.1002/embr.201337983 (2014).

17   Rushe, M. *et al.* Structure of a NEMO/IKK-associating domain reveals architecture of the interaction site. *Structure* **16**, 798-808, doi:10.1016/j.str.2008.02.012 (2008).

18   May, M. J. *et al.* Selective inhibition of NF-kappaB activation by a peptide that blocks the interaction of NEMO with the IkappaB kinase complex. *Science* **289**, 1550-1554 (2000).

19   Strickland, I. & Ghosh, S. Use of cell permeable NBD peptides for suppression of inflammation. *Ann Rheum Dis* **65 Suppl 3**, iii75-82, doi:10.1136/ard.2006.058438 (2006).

20   Rehman, K. K. *et al.* Protection of islets by in situ peptide-mediated transduction of the Ikappa B kinase inhibitor Nemo-binding domain peptide. *The Journal of biological chemistry* **278**, 9862-9868, doi:10.1074/jbc.M207700200 (2003).

21   Delfin, D. A. *et al.* Improvement of cardiac contractile function by peptide-based inhibition of NF-kappaB in the utrophin/dystrophin-deficient murine model of muscular dystrophy. *J Transl Med* **9**, 68, doi:10.1186/1479-5876-9-68 (2011).

22   Garber, S. B., Kingsbury, J. S., Gray, B. L. & Hoveyda, A. H. Efficient and recyclable monomeric and dendritic Ru-based metathesis catalysts. *Journal of the American Chemical Society* **122**, 8168-8179, doi:DOI 10.1021/ja001179g (2000).

23   Bruno, P. A., Morriss-Andrews, A., Henderson, A. R., Brooks, C. L., III & Mapp, A. K. A Synthetic Loop Replacement Peptide That Blocks Canonical NF-kappaB Signaling. *Angewandte Chemie* **55**, 14997-15001, doi:10.1002/anie.201607990 (2016).

24   Kwon, J. H. *et al.* ESE-1, an enterocyte-specific Ets transcription factor, regulates MIP-3alpha gene expression in Caco-2 human colonic epithelial cells. *The Journal of biological chemistry* **278**, 875-884, doi:10.1074/jbc.M208241200 (2003).

25   Kunsch, C., Lang, R. K., Rosen, C. A. & Shannon, M. F. Synergistic transcriptional activation of the IL-8 gene by NF-kappa B p65 (RelA) and NF-IL-6. *J Immunol* **153**, 153-164 (1994).

26   Waugh, D. J. & Wilson, C. The interleukin-8 pathway in cancer. *Clinical cancer research : an official journal of the American Association for Cancer Research* **14**, 6735-6741, doi:10.1158/1078-0432.CCR-07-4843 (2008).

27   Guttridge, D. C., Albanese, C., Reuther, J. Y., Pestell, R. G. & Baldwin, A. S., Jr. NF-kappaB controls cell growth and differentiation through transcriptional regulation of cyclin D1. *Molecular and cellular biology* **19**, 5785-5799 (1999).

28   Daviere, J. M. & Achard, P. Gibberellin signaling in plants. *Development* **140**, 1147-1151, doi:10.1242/dev.087650 (2013).

29   Miklussak, S. *et al.* Application of gibberelic acid (GA) alone or together wih cytostatics in treatment of lung cancer. *Neoplasma* **27**, 203-209 (1980).

30   Muthuraman, P. & Srikumar, K. A comparative study on the effect of homobrassinolide and gibberellic acid on lipid peroxidation and antioxidant status in normal and diabetic rats. *J Enzyme Inhib Med Chem* **24**, 1122-1127, doi:10.1080/14756360802667563 (2009).

31   Kim, K. H. *et al.* Pharbinilic acid, an allogibberic acid from morning glory (Pharbitis nil). *J Nat Prod* **76**, 1376-1379, doi:10.1021/np400326e (2013).

32   KOEHLER, A., N. (129 Franklin Street, #405Cambridge, MA, 02139, US). METHODS FOR MODULATING NF-KB USING GIBBERELLINS. (2010).

33   Reihill, J. A. *et al.* Induction of the inflammatory regulator A20 by gibberellic acid in airway epithelial cells. *Br J Pharmacol* **173**, 778-789, doi:10.1111/bph.13200 (2016).

34   Annand, J. R., Bruno, P. A., Mapp, A. K. & Schindler, C. S. Synthesis and biological evaluation of pharbinilic acid and derivatives as NF-kappaB pathway inhibitors. *Chem Commun (Camb)* **51**, 8990-8993, doi:10.1039/c5cc02918j (2015).

35   Green, N. M. Avidin. 3. The Nature of the Biotin-Binding Site. *The Biochemical journal* **89**, 599-609 (1963).

36   Marttila, A. T. *et al.* Recombinant NeutraLite avidin: a non-glycosylated, acidic mutant of chicken avidin that exhibits high affinity for biotin and low non-specific binding properties. *FEBS letters* **467**, 31-36 (2000).

37   McFedries, A., Schwaid, A. & Saghatelian, A. Methods for the elucidation of protein-small molecule interactions. *Chemistry & biology* **20**, 667-673, doi:10.1016/j.chembiol.2013.04.008 (2013).

38   Ben-Neriah, Y. Regulatory functions of ubiquitination in the immune system. *Nat Immunol* **3**, 20-26, doi:10.1038/ni0102-20 (2002).

39   Espinosa, L., Bigas, A. & Mulero, M. C. Alternative nuclear functions for NF-kappaB family members. *Am J Cancer Res* **1**, 446-459 (2011).

40   Anest, V. *et al.* A nucleosomal function for IkappaB kinase-alpha in NF-kappaB-dependent gene expression. *Nature* **423**, 659-663, doi:10.1038/nature01648 (2003).

41   Yamamoto, Y., Verma, U. N., Prajapati, S., Kwak, Y. T. & Gaynor, R. B. Histone H3 phosphorylation by IKK-alpha is critical for cytokine-induced gene expression. *Nature* **423**, 655-659, doi:10.1038/nature01576 (2003).

42   Huang, W. C., Ju, T. K., Hung, M. C. & Chen, C. C. Phosphorylation of CBP by IKKalpha promotes cell growth by switching the binding preference of CBP from p53 to NF-kappaB. *Molecular cell* **26**, 75-87, doi:10.1016/j.molcel.2007.02.019 (2007).

43   Gavenonis, J., Sheneman, B. A., Siegert, T. R., Eshelman, M. R. & Kritzer, J. A. Comprehensive analysis of loops at protein-protein interfaces for macrocycle design. *Nature chemical biology* **10**, 716-722, doi:10.1038/nchembio.1580 (2014).

44   Wu, Z. *et al.* Targeting the transcriptional machinery with unique artificial transcriptional activators. *Journal of the American Chemical Society* **125**, 12390-12391, doi:10.1021/ja036685v (2003).

45   Hojfeldt, J. W. *et al.* Bifunctional ligands allow deliberate extrinsic reprogramming of the glucocorticoid receptor. *Mol Endocrinol* **28**, 249-259, doi:10.1210/me.2013-1343 (2014).

46   Iniguez-Lluhi, J. A. & Pearce, D. A common motif within the negative regulatory regions of multiple factors inhibits their transcriptional synergy. *Molecular and cellular biology* **20**, 6040-6050 (2000).

47   Livak, K. J. & Schmittgen, T. D. Analysis of relative gene expression data using real-time quantitative PCR and the 2(-Delta Delta C(T)) Method. *Methods* **25**, 402-408, doi:10.1006/meth.2001.1262 (2001).

48   Schmittgen, T. D. & Livak, K. J. Analyzing real-time PCR data by the comparative C(T) method. *Nat Protoc* **3**, 1101-1108 (2008).

Chapter 5

CONCLUSIONS

5.1 CONCLUSIONS

Transcriptional activation hinges on the arrangement and coordination of dozens of proteins to accurately transcribe the genetic material required for healthy cellular function. This complex protein-protein interaction network can accurately integrate cellular signals into the recruitment and assembly of the transcriptional machinery at the appropriate locations on DNA to express genes relevant to that specific cellular process. Critical hubs in these activation pathways are transcriptional coactivators. Coactivators are linchpins between DNA-bound transcriptional activators and the rest of the preinitiation complex necessary for gene expression.[1,2] Transcriptional activation can become dysregulated through many different avenues including overexpression, chromosomal translocations, and mutations to the activator itself or one of its key regulatory partners. As such, therapeutic targeting of the protein-protein interactions (PPI) between activators and coactivators represent a promising strategy for correcting aberrant transcriptional activity in a variety of diseases ranging from developmental disorders to cancers to metabolic diseases.[3] These PPI are historically challenging small molecule targets because of the large surface area and structural plasticity that are hallmarks to many activator-coactivator interactions.[4,5] As a result, successful targeting of these PPI depend on the

use of novel small molecule discovery strategies coupled with studies that enhance our mechanistic understanding of individual activator-coactivator interactions.

In this work, we have sought to mechanistically define activator binding to the Activator Interaction Domain (AcID) of Med25, which is a structurally unique activator binding domain (ABD) within the important Mediator coactivator complex, with the ultimate goal of developing novel small molecule inhibitors of these PPI.[6] The AcID domain is a rare fold known to occur in only one other human protein. A diverse group of transcriptional activators contact Mediator via the AcID domain, including activators that display AcID-dependent expression of genes implicated in a number of different diseases including many cancers.[7,8] As such, molecules capable of modulating these protein interactions have potential therapeutic utility. In order to guide our small molecule development efforts, we first sought to define mechanistic details of activator-AcID interactions. Because of its divergent structure, we sought to compare mechanistic details of AcID-activator binding to the more common helical ABDs like KIX, Taz1, and Taz2 of CBP.

Several groups have previously examined the interactions of VP16 and ERM to AcID.[8-10] These studies revealed the presence of two binding surfaces on opposites faces of AcID, but there were many outstanding questions surrounding the interactions of these activators with AcID including exact binding orientations, the existence of an allosteric network within the AcID domain, and the kinetics of activator-AcID complex formation. Using NMR, we demonstrated that there is considerable conformational heterogeneity in activator binding to AcID. AcID is like other ABDs in that it is very conformationally dynamic. This structural plasticity allows AcID to interact with distinct activators using a shared group of amino acids. The N-terminal TAD of VP16 and

ERM both target the H1 face of AcID using an overlapping binding site. The C-terminal TAD of VP16, ATF6α, and CBP all bind the H2 face of AcID. Although both faces of AcID are used for binding by more than one activator, there are differences in the perturbation patterns induced by each activator sequence. This conformational heterogeneity is similar to the distinct complexes observed with different activators bound to the same binding site on KIX.[11,12] This suggests that it may be possible to selectively inhibit binding of one activator while preserving the binding ability of another activator by using a small molecule capable of inducing and stabilizing individual conformations of AcID.

Because of the structural similarities between the two AcID binding surfaces it is not surprising that activators would display binding affinity for both surfaces of AcID.[6] This makes interpretation of different experiments looking at activator-AcID binding difficult to interpret. To address this and to help map the binding interaction of VP16 with AcID, we utilized a covalent tethering strategy to form covalent VP16-AcID complexes.[13] These complexes are useful because the binding location of the activator is known with much higher certainty. In experiments with a panel of VP16 αH1 disulfide-capped cysteine mutants we showed that activator complexes can be formed at the H1 face using a native cysteine. In the 14 peptides tested, the labeling efficiency increased from the N- to C-terminus with a dramatic increase to full labeling for residues 450-454. This suggests that VP16 binds Med25 with a strong orientational preference and has added to our understanding of how VP16 bridges AcID to simultaneously bind both surfaces of AcID.

Experiments with a tethered construct of VP16 that approximates full length VP16 (VP16 L2L3) in terms of binding affinity and binding location showed that the disulfide tether does not drastically change the binding character of VP16 as assessed by NMR. Tethered VP16 αH1 inhibits

activator binding to Med25, but to a lower degree than might be expected from a peptide that is making such extensive contacts with AcID. This provided confirmation that VP16 can bind both faces of AcID to some degree. As the length of the tethered VP16 construct was increased, inhibition of activator binding to both faces of AcID increased, which suggested that as both binding surfaces of AcID were progressively occluded by the tethered peptide, this promiscuous dual site binding behavior was reduced.

Transient kinetic analysis of activator binding can reveal discrete kinetic parameters guiding activator-coactivator complex formation that are invisible to equilibrium binding experiments. VP16 association to AcID displayed biphasic kinetics consistent with an initial collision followed by a unimolecular conformational change similar to the association of c-Myb to KIX.[14] Dissociation experiments also were consistent with a biphasic mechanism of association followed by a conformational change.

A distinguishing feature of KIX binding is the allosteric network linking the two isolated binding sites. It has been demonstrated that activator binding at one surface can induce positive cooperativity at the opposite binding location.[15-17] Tethering VP16 αH1 to the H1 surface of AcID induced structural perturbations at the H2 face, indicating the presence of some conformational change network linking the two surfaces that can be accessed by transcriptional activators. When this tethered VP16 αH1-AcID complex was used in dissociation kinetics experiments, a 20% reduction in k_{off} was observed for VP16 H2 binding at the H2 face of AcID compared to H2 dissociation from wt Med25 AcID. This is the first demonstration of an allosteric network in AcID capable of producing positive binding cooperativity in a ternary activator-AcID complex.

Taken together, the data revealed that although Med25 AcID has a very different structure from other characterized ABDs, certain mechanistic features are conserved across domains. Like other ABDs, AcID displays conformational heterogeneity when bound to activators of divergent sequences. There is also a communication network that links the two binding surfaces of AcID, promoting positive cooperativity in activator binding similar to activator-KIX ternary complexes. The association and dissociation kinetics of activator-AcID complexes are consistent with a biphasic mechanism of a binding event followed by a conformational change, and the association of VP16 to AcID is roughly 100-fold faster than any KIX-activator association reported. These mechanistic details have enhanced our understanding of AcID biochemistry and have guided our efforts to develop covalent small molecule modulators of AcID-activator complexes.

Small molecules capable of modulating individual activator-AcID complexes are valuable mechanistic tools that will aid the development of molecules with therapeutic utility. We have shown that the two native cysteines on the H1 face of AcID can be alkylated by small molecules while a third AcID cysteine is non-reactive. Further, these two cysteines are functionally relevant. 4-Iodoacetamidosalicylic acid readily alkylates both H1 face cysteines and inhibits binding of VP16 and ERM binding. The presence of both hydrophobicity from the benzyl group and negative charge from the carboxylic acid were necessary for labeling and inhibition. This molecule demonstrated that targeting AcID at these native cysteines can perturb activator binding to AcID.

The inhibition demonstrated by 4-iodoacetamdiosalicylic acid prompted us to perform a Tethering screen to identify site-selective covalent molecules targeting AcID in collaboration with Prof. Jim Wells at UCSF. Tethering has a proven track record of identifying molecules capable of

targeting adaptable protein-protein interfaces.[18,19] We utilized an FP-based tethering format whereby we first assessed the ability of each molecule in the library to inhibit ERM binding followed by a secondary screen to assess the degree of covalent labeling of the most potent inhibitors. This format identified molecules that were effective inhibitors of ERM binding but lacked covalent labeling as well as molecules that efficiently labeled AcID. A third class of molecules, united by the presence of a nipecotic acid moiety, were effective inhibitors of ERM and labelers of AcID.

A fragment, A6, was identified as possessing both inhibitory and covalent character. This compound targeted C506 on AcID, but was unable to fully label AcID while still a disulfide. Converting the A6 disulfide to an iodoacetamide produced an A6 derivative that efficiently labeled C506, while not alkylating C497. This iodoacetamide variant of A6 induced both local and distal conformational changes in AcID in a manner similar to the covalent VP16 αH1 peptide.

Converting A6 from a reversible disulfide to an irreversible iodoacetamide enabled us to test its cellular activity. The expression of the ER chaperone HSPA5 is ATF6α-dependent. Treatment of HeLa cells under stressed conditions with A6 resulted in dose-dependent inhibition of HSPA5 expression suggesting that this molecule can target AcID-activator complexes in the cellular environment.

Targeting activator-coactivator interactions is a challenge. Transcriptional activation is reliant on a network of protein-protein interactions to integrate cellular signals into the expression of target genes. Within this network are other PPIs that can be exploited as a means to regulate or correct aberrant gene expression. The NF-κB pathway is illustrative of a disease-associated transcriptional signaling pathway and notable in its complexity. Proteins involved in

this pathway participate in both canonical and non-canonical NF-κB signaling paths as well as unrelated signaling cascades. The development of a potent cell-active probe capable of selectively inhibiting a single NF-κB signaling pathway would be a valuable mechanistic probe.

Canonical NF-κB signaling is activated by the heterotetrameric IKK kinase complex. Stimulation of cells by cytokines like IL-1β activate this complex which in turns promotes translocation of NF-κB transcription factors into the nucleus. Inhibiting the kinase activity of the IKK complex has been demonstrated to down-regulate NF-κB dependent gene expression. Prior structural analysis of the IKK complex revealed that IKKs interact with NEMO, via a hydrogen bond stabled loop critical for binding. We describe the use of ring closing metathesis to replace this hydrogen bond stabilized loop in the NEMO binding domain with a carbon-carbon bond. This synthetic loop replacement variant of the NBD peptide is 10 times more potent than a non-stabilized NBD peptide and is resistant to proteolytic degradation. Importantly, we show that the NBD2 peptide can inhibit genes regulated by canonical NF-κB signaling but not cyclinD1, the expression of which is regulated via the non-canonical NF-κB pathway. Thus, NBD2 is a cell-active protein-protein inhibitor capable of pathway-specific regulation of transcription.

We also describe the mechanistic characterization of a recently described inhibitor of NF-κB activity, ketogibberellic acid methyl ester (kGAme).[20] We show that this molecule interacts with NF-kB transcriptional activators p65, RelB and c-Rel, but not the transcriptional repressors p50 or p52 via cellular pull-down experiments with a biotinylated variant of kGAme. This biotinylated molecule also pulls-down the IKKα and IKKβ kinases that regulate NF-κB activation. We also show that nuclear translocation of IKKα is inhibited by kGAme while the translocation of p65 is left intact. The nuclear function of IKKα is less well characterized and future work will be

146

focused on validating this observation and linking it to the activity of kGAme[21,22]. We are also

collaborating with Prof. Eranthie Weerapana's lab at Boston College to assess the proteome-wide

binding partners of kGAme via their proteomic expertise.

5.2 FUTURE DIRECTIONS

Next generation covalent small-molecule modulators of AcID structure

The initial Tethering screen conducted in collaboration with the Wells Lab at UCSF utilized

fluorescence polarization as our initial read-out to identify small molecule inhibitors of activator

binding to AcID. This format was successful in identifying the compound A6 which modulates

activator interactions with AcID. Unfortunately, fully labeling Med25 with this molecule or several

other hits from the screen was not possible under conditions where the protein remained folded.

Only after converting A6 from a disulfide to an iodoacetamide were we able to homogenously

label AcID. Mass spectrometry was only used to assess the extent of labeling for compounds that

inhibited activator binding and it was revealed that many of these compounds were non-covalent

(and thus possible artifacts) or only weakly covalent. With these results in mind, we propose that

a full MS-based Tethering screen may yield more effective compounds. When A6 was tethered

to AcID we saw that it did induce structural perturbations and binding cooperativity at the

opposite binding surface. We think we are more likely to find molecules that can capture and

stabilize unique conformations of AcID if we use labeling-efficiency as our primary read out.

In chapter 3 we also show that when 4-iodoacetamidosalicylic acid was alkylated to

Med25, the greatest inhibitory contribution came from C497. C497 is positioned directly within

the H1 face of AcID whereas C506 is positioned on the flexible loop at the bottom of the binding

site. Our NMR analysis suggests that the region immediately surrounding C497 is used for binding

of both ERM and VP16 and thus identifying molecules that specifically target C497 instead of C506 would be useful. To identify compounds capable of targeting this site, we will be conducting an MS-based Tethering screen where we screen the entire 1600 compound library against Med25 followed by a secondary screen of the strongest hits against a Med25 C506A variant to identify fragments that solely target the C497 position.

Regardless of binding site, we are interested in molecules that can efficiently covalently label AcID. Those compounds will be used in NMR, kinetics and direct binding experiments to assess their function. Promising compounds will also be converted to alklyators and used in cell-based assays.

An MS-based Tethering screen of AcID

In collaboration with the Wells Lab at UCSF 1600 compounds were screened against Med25 and tethering efficiency was determined via MS. Initially, Med25 was screened in the presence of 100 equivalents of each disulfide and 1000 equivalents of β-mercaptoethanol (1 μM Med25, 100 μM molecule, 1 mM β-ME). Based on this initial screen, 24 fragments were identified that had labeling efficiencies greater than 3 standard deviations above the mean labeling efficiency (15 % labeled). These 24 compounds were then validated by screening against Med25 at 100 μM β-ME followed by screening against Med25 C506A at 100 μM β-ME (Fig 5.1).

In the initial screen at 1 mM β-ME, two compounds displayed strong bis-labeling (2 cysteines labeled) while at 100 μM β-ME, additional compounds demonstrated enhanced bis-labeling. Following counter screening with Med25 C506A, compounds 10 and 15 displayed the strongest tethering efficiency for C497.

In contrast to the FP Tethering screen reported in chapter 3, compounds were identified that displayed much higher labeling efficiencies suggesting that the MS-based screening format will lead to better overall structural modulators and stabilizers of AcID. Further work will look at the ability of each of these molecules to inhibit activator binding, modulate AcID structure, and alter the binding kinetics of activators in binary or ternary complexes with AcID.

	Original Screen (100 µM Fragment, 1 mM BME)			Follow-up (100 µM Fragment, 100 µM BME)			C506A Follow-up (100 µM Fragment, 100 µM BME)		
Compound #	% 1xTethered	% 2xTethered	Total Tethered	% 1xTethered	% 2xTethered	Total Tethered	% 1xTethered	% 2xTethered	Total Tethered
1	48	18	66	35	21	56	17	1	18
2	43	0	43	73	2	75	3	0	3
3	39	9	48	45	13	58	8	2	10
4	29	0	29	68	2	70	3	0	3
5	23	0	23	74	1	75	1	0	1
6	22	1	23	39	21	60	13	0	13
7	22	9	31	24	18	42	11	12	23
8	21	0	21	49	0	49	0	0	0
9	21	0	21	41	0	41	2	0	2
10	21	42	63	15	8	23	43	17	60
11	20	0	20	59	3	62	4	0	4
12	18	0	18	49	0	49	1	0	1
13	18	0	18	49	1	50	1	0	1
14	18	0	18	52	1	53	1	0	1
15	18	8	26	23	10	33	18	14	32
16	17	0	17	47	0	47	1	0	1
17	17	0	17	46	0	46	1	0	1
18	17	5	22	15	4	19	11	3	14
19	16	1	17	40	11	51	7	0	7
20	16	0	16	51	5	56	6	0	6
21	16	1	17	32	1	33	1	0	1
22	16	0	16	75	0	75	1	0	1
23	16	1	17	47	16	63	8	0	8
24	16	0	16	47	13	60	17	0	17

Figure 5.1 MS-based Tethering screen results The 1600 compound Well's Library was first screened against Med25 (1 µM protein) at 1 mM β-ME and identified 24 compounds that had a labeling efficiency above 15 % (> 3 standard deviations above the mean). These 24 hits were validated by re-screening at 100 µM β-ME and finally by screening against Med25 C506A.

One of the most exciting features of the 1-10 molecule that targeted the KIX domain was its ability to order and stabilize the domain, which facilitated the first crystal structure of KIX. Additionally, this molecule was an effective allosteric regulator of activator-KIX interactions. A screening format that looked at the ability of fragments to stabilize AcID could be a way to specifically identify molecules that possess these traits. ThermoFluor is a high-throughput and

efficient way to assess the thermal stability of proteins and has been extensively used to screen small molecule libraries.[23,24] A ThermoFluor-monitored screen of the Tethering library or another covalent small molecule fragment library would be an effective way of identifying stabilizers of AcID.

We have attempted to crystallize AcID in covalent complex with VP16 and with the small molecule A6. These efforts have thus far been unsuccessful, but the identification of ligands that can induce structural stabilization of AcID, similar to the effect of 1-10 on KIX, may capture a conformation of AcID that can be crystallized.

Cellular assessment of AcID-activator covalent inhibitors

We would like to assess the ability of covalent inhibitors identified from the Tethering screen reported in chapter 3 and molecules identified in future screens to both covalently engage Med25 in cells and to inhibit gene expression regulated by AcID-activator interactions. Molecules with promising cellular activity can modified through attachment of a biotinylated linker and used in pull-down experiments to verify that Med25 is targeted. This can be further confirmed via proteomics to assay the proteome-wide binding profile of these covalent molecules. More significantly, we are interested in the ability of these molecules to inhibit PEA3-dependent expression of cancer associated genes including the matrix metalloproteinases MMP-1, MMP-2, and MMP-9.[25-27] Silencing of Med25 via siRNA or squelching via overexpression of Med25 reduced PEA3-dependent transcription in cells.[7] The effects that these molecules exert on the expression of these genes will be monitored via RT-qPCR. Additionally, we have demonstrated that ATF6α targets the opposite binding surface of AcID. Monitoring the expression of ATF6α-mediated genes, including the ER chaperone HSPA5, would be an interesting way to assess the

functional consequences of allosteric changes induced in the H2 face via small molecules targeting the H1 face of AcID.[28-30]

5.3 REFERENCES

1   Allen, B. L. & Taatjes, D. J. The Mediator complex: a central integrator of transcription. *Nature reviews. Molecular cell biology* **16**, 155-166, doi:10.1038/nrm3951 (2015).
2   Goodman, R. H. & Smolik, S. CBP/p300 in cell growth, transformation, and development. *Genes & development* **14**, 1553-1577 (2000).
3   Mapp, A. K., Pricer, R. & Sturlis, S. Targeting transcription is no longer a quixotic quest. *Nature chemical biology* **11**, In Press (2015).
4   Cesa, L. C., Mapp, A. K. & Gestwicki, J. E. Direct and Propagated Effects of Small Molecules on Protein-Protein Interaction Networks. *Front Bioeng Biotechnol* **3**, 119, doi:10.3389/fbioe.2015.00119 (2015).
5   Thompson, A. D., Dugan, A., Gestwicki, J. E. & Mapp, A. K. Fine-tuning multiprotein complexes using small molecules. *ACS chemical biology* **7**, 1311-1320, doi:10.1021/cb300255p (2012).
6   Bontems, F. *et al.* NMR structure of the human Mediator MED25 ACID domain. *Journal of structural biology* **174**, 245-251, doi:10.1016/j.jsb.2010.10.011 (2011).
7   Verger, A. *et al.* The Mediator complex subunit MED25 is targeted by the N-terminal transactivation domain of the PEA3 group members. *Nucleic acids research* **41**, 4847-4859, doi:10.1093/nar/gkt199 (2013).
8   Landrieu, I. *et al.* Characterization of ERM transactivation domain binding to the ACID/PTOV domain of the Mediator subunit MED25. *Nucleic acids research* **43**, 7110-7121, doi:10.1093/nar/gkv650 (2015).
9   Vojnic, E. *et al.* Structure and VP16 binding of the Mediator Med25 activator interaction domain. *Nature structural & molecular biology* **18**, 404-409, doi:10.1038/nsmb.1997 (2011).
10   Milbradt, A. G. *et al.* Structure of the VP16 transactivator target in the Mediator. *Nature structural & molecular biology* **18**, 410-415, doi:10.1038/nsmb.1999 (2011).
11   Law, S. M., Gagnon, J. K., Mapp, A. K. & Brooks, C. L., III. Prepaying the entropic cost for allosteric regulation in KIX. *Proceedings of the National Academy of Sciences of the United States of America*, doi:10.1073/pnas.1405831111 (2014).
12   Thakur, J. K., Yadav, A. & Yadav, G. Molecular recognition by the KIX domain and its role in gene regulation. *Nucleic acids research* **42**, 2112-2125, doi:10.1093/nar/gkt1147 (2014).
13   Sadowsky, J. D. *et al.* Turning a protein kinase on or off from a single allosteric site via disulfide trapping. *Proceedings of the National Academy of Sciences of the United States of America* **108**, 6056-6061, doi:10.1073/pnas.1102376108 (2011).
14   Shammas, S. L., Travis, A. J. & Clarke, J. Remarkably fast coupled folding and binding of the intrinsically disordered transactivation domain of cMyb to CBP KIX. *J Phys Chem B* **117**, 13346-13356, doi:10.1021/jp404267e (2013).
15   Shammas, S. L., Travis, A. J. & Clarke, J. Allostery within a transcription coactivator is predominantly mediated through dissociation rate constants. *Proceedings of the National Academy of Sciences of the United States of America* **111**, 12055-12060, doi:10.1073/pnas.1405815111 (2014).

16   Wang, N., Lodge, J. M., Fierke, C. A. & Mapp, A. K. Dissecting allosteric effects of activator-coactivator complexes using a covalent small molecule ligand. *Proceedings of the National Academy of Sciences of the United States of America* **111**, 12061-12066, doi:10.1073/pnas.1406033111 (2014).

17   Law, S. M., Gagnon, J. K., Mapp, A. K. & Brooks, C. L., III. Prepaying the entropic cost for allosteric regulation in KIX. *Proceedings of the National Academy of Sciences of the United States of America* **111**, 12067-12072, doi:10.1073/pnas.1405831111 (2014).

18   Arkin, M. R. *et al.* Binding of small molecules to an adaptive protein-protein interface. *Proceedings of the National Academy of Sciences of the United States of America* **100**, 1603-1608, doi:10.1073/pnas.252756299 (2003).

19   Arkin, M. R., Tang, Y. & Wells, J. A. Small-molecule inhibitors of protein-protein interactions: progressing toward the reality. *Chemistry & biology* **21**, 1102-1114, doi:10.1016/j.chembiol.2014.09.001 (2014).

20   Annand, J. R., Bruno, P. A., Mapp, A. K. & Schindler, C. S. Synthesis and biological evaluation of pharbinilic acid and derivatives as NF-kappaB pathway inhibitors. *Chem Commun (Camb)* **51**, 8990-8993, doi:10.1039/c5cc02918j (2015).

21   Anest, V. *et al.* A nucleosomal function for IkappaB kinase-alpha in NF-kappaB-dependent gene expression. *Nature* **423**, 659-663, doi:10.1038/nature01648 (2003).

22   Espinosa, L., Bigas, A. & Mulero, M. C. Alternative nuclear functions for NF-kappaB family members. *Am J Cancer Res* **1**, 446-459 (2011).

23   Makley, L. N. *et al.* Pharmacological chaperone for alpha-crystallin partially restores transparency in cataract models. *Science* **350**, 674-677, doi:10.1126/science.aac9145 (2015).

24   Cummings, M. D., Farnum, M. A. & Nelen, M. I. Universal screening methods and applications of ThermoFluor. *J Biomol Screen* **11**, 854-863, doi:10.1177/1087057106292746 (2006).

25   Bieche, I. *et al.* Expression of PEA3/E1AF/ETV4, an Ets-related transcription factor, in breast tumors: positive links to MMP2, NRG1 and CGB expression. *Carcinogenesis* **25**, 405-411, doi:10.1093/carcin/bgh024 (2004).

26   Davidson, B. *et al.* PEA3 is the second Ets family transcription factor involved in tumor progression in ovarian carcinoma. *Clinical cancer research : an official journal of the American Association for Cancer Research* **9**, 1412-1419 (2003).

27   de Launoit, Y. *et al.* The Ets transcription factors of the PEA3 group: transcriptional regulators in metastasis. *Biochimica et biophysica acta* **1766**, 79-87, doi:10.1016/j.bbcan.2006.02.002 (2006).

28   Wang, J., Lee, J., Liem, D. & Ping, P. HSPA5 Gene encoding Hsp70 chaperone BiP in the endoplasmic reticulum. *Gene* **618**, 14-23, doi:10.1016/j.gene.2017.03.005 (2017).

29   Okada, T., Yoshida, H., Akazawa, R., Negishi, M. & Mori, K. Distinct roles of activating transcription factor 6 (ATF6) and double-stranded RNA-activated protein kinase-like endoplasmic reticulum kinase (PERK) in transcription during the mammalian unfolded protein response. *The Biochemical journal* **366**, 585-594, doi:10.1042/BJ20020391 (2002).

30   Sela, D. *et al.* Endoplasmic reticulum stress-responsive transcription factor ATF6alpha directs recruitment of the Mediator of RNA polymerase II transcription and multiple

histone acetyltransferase complexes. *The Journal of biological chemistry* **287**, 23035-23045, doi:10.1074/jbc.M112.369504 (2012).